MICHIGAN STATE UNIVERSITY LIBRARIES
3 1293 00634 3226

L

This is to certify that the

dissertation entitled

THE ELECTRONIC AND GEOMETRIC STRUCTURE OF
I. DILITHIOMETHANE, CH_2Li_2, AND
II. VARIOUS SMALL CATIONS CONTAINING
SCANDIUM AND CHROMIUM

presented by

Aileen Evelyn Alvarado-Swaisgood

has been accepted towards fulfillment
of the requirements for

Ph.D. degree in Chemistry

James F Harrison
Major professor

Date 10-31-86

MSU is an Affirmative Action/Equal Opportunity Institution

MSU
LIBRARIES

RETURNING MATERIALS:
Place in book drop to remove this checkout from your record. FINES will be charged if book is returned after the date stamped below.

216

THE ELECTRONIC AND GEOMETRIC STRUCTURE OF
I. DILITHIOMETHANE, CH_2Li_2, AND
II. VARIOUS SMALL CATIONS CONTAINING SCANDIUM AND CHROMIUM

By

Aileen Evelyn Alvarado-Swaisgood

A DISSERTATION

Submitted to
Michigan State University
in partial fulfillment of the requirements
for the degree of

DOCTOR OF PHILOSOPHY

Department of Chemistry

1986

ABSTRACT

THE ELECTRONIC AND GEOMETRIC STRUCTURE OF
I. DILITHIOMETHANE, CH_2Li_2, AND
II. VARIOUS SMALL CATIONS CONTAINING SCANDIUM AND CHROMIUM

By

Aileen Evelyn Alvarado-Swaisgood

Dilithiomethane

The electronic structure of the lowest singlet and triplet states of CH_2Li_2 has been studied with the goal of understanding the bonding in this unusual molecule. Previous work placed the lowest triplet approximately 2 kcal/mol above the lowest singlet with the calculated dipole moment of the singlet being +5.42 D and that of the triplet being -0.76 D. We have constructed MCSCF functions at the optimal SCF geometry and predict a similar shift in the dipole moment in going from the singlet to the triplet state. In addition, these MCSCF calculations suggest an orbital interpretation of the bonding consistent with the dipole moments. Density difference plots, orbital contours, and a population analysis of the various MCSCF functions are presented.

Small Cations Containing Scandium and Chromium

The electronic and geometric structure of the Cr cations CrH^+, $CrCH_3^+$, $CrCH_2^+$, $CrCH^+$, and $CrCl^+$, and of the Sc cations ScH^+, $ScCH_3^+$, $ScCH_2^+$, $ScCH^+$, and ScH_2^+ have been studied by ab initio MCSCF and CI (MCSCF+1+2) techniques. The resulting bond energies, bond lengths, and electron distribution suggest: Cr^+ forms a single, double, and triple bond with the ligands CH_3, CH_2, and CH, respectively, while Sc^+ forms a single, double, and double bond with the same ligand series; the transition metal-carbon bonds become more ionic and the bond lengths become shorter as the bond order increases; the bonding in the low lying states of $CrCl^+$ have large ionic character due to the charge transfer from Cr to Cl and the differences between the $^5\Sigma^+$ and $^5\Pi$ states of $CrCl^+$ are very subtle; the ground state of ScH_2^+ has a non-linear structure and, based on the calculated energetics, the reductive elimination of H_2 from ScH_2^+ will be endothermic. An analysis of the exchange energy loss of the metal ion upon bond formation suggests that there is an intrinsic metal-carbon bond energy for these species given by the sum of the exchange energy loss and the calculated bond energies. The calculated bond energies are compared with available (ion beam) experimental values and a detailed analysis of the role played by the metal ion 4s and $3d_\sigma$ electrons in the bonding, as well as, the varying degrees of charge transfer is presented.

TO THE "CONSTANT FACTOR IN MY LIFE"—
MY FAMILY

ACKNOWLEDGEMENTS

One may accomplish many mile stones in one's life but those accomplishments are greatly possible by the love, support, advice and encouragement of those fine individuals we come across each day.

I wish to thank Dr. James Harrison for what seemed like a boundless source of knowledge, guidance and encouragement during the course of my graduate studies.

Also, I wish to extend my appreciation to the members of my Guidance Committee (Dr. Schwendeman, Dr. Allison, Dr. Eick, and Dr. Pinnavaia) for their valuable suggestions. It is a pleasure to thank Drs. Paul and Kathy Hunt, and Dr. Frederick Horne for the opportunity they have given me to come to Michigan State University to pursue a degree in Theoretical Chemistry.

A special acknowledgement to my family, in particular to my parents, Hector I. Alvarado Rivera and Carmen E. Santiago de Alvarado, and my dear husband, Mark, for the love and moral support throughout the many stages of my life.

Thanks are extended to Michigan State University for financial support as a graduate assistant throughout the course of this research. Finally, I would like to thank the Department of Urban Affairs (MSU), the Dow Chemical Co., the

College of Natural Science (MSU), and the Department of Chemistry (MSU) for various academic fellowships.

TABLE OF CONTENTS

Page

LIST OF TABLES viii

LIST OF FIGURES xi

KEY TO SYMBOLS AND ABBREVIATIONS xvii

CHAPTER I

INTRODUCTION 1

CHAPTER II

The Bonding, Dipole Moment, and Charge Distribution in the Lowest Singlet and Triplet States of Dilithiomethane, CH_2Li_2.

INTRODUCTION 3

A. Bonding of C with Li_2 5

ELECTRONIC STRUCTURE OF DILITHIOMETHANE, CH_2Li_2 .. 11

A. Orbital Description and Development of Wavefunctions 11

B. Computational Details 16

C. Results and Discussion 16

1. Orbital Characterization 20

2. Charge Distribution and Dipole Moment 28

3. On the Role of the Li p Orbitals 35

Page

CONCLUSIONS 36

REFERENCES 40

CHAPTER III

The Electronic and Geometric Structure of Various Small Cations Containing Scandium and Chromium.

INTRODUCTION 42

BASIS SETS AND MOLECULAR CODES 45

SIZE CONSISTENCY 46

NATURE OF THE FRAGMENTS: TRANSITION METAL IONS ... 48

BONDING OF Sc^+ AND Cr^+ WITH H, CH_3, CH_2, AND CH .. 51

A. CrH^+ and $CrCH_3^+$ 56

B. ScH^+ and $ScCH_3^+$ 66

Comparison between ScH^+ and ScH 77

C. $CrCH_2^+$ 83

D. $ScCH_2^+$ 94

E. $CrCH^+$ 101

F. $ScCH^+$ 108

Comparison between Cr-C and C-C Bonds .. 114

BONDING OF Sc^+ WITH H_2 116

Results and Discussion 116

BONDING OF Cr^+ WITH Cl 123

A. Wavefunctions and Computational Details .. 123

B. Energetics and Geometric Structure 126

C. Potential Energy Curves and Charge Distribution 126

D. Long Range Interactions 135

CONCLUSIONS: COMPARISON BETWEEN THE
Sc AND Cr COMPOUNDS ....
REFERENCES ....
APPENDIX A
Electronic Structure Theory: Techniques
INTRODUCTION ....
DEVELOPMENT OF WAVEFUNCTIONS ....
REFERENCES ....
APPENDIX B
Listing of Publications ....

LIST OF TABLES

Table Page

CHAPTER II

1. Comparison of Laidig and Schaefer (LS) Results with Those of the Current Study 18

2. The Principal Natural Orbitals of the Planar Singlet and Their Contributions to the Dipole Moment and Population Analysis 29

3. The Principal Natural Orbitals of the Tetrahedral Singlet and Their Contributions to the Dipole Moment and Population Analysis 30

4. The Principal Natural Orbitals of the Planar Triplet and Their Contributions to the Dipole Moment and Population Analysis 31

5. The Principal Natural Orbitals of the Tetrahedral Triplet and Their Contributions to the Dipole Moment and Population Analysis 32

CHAPTER III

1. Experimental Bond Energies for Selected Scandium, Chromium, and Vanadium Cations 53

Table Page

2. Calculated Energies, Bond Strengths, and Geometric Parameters for Various Chromium Cations 54

3. Calculated Energies, Bond Strengths, and Geometric Parameters for Various Scandium Cations 55

4. Equilibrium Properties of ScH^+ in the $^2\Delta$, $^2\Pi$, and $^2\Sigma^+$ States Calculated with the **spd** and **spdf** Basis Sets Using the MCSCF and MCSCF+1+2 Functions 71

5. Equilibrium Properties of Neutral ScH in Several Low-Lying Electronic States Calculated with the **spd** Basis Set Using the MCSCF+1+2 Functions......................... 78

6. Equilibrium Properties of ScH_2^+ in the Ground $^1A_1$ State Calculated with the **spd** and **spdf** Basis Sets Using the MCSCF and MCSCF+1+2 Functions 118

7. Equilibrium Properties of $CrCl^+$ in the $^5\Sigma^+$ and the $^5\Pi$ States Calculated Using the MCSCF and MCSCF+1+2 Functions 127

8. Long Range Interaction Energies of a Chlorine Atom Approaching a Point Charge 138

Table Page

9. Comparison of the Transition Metal (TM) Contribution to the σ Bond, the Percentage of 4s and $3d_\sigma$ Orbital Character, and the Bond Lengths in Each of the Sc^+-C and Cr^+-C Bonds 142

LIST OF FIGURES

Figure Page

CHAPTER II

1. The Optimized SCF Geometries of Laidig and Schaefer 17
2. The Contours of the (GVB) Valence Orbitals in the Planar and Tetrahedral Singlets 21
3. The Contours of the $2\sigma_g$ Orbital of Li_2^+ 23
4. The Contours of the (GVB) Valence Orbitals in the Planar and Tetrahedral Triplets 25
5. Density Difference Plots (molecule - atom) in Several Planes for the Planar Singlet and Triplet States of CH_2Li_2 27

CHAPTER III

1. Flow chart for the QUEST-164 collection of codes as implemented at MSU 47
2. Comparison of experimental sd^N-d^{N+1} energy separation with SCF and MCSCF results 49
3. Potential energy curve for the lowest $^5\Sigma^+$ state of CrH^+ 57
4. GVB orbitals for the Cr-H bond in $^5\Sigma^+$ CrH^+ at equilibrium geometry 59

Figure Page

5. Electron population of selected atomic orbitals from the bonding natural orbitals of the 7 CSF MCSCF wavefunction of $^6\Sigma^+$ CrH^+ 60

6. Potential energy curve for the lowest $^5A'$ state of $CrCH_3{}^+$ 63

7. Electron population of selected atomic orbitals from the bonding natural orbitals of the 7 CSF MCSCF wavefunction of $^5A'$ $CrCH_3{}^+$ 64

8. GVB orbitals for the Cr-C bond in $CrCH_3{}^+$ at its equilibrium geometry 65

9. Binding energy of ScH^+ in the $^2\Delta$ state as a function of R for the **spd** and **spdf** basis sets in both the MCSCF and MCSCF+1+2 calculations 67

10. Binding energy of ScH^+ in the $^2\Pi$ state as a function of R for the **spd** and **spdf** basis sets in both the MCSCF and MCSCF+1+2 calculations 68

11. Binding energy of ScH^+ in the $^2\Sigma^+$ state as a function of R for the **spd** and **spdf** basis sets in both the MCSCF and MCSCF+1+2 calculations 70

12. Electron population of selected atomic orbitals of σ symmetry from the bonding natural orbitals of the MCSCF wave function (**spd** basis) of $^2\Delta$ ScH^+ 73

Figure Page

13. Electron population of selected atomic orbitals of σ symmetry from the bonding natural orbitals of the MCSCF wave function (**spd** basis) of $^2\Pi$ ScH^+ 74

14. Electron population of selected atomic orbitals of σ symmetry from the bonding and nonbonding natural orbitals of the MCSCF wave functions (**spd** basis) of $^2\Sigma^+$ ScH^+ 75

15. Potential energy curve for the lowest $^2A''$ state of $ScCH_3{}^+$ 80

16. Electron population of selected atomic orbitals from the bonding natural orbitals of the 4 CSF MCSCF wavefunction of $^2A''$ $ScCH_3{}^+$ 82

17. Potential energy curves for the $^6B_1$ (filled circles) and $^4B_1$ (open circles) states of $CrCH_2{}^+$ 85

18. Electron population of selected atomic orbitals from the bonding sigma natural orbitals of the 7 CSF MCSCF wavefunction of $^6B_1$ $CrCH_2{}^+$... 86

19. Electron population of selected atomic orbitals from the bonding sigma natural orbitals of the 34 CSF MCSCF wavefunction of $^4B_1$ $CrCH_2{}^+$.. 87

20. GVB orbitals for the Cr-C σ bond and the singly occupied π orbitals of $^6B_1$ $CrCH_2{}^+$ at its equilibrium geometry 88

Figure Page

21. GVB orbitals for the Cr-C σ and π bonds of $^4B_1$ $CrCH_2^+$ at its equilibrium geometry 89

22. Natural orbital occupation numbers for the valence π orbitals of the MCSCF wavefunctions of $CrCH_2^+$ ($^4B_1$) and $CrCH^+$ ($^3\Sigma^-$) 92

23. Electron population of selected atomic orbitals from the bonding π natural orbitals of the MCSCF wavefunctions for $CrCH_2^+$ ($^4B_1$) and $CrCH^+$ ($^3\Sigma^-$) 93

24. Potential energy curves for the lowest $^1A_1$ state of $ScCH_2^+$ 95

25. Potential energy curves for the lowest $^3A_1$ state of $ScCH_2^+$ 97

26. Electron population of selected atomic orbitals from the bonding σ and π natural orbitals of the 10 CSF MCSCF wavefunction of $^1A_1$ $ScCH_2^+$.. 98

27. Electron population of selected atomic orbitals from the bonding sigma natural orbitals of the 7 CSF MCSCF wavefunction of $^3A_1$ $ScCH_2^+$... 99

28. Potential energy curves for the lowest $^3\Sigma^-$ states of $CrCH^+$ 103

29. Electron population of selected atomic orbitals from the bonding σ natural orbitals of the 126 CSF MCSCF wavefunction of $^3\Sigma^-$ $CrCH^+$ 104

Figure Page

30. GVB orbitals for the Cr-C σ and π bonds of $^3\Sigma^-$ CrCH$^+$ 106

31. Potential energy curves for the lowest $^2\Pi$ state of ScCH$^+$ 109

32. Electron population of selected atomic orbitals from the bonding σ natural orbitals of the 17 CSF MCSCF wavefunction of $^2\Pi$ ScCH$^+$ 110

33. Bond energy and Sc-C bond lengths of various states of ScCH$^+$ which dissociate to Sc(^{3}D) + CH($^4\Sigma^-$) 113

34. Correlation of predicted (Cr-R)$^+$ bond lengths with standard R-R bond lengths 115

35. Computed dissociation energies of various combinations of Sc$^+$ and two H atoms relative to the separated ground state atoms 122

36 Potential energy curves for the lowest $^6\Sigma^+$, $^6\Pi$, and $^7\Pi$ states of CrCl$^+$ 128

37. Electron population of selected atomic orbitals from the bonding natural orbitals of the 7 CSF MCSCF wavefunction of $^6\Sigma^+$ CrCl$^+$ 129

38. Electron population of selected atomic orbitals from the bonding natural orbitals of the 14 CSF MCSCF wavefunction of $^6\Pi$ CrCl$^+$ 130

Figure Page

39. Comparison of the calculated bond energies and geometric parameters for various Sc and Cr compounds 140

APPENDIX A

1. Spin Eigenfunction Branching Diagram 168

KEY TO SYMBOLS AND ABBREVIATIONS

Symbol and/or Abbreviation	Meaning
SCF	Self-Consistent-Field
GVB	Generalized Valence Bond
MCSCF	Multiconfiguration SCF
SOGVB	Spin Optimized GVB
CI	Configuration Interaction
SCF+1+2	Single and double excitations from SCF reference space (CI)
MCSCF+1+2	Single and double excitations from MCSCF reference space (CI)
b_l, b_r	Bonding Orbitals
l_Y, l_Y	Lobe Orbitals
LS	Laidig and Schaefer
ΔE	Relative Energies
μ	Dipole Moment
S	(GVB) Orbital Overlap
PS	Planar Singlet (CH_2Li_2)
PT	Planar Triplet (")
TS	Tetrahedral Singlet (CH_2Li_2)
TT	Tetrahedral Triplet (")
P	With Li p Orbitals

Symbol and/or Abbreviation	Meaning
NO-P	Without Li p Orbitals
$\Delta\rho$	Density Difference ($\rho_{molecule} - \rho_{atom}$)
$\mu^{(e)}$	Electronic Contribution to the Dipole Moment
$\mu^{(N)}$	Nuclear Contribution to the Dipole Moment
TM	Transition Metal
ICR	Ion Cyclotron Resonance
m/z	Mass Ratio
R_{eq} or R_e	Equilibrium (Bond) Distance
D_e	Dissociation Energy ($E_{R=\infty} - E_{R=eq}$)
au	Atomic units: for Energies ... hartree for Distance ... bohrs
mH	Millihartree
2X2 MCSCF	Two Configuration MCSCF
$3d_{\sigma}$	m=0; $3d_{z^2}$ Orbital a_1 orbital (C_{2v} symm.)
$3d_{\pi_x}$	|m|=1; $3d_{XZ}$ Orbital b_1 orbital (C_{2v} symm.)
$3d_{\pi_y}$	|m|=1; $3d_{YZ}$ Orbital b_2 orbital (C_{2v} symm.)
$3d_{\delta_+}$	|m|=2; $3d_{X^2-Y^2}$ Orbital a_1 orbital (C_{2v} symm.)

Symbol and/or Abbreviation	Meaning
$3d_{\delta_-}$	$\|m\|=2$; $3d_{XY}$ Orbital a_2 orbital (C_{2v} symm.)
$\alpha(\omega),\beta(\omega)$	Orthogonal Spin Functions
$(\alpha\beta-\beta\alpha)$	Singlet-Coupled Spin Functions
$\alpha\alpha\alpha\ldots$	High-Spin-Coupled Spin Functions
CSF	Configuration State Functions
ω_e	Equilibrium Vibrational Frequency
$\alpha_{\alpha\beta}$	Polarizability Tensor
$\theta_{\alpha\beta}$	Quadrapole Moment Tensor
F_α,F_β	Electric Field
$F'_{\alpha\beta}$	Electric Field Gradient
Ψ	Total Wavefunction of the System
H	Hamiltonian (Energy) Operator
∇_i^2	Laplacian Operator Associated with the i^{th} particle
M_A	Mass Ratio between nucleus A and an electron
Z_A	Atomic Number
r_{iA}	Distance between i^{th} electron and nucleus A
r_{ij}	Distance between two electrons
R_{AB}	Distance between two nuclei
$<\ \|\ \|\ >$	Braket Notation for an Integral
Φ_i	One-electron Functions

Symbol and/or Abbreviation	Meaning
$\mathcal{A}$	Antisymmetrization Operator
$[\Phi_1(\underset{\sim}{q}_1)\ \Phi_2(\underset{\sim}{q}_2)\ \ldots]$	Electronic Configuration
$\Phi(\underset{\sim}{r})$	One-electron Spatial Function
χ_μ	Atomic Basis Functions
δ_{ij}	Kronecker Delta
$\langle\Psi\|H\|\Psi\rangle$	Expectation Value of the Energy
$\langle i\|i\rangle$	One-electron Integral
$\langle ij\|ij\rangle$	Coulomb Two-electron Integral
$\langle ij\|ji\rangle$	Exchange Two-electron Integral
$f(\underset{\sim}{r}_1)$	Fock Operator
$\mathbf{F}$	Fock Matrix
ε_i	One-electron Energy
ζ_+,ζ_-	Localized (GVB) Orbitals

CHAPTER I

INTRODUCTION

The main objective of this dissertation is to determine a) the electronic structure of dilithiomethane, CH_2Li_2, and b) the electronic and geometric structure of various small cations containing scandium (Sc) and chromium (Cr). Electronic Structure Theory has developed into a useful technique for elucidating the factors which dictate the electronic and geometric structure of molecules and understanding the role of these factors in the observed chemistry. In the past, ab initio calculations were limited to small systems containing few electrons while the study of larger systems involved higher levels of approximation (e.g., Huckel Theory). However, increased computer power and highly optimized computer codes have allowed for the investigation of a whole new array of molecules.

In Chapter II, the electronic structure of the low lying states of dilithiomethane, CH_2Li_2, is evaluated using ab initio MCSCF and CI techniques with the goal of understanding the bonding in this unusual molecule. Dilithiomethane falls into the group of interesting compounds where the carbon central atom, most commonly found in the "tetra-

hedral" form when bound to four substituents, may also exist in a low energy planar form. A study of this system contributes to the understanding of the effect of substituents on the stability of the planar tetracoordinate carbon.

The electronic and geometric structure of various cations containing scandium and chromium, obtained by the use of ab initio MCSCF and CI techniques, is discussed in Chapter III. This study complements efforts made through the use of mass spectroscopic techniques, in understanding the nature of the chemical bond between the transition metal cation and different ligands which, in turn, provides us with the necessary information to understand the observed chemical reaction processes.

A general discussion of the techniques used to characterize the electronic structure of the various molecular systems described in this dissertation, is found in Appendix A. Special emphasis is given to the development of wavefunctions (MCSCF: GVB, SOGVB; CI: MCSCF+1+2) used in the calculations, though specific applications are discussed in the main text (Chapters II and III). A Key to Symbols and Abbreviations was included (found prior to Chapter I) for quick reference to the many "common" symbols and acronyms used in this dissertation.

A listing of publications resulting from this dissertation can be found in Appendix B.

CHAPTER II

THE BONDING, DIPOLE MOMENT, AND CHARGE DISTRIBUTION IN THE LOWEST SINGLET AND TRIPLET STATES OF DILITHIOMETHANE, CH_2Li_2

INTRODUCTION

Experimental determination of the structure of organolithium compounds is difficult primarily because they tend to aggregate in the solid and are highly solvated in solution[1]. Since ab initio calculations have been able to provide useful structural information[2] from molecules containing main group elements, which is comparable to that obtained experimentally, we anticipate similar calculations on CH_2Li_2 will shed light on the bonding structure of this molecule (not yet characterized by experiment).

Dilithiomethane, CH_2Li_2, falls into the group of interesting compounds where the carbon central atom, most commonly found in the tetrahedral form when bound to four substituents, may also exist in a low energy planar form. As suggested by Hoffmann[3], the stabilization of tetracoordinate carbon depends on the nature of the substituents. For example, if the hydrogens in methane were substituted by electron-withdrawing groups, the energy difference between

the planar form of the molecule and that of the nonplanar "tetrahedral" would be reduced. $C(CN)_4$ results in a planar-tetrahedral energy difference of 78 kcal/mol compared to 150 kcal/mol needed to make methane planar. This lowering in energy is due to the delocalization of the lone pair of the planar tetracoordinate carbon among the cyano groups. Substitution of hydrogen by less electronegative groups also lower the planar-tetrahedral energy difference. In $C(SiH_3)_4$, Si serves as both a σ donor and π acceptor by inclusion of 3d orbitals resulting in an energy difference of 67 kcal/mol.

Lithium atoms are very electropositive species and play an important role in stabilizing the planar form of CH_2Li_2. According to Collins et al.[4], CH_2Li_2 has a planar-tetrahedral energy difference of 10.35 kcal/mol based on a RHF (4-31G) ab initio calculation with the tetrahedral being lower. The dissociation energy of LiC-Li is around 20 kcal/mol[5] and that of C-Li is about 50 kcal/mol[5] leading us to believe that CH_2Li_2 would rather take the planar form than dissociate by breaking a C-Li bond.

Laidig and Schaefer[6] (LS) have also studied the lowest singlet and triplet electronic states of CH_2Li_2 and, on the basis of the calculated dipole moments, suggested a C^-Li^+ polarity for both planar and tetrahedral singlet states while the same molecule has reversed polarity C^+Li^- in both triplet states. Unfortunately no interpretaton of this remarkable observation was attempted.

We are interested in using the MCSCF and CI ab initio techniques to understand the bonding in the low lying states of CH_2Li_2 and to relate the structure of Li-C-Li in CH_2Li_2 with that in free $C\text{-}Li_2$[5] (which has been studied by our group). A study of these systems could shed light into the understanding of the stability of planar tetracoordinate carbon. In addition, CH_2Li_2 serves as a model for metal-carbene interactions.

A. Bonding of C with Li_2.

Before presenting the results of our calculations on the structure of CH_2Li_2, a review of studies done on small organo-lithium systems would be beneficial. Organo-lithium compounds, R-Li, have gained a reputation as being very useful synthetically, approaching the importance that Grignard reagents[7], R-MgX (X = Cl, Br, I), have in organic chemistry and other related fields. The carbon-metal ligand bond has been described to be of high ionic character (more like a hybrid between R-M and R^-M^+)[5,7,8]. Since lithium is more electropositive than the MgX ligand, C-Li bonds are more "ionic" than C-Mg bonds and, thus, organolithium compounds are more reactive than Grignard reagents.

In spite of their importance and interest, little has been done to study the electronic structure of lithium-containing organic molecules[5]. Lithium is a three electron system, making simple C-Li systems excellent models in the

study of organometallic compounds.

Throughout the years, our group[5,8] and others(see for example: refs.4,6,9) have developed a keen interest in the study of lithium-substituted carbynes, carbenes and other lithiated hydrocarbons. Mavridis and Harrison[5] reported the results obtained from the study of the electronic structure of the carbyne C-Li and the carbene CLi_2. The ab initio techniques used were SCF, GVB, and CI (see Appendix A) with a C (6s,4p,1d), Li (3s,1p) contracted basis set[5]. They noted that C-Li has a $^4\Sigma^-$ ground state with an excited state, $^2\Pi_r$, about 34 kcal/mol higher in energy. In contrast, C-H has a $^2\Pi_r$ ground state and a $^4\Sigma^-$ excited state 17 kcal/mol higher in energy. Also, in C-Li, a $^2\Pi_i$ state was found to be 49 kcal/mol higher than the $^4\Sigma^-$ ground state. The GVB representations of the $^4\Sigma^-$, $^2\Pi_r$, and $^2\Pi_i$ states of CLi[5] are as follows:

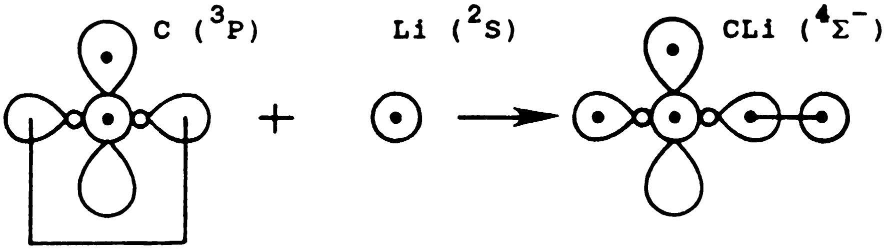

$$| {}^4\Sigma^- \rangle = | (\text{core}) (b_r b_l + b_l b_r) \sigma \pi_x \pi_y \alpha\beta\alpha\alpha\alpha \rangle$$

study of organometallic compounds.

Throughout the years, our group[5,8] and others(see for example: refs.4,6,9) have developed a keen interest in the study of lithium-substituted carbynes, carbenes and other lithiated hydrocarbons. Mavridis and Harrison[5] reported the results obtained from the study of the electronic structure of the carbyne C-Li and the carbene CLi_2. The ab initio techniques used were SCF, GVB, and CI (see Appendix A) with a C (6s,4p,1d), Li (3s,1p) contracted basis set[5]. They noted that C-Li has a $^4\Sigma^-$ ground state with an excited state, $^2\Pi_r$, about 34 kcal/mol higher in energy. In contrast, C-H has a $^2\Pi_r$ ground state and a $^4\Sigma^-$ excited state 17 kcal/mol higher in energy. Also, in C-Li, a $^2\Pi_i$ state was found to be 49 kcal/mol higher than the $^4\Sigma^-$ ground state. The GVB representations of the $^4\Sigma^-$, $^2\Pi_r$, and $^2\Pi_i$ states of CLi[5] are as follows:

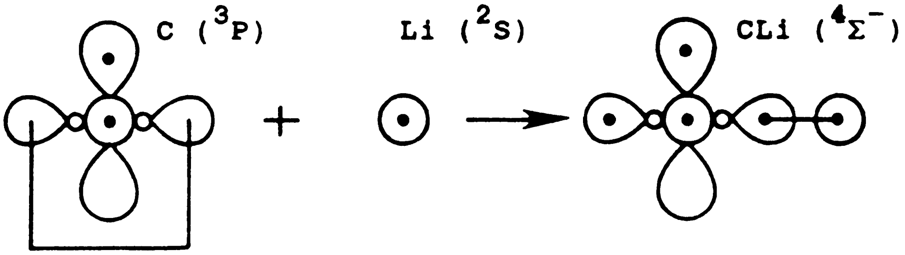

$$| {}^4\Sigma^- \rangle = | \text{(core)} (b_r b_l + b_l b_r) \sigma \pi_x \pi_y \alpha\beta\alpha\alpha\alpha \rangle$$

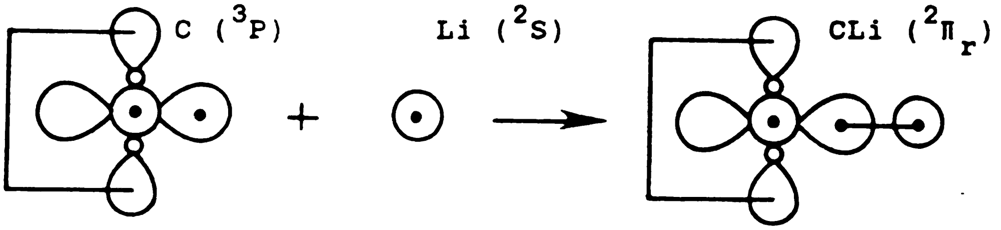

$$| {}^2\Pi_r > = | (\mathrm{core})\,(b_r b_l + b_l b_r)\,(l_y l_y + l_y l_y)\,\alpha\beta\alpha\beta\pi_x\alpha >$$

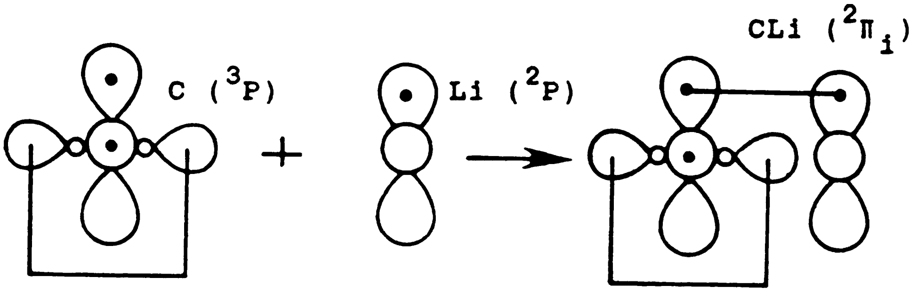

$$| {}^2\Pi_i > = | (\mathrm{core})\,(l_y l_y + l_y l_y)\,(\pi_{yr}\pi_{yl} + \pi_{yl}\pi_{yr})\,\pi_x\alpha\beta\alpha\beta\alpha >$$

where terms in parenthesis represent bonding orbitals on the right (r) and left (l) atom with the exception of l_y, l_y which represent the singlet coupled lobe orbitals (result of correlated carbon 2s orbital).

The $^4\Sigma^-$, $^2\Pi_r$, and $^2\Pi_i$ states were optimized at the SCF+1+2 level and the results[5] from the three states agree in one aspect: the C-Li bond has high ionic character due to considerable electron transfer from Li to C.

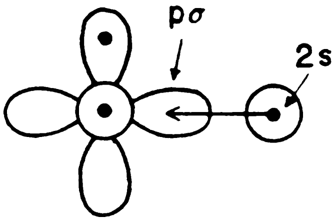

The $^4\Sigma^-$ and $^2\Pi_r$ states are composed of ground state fragments while the $^2\Pi_i$ state is composed of a ground state carbon and an excited state (^2P) lithium atom.

In a study of the multiplicity of substituted acyclic carbenes, Harrison et al.[8] concluded that acyclic carbenes with very electropositive substituents favor a triplet ground state. Consistent with this we find that in CLi_2 there are three triplets before the first singlet state[5]:

$^3\Sigma_g^-$	R= 3.717 a.
$^3\Pi_g(3)$	R= 3.507 a.
$^3A_2$	R= 3.815 a.; θ= 88.1°

The GVB description of how the linear $^3\Sigma_g^-$ state of CLi_2 is formed shows two ground state (^2S) lithium atoms bonding to both lobe orbitals in C(^3P). Calculations at the SCF+1+2 level[5] suggest that this state is a carbon-centered "carbene state". Bonding in the linear CLi_2 $^3\Pi_g(3)$ state is similar to the bonding scheme in the C-Li $^2\Pi_i(3)$ state but the second lithium (^2S) atom binds to the opposite lobe orbital.

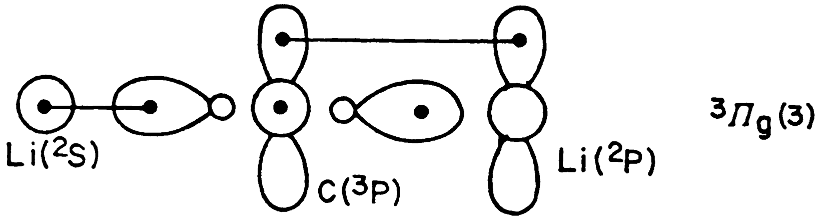

The results obtained for this state[5] suggest that the lobe orbital bonded to the Li(^{2}S) atom is more 2s-like and essentially doubly occupied (due to the ionic character of a C-Li bond).

The $^3A_2$ state is obtained when the Y-component of the $^3\Pi_g(3)$ state is bent in the XZ plane with X as the C_2 axis. Self-consistently optimized orbitals[5] lead to a Li_2 separation of 5.374 a_0 which lies between the Li_2^+ separation [10] and the experimental Li_2 separation[11]. As a result the $^3A_2$ state is described[5] as resulting from valence electrons from the Li_2 $2\sigma_g$ orbital being donated to an empty p_σ orbital on C.

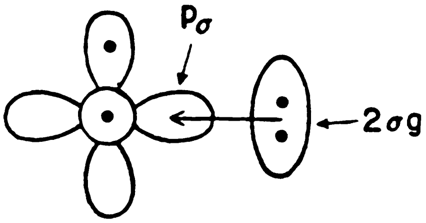

Before discussing the importance of this conclusion, it is useful to comment on the relative energies of the $^3\Sigma_g^-$ state and that of the $^3A_2$ state. At the SCF+1+2 level of calculation[5], $^3\Sigma_g^-$ is the ground state and $^3A_2$ is an excited state 6.2 kcal/mol higher in energy. By including corrections for unlinked clusters[5] the role switches, i.e., the $^3A_2$ is the ground state while the $^3\Sigma_g^-$ state is 0.2 kcal/mol higher. What we see are two low lying states, nearly degenerate but with very different geometries. At this level of calculation the ground state cannot be distinguished.

Generally, carbon compounds have tetrahedral, planar, or linear carbon centers depending on whether or not the carbon atom is singly, doubly, or triply bonded. Usually the energy difference between a planar and tetrahedral form of a tetracoordinate carbon is quite large; for example, for methane it is ~150 kcal/mol. By appropriate substitution[1,4,6] this energy difference can be lowered. The simplest candidate for planar tetracoordinate carbon is dilithiomethane, CH_2Li_2. Research to date suggests that there are three main factors[1,4,6] leading to the stabilization of a planar tetracoordinate carbon:

1) delocalization of the lone pair electrons of the planar carbon into the vacant π orbitals of the substituents.
2) σ electron donation from substituent to carbon atom.
3) angle reduction if the carbon atom is embodied into small rings.

ELECTRONIC STRUCTURE OF DILITHIOMETHANE, CH_2Li_2.

A. Orbital Description and Development of Wavefunctions

Understanding how carbon can find itself in a relatively stable tetracoordinate form would require some study of the orbitals involved in such a molecule. In CH_4,each bond can be described as:

$$B = (sp^3)_C + (s)_H$$

Depending on equilibrium geometries, nonplanar CH_2Li_2 bonds can be thought of as:

$$B_i = \lambda(sp^3)_i + \mu(s)_i$$

in which λ and μ would be determined by the variational principle. CH_2Li_2 has 8 valence (bonding) electrons.

By constructing symmetry orbitals (in C_{2v}) from each bond orbital, B_i, we would obtain

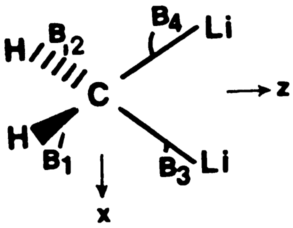

$B_1 + B_2 \rightarrow a_1$

$B_1 - B_2 \rightarrow b_2$ (node in LiCLi plane)

$B_3 + B_4 \rightarrow a_1$

$B_3 - B_4 \rightarrow b_1$ (node in HCH plane)

Now

$$B_3 + B_4 = \lambda(sp^3)_3 + \mu s_3 + \lambda(sp^3)_4 + \mu s_4$$

but

$$(sp^3)_3 \sim s + p_z + p_x$$
$$(sp^3)_4 \sim s + p_z - p_x$$

Therefore,

$$B_3 + B_4 \approx \lambda(s+p_z) + \mu(s_3+s_4) \rightarrow a_1$$

and

$$B_3 - B_4 \approx \lambda(p_x) + \mu(s_3-s_4) \quad \rightarrow b_1 \quad .$$

So the symmetry orbitals involved in the bonding of C with the two Li atoms in the nonplanar CH_2Li_2 can be visualized as follows:

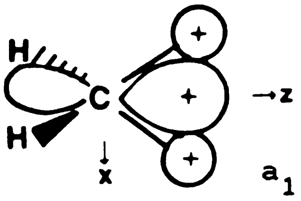

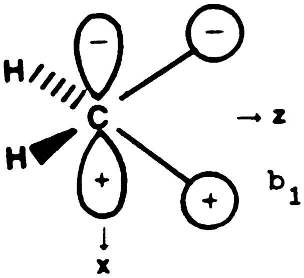

Keeping the hydrogens fixed and "twisting" the lithiums so they also lie on the YZ plane,

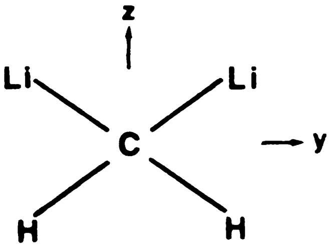

would give the cis-planar form for CH_2Li_2. The trans-planar

form is higher in energy and will not be considered. The symmetry orbitals, a_1 and b_1 in the nonplanar form, must also conform to the change in the geometry. The a_1 orbital retains a_1 symmetry in the planar form, but the two parts of the b_1 orbital have different symmetry in the planar form.

$\lambda(p_x) \rightarrow b_1$ (nonbonding: node in the molecular plane)

$\mu(s_3 - s_4) \rightarrow b_2$ (antibonding: node between the Li ligands)

Having two electrons in a b_1 orbital, where p_x on carbon is a π nonbonding orbital, is the preferred choice. This would involve backbonding to the Li π system.

The planar ${}^1A_1$ state of CH_2Li_2 is characterized by the configuration

$$1a_1^2 2a_1^2 1b_2^2 3a_1^2 2b_2^2 4a_1^2 1b_1^2 \qquad (1)$$

The $1a_1$ orbital is the carbon 1s function, the $2a_1$ and $1b_2$ are the symmetric and antisymmetric combinations of the Li 1s orbitals, and the $2b_2$ and $3a_1$ orbitals represent the two C-H bonds. The remaining two orbitals, $4a_1$ and $1b_1$, host the four electrons which must be responsible for binding the two Li atoms to C.

Since we are interested in the bonding between C and the two lithium atoms, the C-H bonding orbitals were

"fixed" at the SCF level. The remaining 4 valence electrons in the SCF wavefunction (1) are correlated as in the following example for the $^1A_1$ case:

$$\begin{array}{ll} \text{core} & (1a_1^2 2a_1^2 1b_2^2 3a_1^2 2b_2^2) \\ \text{valence} & (4a_1^2 1b_1^2) \qquad \text{SCF} \\ & \left.\begin{array}{l} (5a_1^2 1b_1^2) \\ (3b_2^2 1b_1^2) \\ (2b_1^2 1b_1^2) \\ (1a_2^2 1b_1^2) \\ (4a_1^2 6a_1^2) \\ (4a_1^2 4b_2^2) \\ (4a_1^2 3b_1^2) \\ (4a_1^2 2a_2^2) \end{array}\right\} \begin{array}{c} \text{Diagonal Double} \\ \text{Excitations} \end{array} \end{array}$$

Here, the $4a_1^2$ pair is excited into the $5a_1$, $2b_1$, $3b_2$, and $1a_2$ orbitals and the $1b_1^2$ pair is excited into the $6a_1$, $3b_1$, $4b_2$, and $2a_2$ orbitals. Thus, the MCSCF function for the $^1A_1$ state of CH_2Li_2 consists of nine configurations. The CI function was a full four electron CI over the MCSCF orbital reference space consisting of a total of 153 configurations.

The nonplanar $^1A_1$ state of CH_2Li_2 is characterized by the configuration

$$1a_1^2 2a_1^2 1b_1^2 3a_1^2 1b_2^2 4a_1^2 2b_1^2 \ .$$

This SCF wavefunction was then correlated, as in the planar

form, to give a MCSCF funtion consisting of 9 configurations and a CI function of 153 configurations.

If the $(1b_1^2)$ electron pair were "split" to give $(1b_1 5a_1)$, this would lead us to the $^3B_1$ state:

$$| \, ^3B_1 > \approx (\text{core})^2 \; 4a_1^2 1b_1 5a_1 \; \alpha\beta\alpha\alpha \qquad \text{SCF}$$

Keeping the orbitals involved with the core (including the C-H bond orbitals) frozen, the remaining four electrons were correlated in the following way:

For example,

$^3B_1$ planar

core $(1a_1^2 2a_1^2 1b_2^2 3a_1^2 2b_2^2)$

valence $(4a_1^2 1b_1 5a_1)$ SCF

$$\left.\begin{array}{l} (6a_1^2 1b_1 5a_1) \\ (2b_1^2 1b_1 5a_1) \\ (3b_2^2 1b_1 5a_1) \\ (1a_2^2 1b_1 5a_1) \end{array}\right\} \text{Diagonal Double Excitations}$$

$$\left.\begin{array}{l} (4a_1^2 3b_1 7a_1) \\ (4a_1^2 4b_2 2a_2) \end{array}\right\} \text{Off-diagonal Double Excitations (maintaining overall symmetry)}$$

The MCSCF function for the $^3B_1$ state of CH_2Li_2 consists of seven configurations and a full four-electron CI function from the MCSCF valence orbital reference space consists of 316 configurations. The wave functions for the nonplanar $^3B_1$ were also constructed in a similar fashion.

B. Computational Details

All wave functions used in this study were constructed with the ALIS[12] collection of codes as implemented on the MSU CYBER 750. The basis sets for carbon and lithium are the Duijneveldt[13] 11s6p and 9s augmented with a set of d functions (α= 0.75) on carbon and a set of four p functions on each lithium[14]. The hydrogen basis is the Huzinaga[15] 4s augmented with a set p functions (α= 1.00). The basis set was contracted following Raffenetti[16] to 4s2p1d on carbon, 3s2p on lithium, and 2s1p on hydrogen.

All calculations were done at the optimal (SCF) geometries reported by Laidig and Schaefer[6] (LS) as seen in Figure 1.

C. Results and Discussion

Relative energies (ΔE) and dipole moments (μ) were calculated for each of the low lying states of CH_2Li_2. Our results, which are compared to those reported by Laidig and Schaefer[6] (LS), appear in Table 1. The CI wavefunction used was not as extensive as that used by LS (7000 to 9000 configurations) but could adequately track the previously reported energy differences and dipole moments. We believe the wavefunction we have chosen is sufficiently accurate so as to capture the essential characteristics of the electronic structure of CH_2Li_2. In other words, the MCSCF wave functions and its corresponding CI functions used in

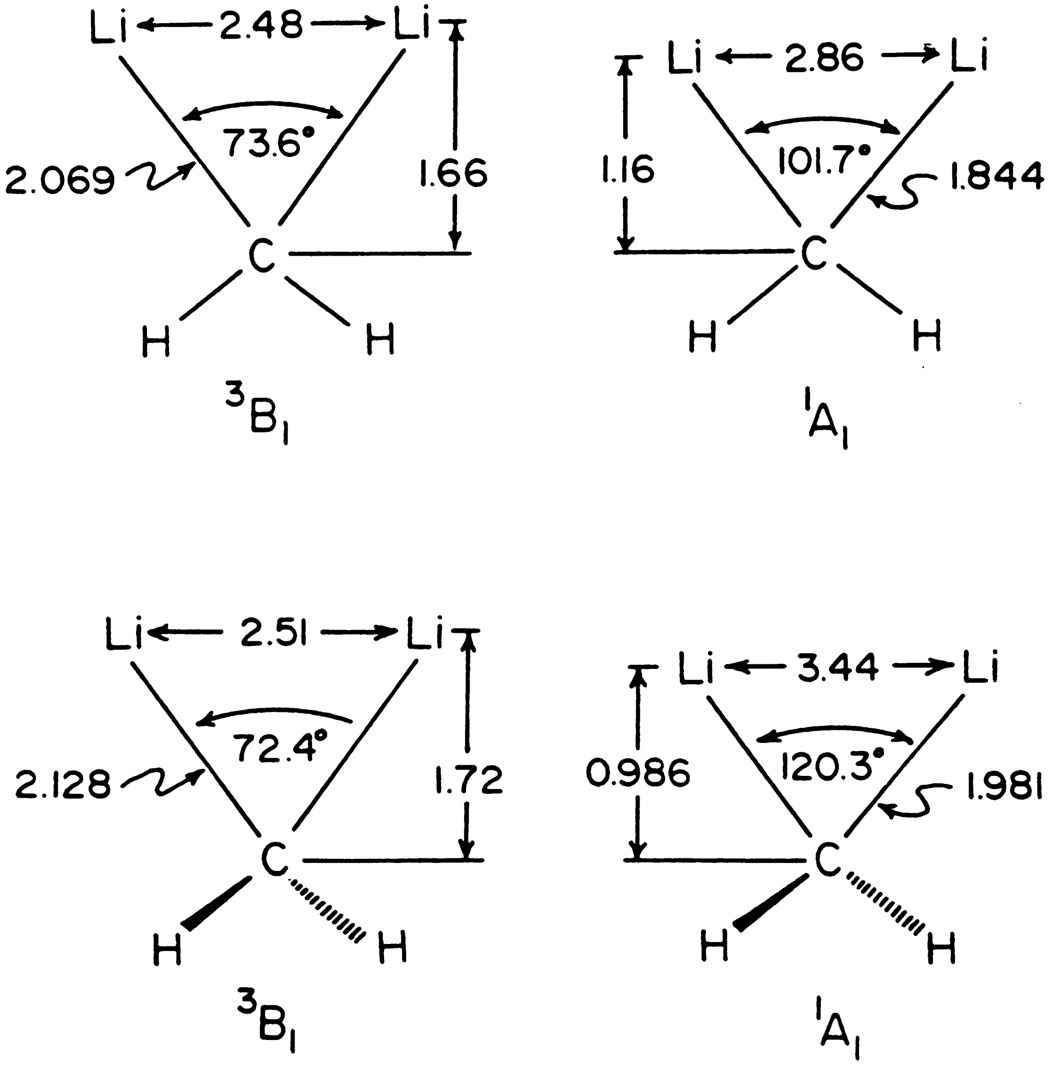
Li
2.48
Li
73.6°
2.069
1.66
C
H
H
$^3B_1$
Li
2.86
Li
1.16
101.7°
1.844
C
H
H
$^1A_1$
Li
2.51
Li
72.4°
2.128
1.72
C
H
H
$^3B_1$
Li
3.44
Li
0.986
120.3°
1.981
C
H
H
$^1A_1$

Figure 1. The Optimized SCF Geometries of Laidig and Schaefer. All distances are in angstroms.

Table 1. Comparison of Laidig and Schaefer (LS) Results with Those of the Current Study[a]

	ΔE(SCF)			μ(SCF)			ΔE(CI)			μ(CI)	
	LS	P	NO-P	LS	P	NO-P	LS	P	NO-P	P	NO-P
PS	+3.2	+2.0	+21.3	4.85	+4.95	+7.88	4.0 (4.2)	1.1	24.5	4.32	7.58
PT	-15.8	-15.3	-10.3	-1.22	-1.23	+2.57	2.4 (5.9)	3.8	8.2	-1.34	2.58
TS	0.0	0.0	0.0	5.42	+5.25	+5.10	0.0 (0.0)	0.0	0.0	+4.86	4.14
TT	-16.6	-15.9	-10.6	-0.76	-0.89	+2.90	1.3 (4.7)	3.5	8.0	-0.96	2.79

[a] Energies are relative to the tetrahedral singlet (TS) and are in kcal/mol, and the dipole moments are in debyes. The column headed P contains the results obtained on lithium while the NO-P column lists the corresponding quantities when the p orbitals on lithium were deleted from the basis. Other symbols include PS: planar singlet, PT: planar triplet, TT: tetrahedral triplet, and energy values in parenthesis are the unlinked-cluster corrections.

this study include those configurations needed to essentially describe the bonding in CH_2Li_2 with special emphasis in the C-Li_2 moiety.

We have included two sets of calculations in Table 1: one using the basis described previously (P) and another (NO-P) where the lithium p orbitals were deleted from the basis. Our intention is to understand the effect these p functions have in the overall bonding of CH_2Li_2. These effects will be discussed at a later time. For now, we will concern ourselves with those results where the lithium p functions were included.

The tetrahedral (nonplanar) singlet ($^1A_1$) state is the lowest lying state at the CI level followed by the planar singlet 1.1 kcal/mol higher in energy. The $^3B_1$ states are higher in energy relative to the singlet states. The tetrahedral $^3B_1$ and the planar $^3B_1$ states are 3.5 and 3.8 kcal/mol, respectively, higher than the tetrahedral singlet. The difference in energy between the tetrahedral and planar structures among the spin states are very low. As mentioned before, for the singlet states the tetrahedral-planar energy difference is 1.1 kcal/mol and that for the triplet states is 0.3 kcal/mol.

The dipole moments calculated at the CI level show positive values for the singlet states and small negative values for the triplet states. These results suggest a C^-Li^+ polarity for the singlet states and a C^+Li^- polarity for the triplet states (also observed by LS). Note that

this is a consequence of the difference in the electronic states ($^3B_1$ vs. $^1A_1$) and not because of the symmetry of the geometric structure (planar vs. nonplanar).

While these results compare favorably with those found in the literature[1,4,6], many questions remain unanswered and we believe a more detailed analysis of the charge distribution and orbital characteristics of the predicted structures of CH_2Li_2 is useful.

1. Orbital Characterization

The three most important terms in the CI function for both the tetrahedral and planar $^1A_1$ states are:

$4a_1^2 1b_1^2$	SCF[17]	
$5a_1^2 1b_1^2$	correlating	a_1 pair
$4a_1^2 2b_1^2$	"	b_1 pair

Using the relative weights of these configurations, we defined the GVB (generalized valence bond) bonding pairs from the two a_1 and the two b_1 orbitals, and these are contoured in Figure 2. The plotted coordinate system is as follows:

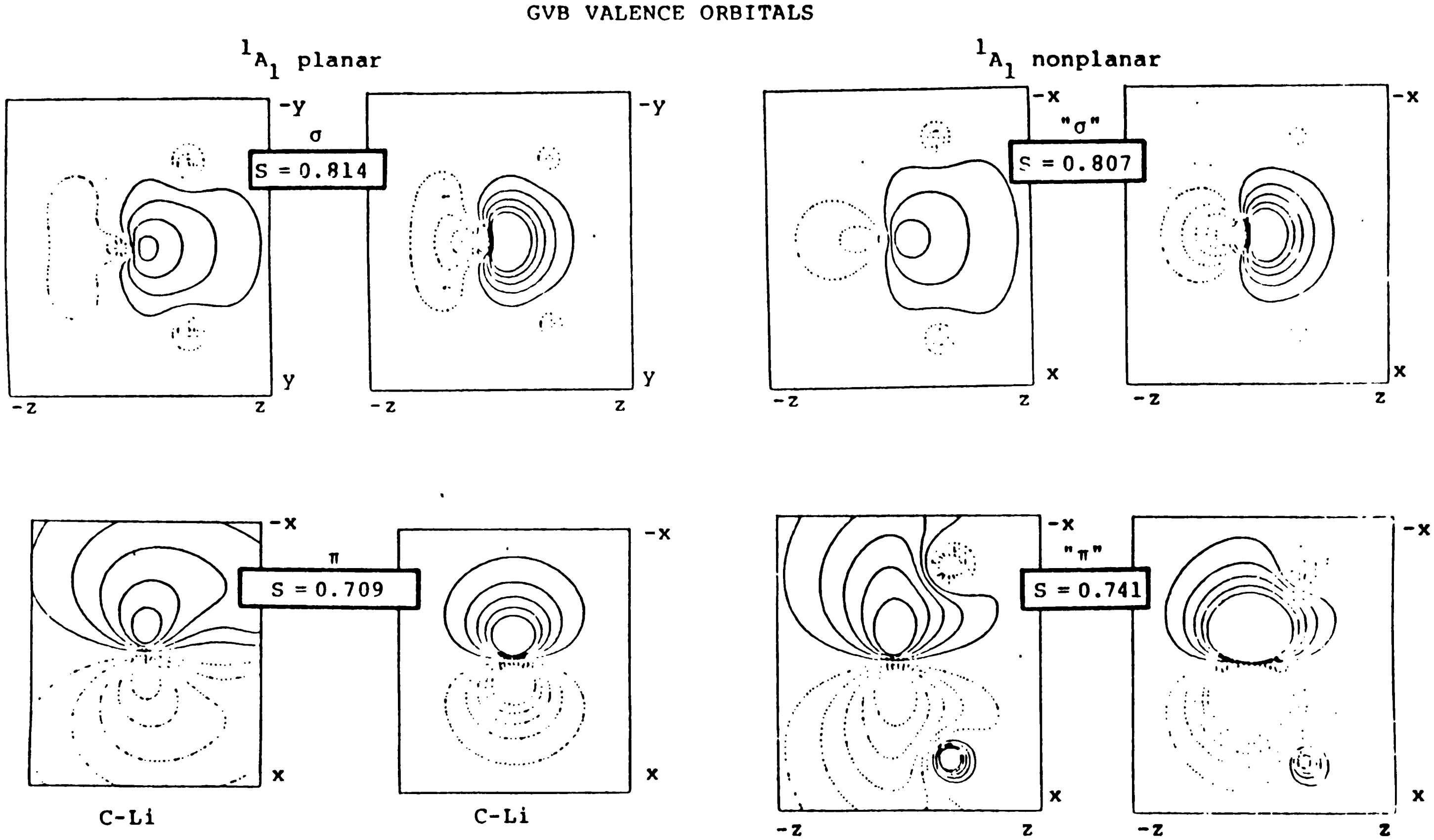

Figure 2. **The Contours of the (GVB) Valence Orbitals in the Planar and Tetrahedral Singlets.** The plots have uniformly spaced contours with increments of 0.5 au. Positive contours are indicated by solid lines and negative contours by dotted lines. All orbital contour plots follow this convention.

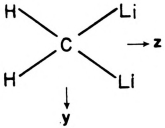

Planar (molecule in
YZ plane)

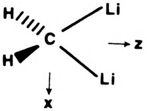

Nonplanar (CLi_2
in XZ plane and
CH_2 in YZ plane)

The calculated overlaps (S) of the GVB pairs are around 0.7 and 0.8. These values attest to the inadequacy of the SCF function (which does not allow the correlation of the valence a_1,b_1 electrons; S=1) to describe these states. Also, we note from the contours the "ionic" characteristic of the GVB π orbitals which are largely centered on the carbon. The GVB σ orbitals are more "covalent", where one orbital (centered on carbon) looks like an sp^2 orbital while the other resembles the Li^{2+} $2\sigma_g$ orbital. For comparison we contoured the $2\sigma_g$ bonding orbital of Li_2^+ at the Li-Li separation in CH_2Li_2, and show the results in Figure 3.

The interaction of C with Li_2 is similar in the "σ" system for both singlet states and the main difference in the "π" system lies on the symmetry of the carbon p_x orbital relative to the Li-C-Li molecular plane. In the planar state, the p_x orbital on carbon can only interact with the p_x orbitals on the lithium atoms (out-of-plane) while in the nonplanar state, it can interact with both the s and p

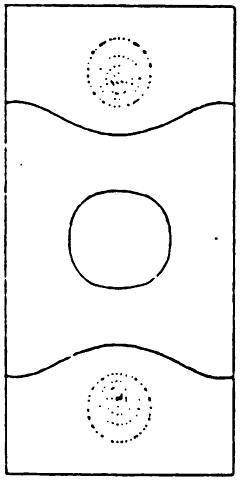

Figure 3. The Contours of the $2\sigma_g$ Orbital of Li_2^+.

orbitals on the Li atoms (in-plane).

The most important terms in the CI function for both the tetrahedral and planar $^3B_1$ states are:

$4a_1^2 1b_1 5a_1$ SCF[17]
and $6a_1^2 1b_1 5a_1$ correlating a_1 pair

Using the relative weights of these configurations, we constructed the GVB σ-bonding pair and these, as well as the $5a_1$ and $1b_1$ orbitals, are contoured in Figure 4.

The σ-bonding pair in the triplet states are very similar to those of the singlet states (and essentially identical to each other) yet have more carbon character than the singlet states. This is due to the presence of the $5a_1$ orbital in the triplet states. The $5a_1$ orbital is rather remarkable in that it is, in large measure, localized on the side of the Li_2 away from the carbon atom.

The $5a_1$ orbital has a node between the C and Li_2 group; in the $^3B_1$ states this accounts for the increased C-Li_2 separation as compared to the $^1A_1$ states (planar: 1.16A → 1.66A; nonplanar: 0.986A → 1.72A). The change in the nonplanar form is the most dramatic. Also the $5a_1$ orbital increases the Li_2 bond strength, thus, decreasing the Li_2 separation (planar: 2.86A → 2.48A; nonplanar: 3.44A → 2.51A). In both triplet states, the b_1 orbital is centered around carbon.

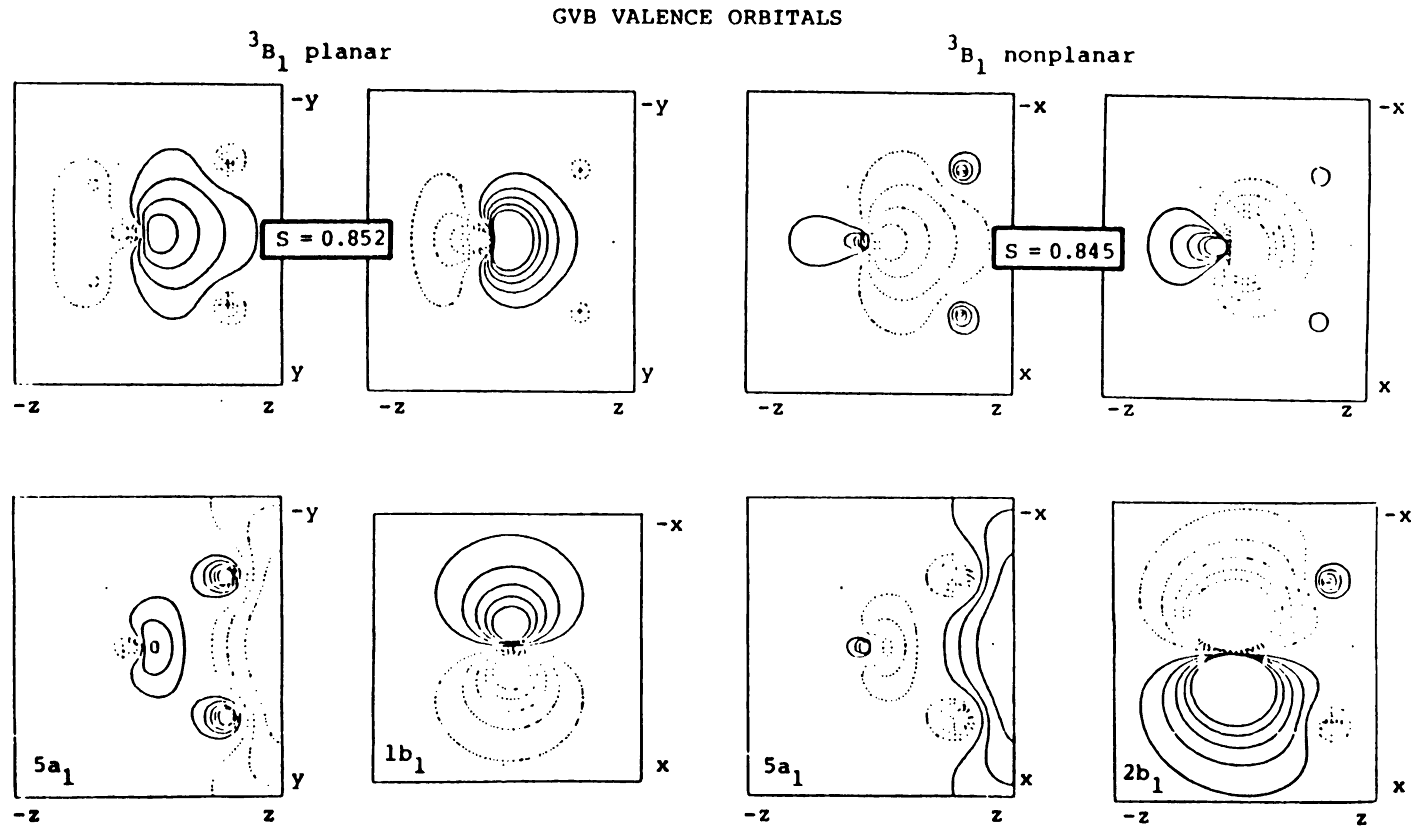

Figure 4. The Contour of the (GVB) Valence Orbitals in the Planar and Tetrahedral Triplets.

The differences in energy between the tetrahedral and planar structures among the spin states are very low: 1.1 kcal/mol between the singlet states and 0.3 kcal/mol between the triplet states. From the orbital contours we could see that the change from planar to tetrahedral in the singlet states is more noticeable than for the triplet states. This is due to the doubly occupied b_1 orbitals and its change in character (with its accompanied influence on Li_2) between the two geometric structures. In the triplet states, the larger C-Li_2 separation appears to lead to an indifference of the C p_π orbital to the Li_2 orientation, an effect that lowers the energy difference between the two geometric structures. Therefore, the rotation of Li_2 about the C_2 axis of CH_2 is essentially barrier-free.

A useful interpretative tool is the electron density difference plots for the planar $^1A_1$ and $^3B_1$ states which appear in Figure 5. In these plots the electron density of the molecule is compared to that of the separated atoms. The solid lines represent an increase in electron density over the separated atom values and the dotted lines represent a decrease. These plots were also contoured in several different planes: first, in the molecular plane; second, along a C-Li bond in a plane perpendicular to the molecular plane; and third, along the Li-Li bond in a plane also perpendicular to the molecular plane. While the C-H bonds are clearly visible as an enhanced electron density along the line connecting the C and H nuclei, the

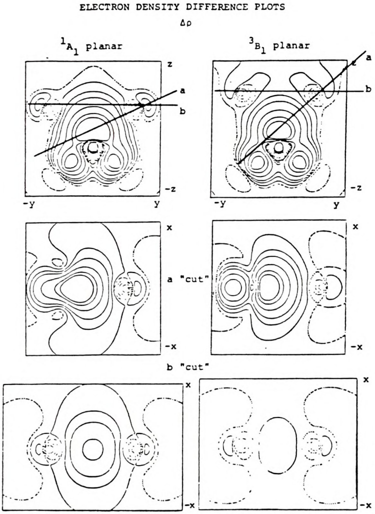

Figure 5. Density Difference Plots (molecule - atom) in Several Planes for the Planar Singlet and Triplet States of CH_2Li_2. The carbon atom for the singlet difference plot was taken as

$$1s^2\ (sp^2)^1_{H_1}\ (sp^2)^1_{H_2}\ p^2_\pi$$

where $(sp^2)_H$ is an sp^2 hybrid orbital directed toward an H atom and p_π is a 2p orbital perpendicular to the molecular plane. For the triplet difference plot the carbon configuration was

$$1s^2\ (sp^2)^1_{H_1}\ (sp^2)^1_{H_2}\ (sp^2)^1\ p^1_\pi$$

where the unsubscripted sp^2 orbital is directed toward the midpoint of the Li_2 group.

enhancement in the density between C and Li_2 seems delocalized over a significant region between them and is consistent with the carbon p_σ bonding with the Li_2 $2\sigma_g$ orbital (i.e., a three center bond). In the triplet state, the presence of the delocalized $5a_1$ orbital is apparent with the increase in electron density behind Li_2 away from the CH_2 group. The plane perpendicular to the molecule plane and containing the Li nuclei the strong Li-Li bonding interaction in the $^1A_1$ state while there is less enhancement of electron density between the two Li nuclei in the $^3B_1$ state. Much of the differential enhancement in the $^1A_1$ state seems to be due to the π electrons delocalized onto Li_2 from C. This is considerably reduced in the triplet state because, as noted above, the Li_2 group is much further away from the C p_π orbital, preventing a significant delocalization.

2. Charge Distribution and Dipole Moment

In the previous section we were able to obtain a feeling for the spatial extension of those valence orbitals crucial in the bonding of C with the two Li atoms. To further aid our understanding of the electronic structure of these states, we gathered the contribution of the most prominent natural orbitals to the population analysis and dipole moments for each of the states of CH_2Li_2 and are collected in Tables 2-5.

The dipole moment μ_z is the sum of an electronic

Table 2. The Principal Natural Orbitals of the Planar Singlet and Their Contributions to the Dipole Moment and Population Analysis

			Contribution to dipole moment	Net atomic population		
Natural Orbital	Occupation number (n_i)	COMMENT	$-n_i\langle \psi_i \| z \| \psi_i \rangle$(au)	C ..	H ..	Li ..
1a	2.000	1s on C	0.000	2.000	0.000	0.000
$2a_1$	2.000	1s on Li	-4.401	0.010	0.001	0.994
$3a_1$	2.000	C-H bond	+1.948	1.055	0.454	0.019
$1b_2$	2.000	1s on Li	-4.402	0.011	-0.001	0.995
$2b_2$	2.000	C-H bond	+1.283	0.831	0.497	0.087
$4a_1$	1.955	C-Li_2 bond	-2.128	1.355	-0.019	0.318
$1b_1$	1.924	π ORBITAL	-1.018	1.351	0.006	0.280
$2b_1$	0.069	CORRELATING	-0.084	0.037	0.000	0.016
$5a_1$	0.037	CORRELATING	-0.072	0.024	0.000	0.006
TOTAL	13.985		-8.874	6.674	0.938	2.715
$\mu_z^{(N)}$ (au)			+10.578			
$\mu_z^{(T)}$ (au)			+1.700			

Table 3. The Principal Natural Orbitals of the Tetrahedral Singlet and Their Contributions to the Dipole Moment and Population Analysis

Natural Orbital	Occupation number (n_i)	COMMENT	Contribution to dipole moment	Net atomic population		
			$-n_i\langle\psi_i\|z\|\psi_i\rangle$(au)	C ..	H ..	Li ..
$1a_1$	2.000	1s on C	0.000	2.000	0.000	0.000
$2a_1$	2.000	1s on Li	-3.729	0.008	0.000	0.996
$3a_1$	2.000	C-H bond	+1.876	1.226	0.380	0.008
$1b_2$	2.000	C-H bond	+1.243	0.993	0.488	0.015
$1b_1$	2.000	1s on Li	-3.729	0.008	0.000	0.996
$4a_1$	1.948	$C\text{-}Li_2$	-2.281	1.411	-0.004	0.273
$2b_1$	1.927	$Cp_\pi/Li_2\sigma_u$	-0.057	1.212	0.006	0.352
$3b_1$	0.062	CORRELATING	-0.011	0.032	0.000	0.015
$5a_1$	0.043	CORRELATING	-0.088	0.029	0.000	0.007
TOTAL	13.980		-6.776	6.919	0.870	2.662
$\mu_z^{(N)}$ (au)			+8.689			
$\mu_z^{(T)}$ (au)			+1.913			

Table 4. The Principal Natural Orbitals of the Planar Triplet and Their Contributions to the Dipole Moment and Population Analysis

			Contribution to dipole moment	Net atomic population		
Natural Orbital	Occupation number (n_i)	COMMENT	$-n_i\langle\psi_i\|z\|\psi_i\rangle$(au)	C ..	H ..	Li ..
$1a_1$	2.000	1s on C	0.000	2.000	0.000	0.000
$2a_1$	2.000	1s on Li	-6.264	0.008	0.000	0.996
$3a_1$	2.000	C-H bond	+2.006	1.112	0.450	-0.006
$1b_2$	2.000	1s on Li	-6.266	0.007	-0.001	0.997
$2b_2$	2.000	C-H bond	+1.233	0.997	0.472	0.030
$4a_1$	1.969	C-Li_2 bond	-1.987	1.595	-0.020	0.207
$1b_1$	0.997	π ORBITAL	-0.149	0.926	0.003	0.032
$2b_1$	0.008	CORRELATING	-0.019	0.002	0.000	0.003
$5a_1$	0.996	Li_2 bonding	-5.238	-0.018	0.002	0.505
TOTAL	13.970		-16.684	6.629	0.906	2.764
$\mu_z^{(N)}$ (au)			+16.189			
$\mu_z^{(T)}$ (au)			-0.495			

Table 5. The Principal Natural Orbitals of the Tetrahedral Triplet and Their Contributions to the Dipole Moment and Population Analysis

			Contribution to dipole moment	Net atomic population		
Natural Orbital	Occupation number (n_i)	COMMENT	$-n_i\langle\phi_i\|z\|\psi_i\rangle$(au)	C	H	Li
$1a_1$	2.000	1s on C	0.000	2.000	0.000	0.000
$2a_1$	2.000	1s on Li	-6.494	0.006	0.000	0.997
$3a_1$	2.000	C-H bond	+1.971	1.204	0.408	-0.010
$1b_2$	2.000	C-H bond	+1.233	1.057	0.467	0.004
$1b_1$	2.000	1s on Li	-6.495	0.002	0.000	0.999
$4a_1$	1.967	C-Li_2	-2.053	1.603	-0.014	0.196
$2b_1$	0.998	Cp_π	-0.077	0.901	0.003	0.046
$3b_1$	0.005	CORRELATING	-0.008	0.003	0.000	0.001
$5a_1$	0.996	Li_2 bonding	-5.363	-0.015	0.000	0.506
TOTAL	13.966		-17.286	6.761	0.864	2.739
$\mu_z^{(N)}$ (au)			16.957			
$\mu_z^{(T)}$ (au)			-0.329			

contribution, $\mu_z^{(e)}$, and a nuclear contribution, $\mu_z^{(N)}$, with the z axis being the C_2 axis:

$$\mu_z = \mu_z^{(e)} + \mu_z^{(N)} = -\sum_{i=1}^{N} \eta_i \langle \Psi_i | z | \Psi_i \rangle + (6z_{Li} + 2z_H)$$

In this expresion z_{Li} and z_H are the z coordinates of the nuclei, Ψ_i is a natural orbital of the appropriate wave function, η_i is the corresponding occupation number, and the sum is over all the natural orbitals of the system.

For both $^1A_1$ states, $\mu_z^{(N)} > |\mu_z^{(e)}|$ and the total dipole moment is positive, suggesting a shift of electrons from Li_2 to CH_2. This is consistent with the charge distribution of both states where ~0.6 electrons shifts to CH_2 from Li_2.

In forming the $^3B_1$ state, the $1b_1^2$ pair was split placing an electron in the $5a_1$ orbital. This $5a_1$ orbital is diffuse and localized to the side of the Li_2 away from the CH_2 group. This spatially extended orbital dominates the valence electron contribution to $\mu_z^{(e)}$ and results in the electronic contribution outweighing the nuclear and produces a negative dipole moment.

As a schematic example, the overall charge distribution and the σ,π components of the planar $^1A_1$ state is shown as follows:

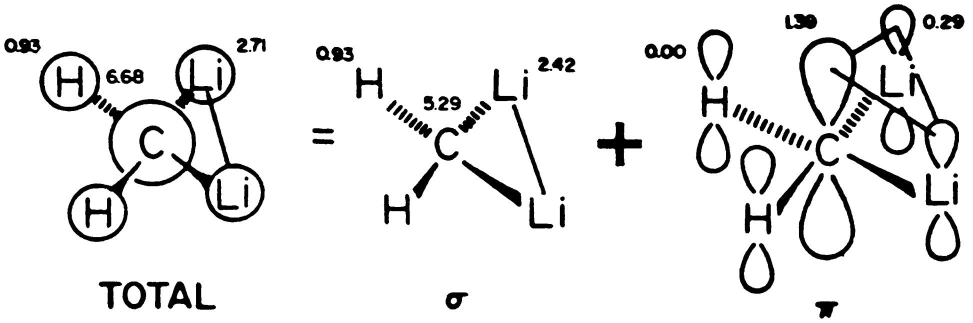
0.93
H
6.68
2.71
Li
C
H
Li
TOTAL
=
0.93
H
5.29
Li
2.42
C
H
Li
σ
+
0.00
1.39
0.29
H
C
Li
H
Li
π

and that of the planar $^3B_1$ state:

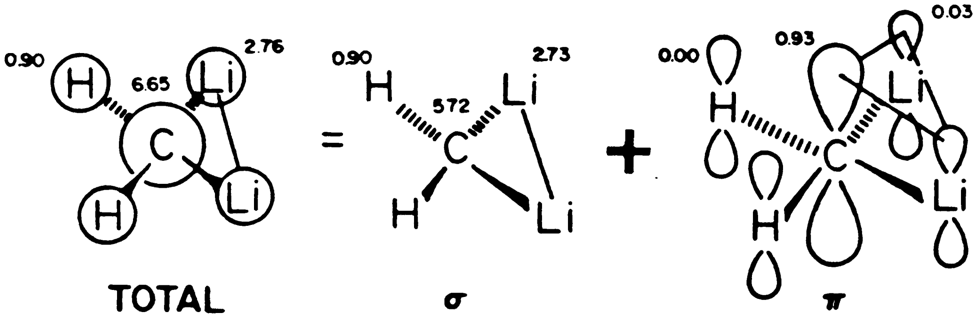
0.90
H
6.65
2.76
Li
C
H
Li
TOTAL
=
0.90
H
5.72
2.73
Li
C
H
Li
σ
+
0.00
0.93
0.03
H
C
Li
H
Li
π

Note the similarities in the overall charge distribution even though the dipole moments have different signs. When a b_1 electron from the $^1A_1$ state is placed in the $5a_1$ orbital (defining the $^3B_1$ state), 0.26 electron is removed from the p_π orbital on each Li atom and replaced with 0.31 electron in the Li "σ" orbitals. At the same time, lithium's contribution to the σ bond ($4a_1$ orbital) is reduced. Therefore, the σ and π components of the charge distribution for the two spin states are quite different but the similarity lies on the net charge. This is also observed for the nonplanar molecules.

3. On the Role of the Li p Orbitals

The data in Table 1. suggest that the Li p orbitals are crucial for a balanced description of either the singlet or the triplet states. In particular, one sees that the energy separation between the planar and tetrahedral singlet is far more sensitive to the presence of Li p orbitals than to the level (SCF, MCSCF, or CI) of calculation. In addition, the dipole moment of the planar singlet increases in both the SCF and CI approximations by more than 3 debyes when the p orbitals are removed, reflecting the lost opportunity for back donation via the Li p_π orbitals. Note that the tetrahedral singlet does not suffer so because the carbon p_π can donate electrons to Li via the σ_u orbitals on Li_2. The triplet states respond differently than the singlets to the absence of Li p orbitals. In this case they have little effect on the energy separation between planar and tetrahedral forms but result in an increase of ~3 debyes in the dipole moment of both conformations. This is clearly a result of the ability to properly polarize the $5a_1$ orbital (see Figure 4) without the Li p orbitals.

CONCLUSIONS

While there are eight valence electrons in CH_2Li_2, four are involved in C-H bonds leaving the remaining four to bind the two lithium atoms to carbon. How these four electrons are distributed among the C-Li_2 moiety will determine the essential characteristics of each of the low-lying states of CH_2Li_2. A qualitative model of the bonding in CH_2Li_2 which is consistent with the charge distribution, low barrier of rotation (tetrahedral → planar), dipole moment, and the geometric changes which accompany the planar-tetrahedral rotations in either the singlet or triplet states can be abstracted from these calculations.

For the planar $^1A_1$ state, the four "CLi_2" valence electrons are in the $4a_1$ and $1b_1$ orbitals. The $4a_1$ orbital seems to be a combination of a p_σ orbital on CH_2 and the $2\sigma_g$ bonding orbital on Li_2 while the $1b_1$ orbital is a mixture of the p_π on CH_2 and the Li p_π orbitals. The resulting bonding structure, relative to the free CH_2 ($^1A_1$) and Li_2 ($^1\Sigma^+$) fragments, shows an electron donation from the Li_2 $2\sigma_g$ bonding orbital to the formally empty p_σ orbital on CH_2 with a concurrent delocalization of the CH_2 p_π electrons into the Li p_π orbitals.

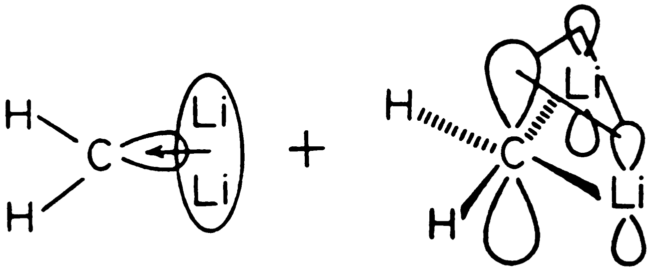

If the Li_2 group is rotated 90° the σ bond remains intact while the π bond changes. Specifically, the ability of the CH_2 p_π to donate electrons into the formally empty Li p_π orbitals is lost. However, the Li_2 $2\sigma_u$ orbital has the correct symmetry to interact with the doubly occupied CH_2 p_π orbital.

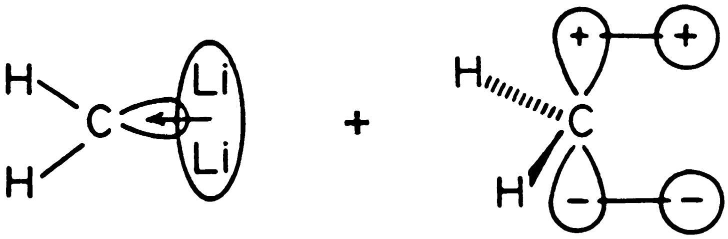

This results in significant increase in the Li-Li distance (2.86 A planar → 3.44 A nonplanar) while the C-Li_2 separation decreases (1.16 A → 0.99 A) permitting a stronger overlap between the CH_2 p_π and Li_2 σ_u orbitals. Note that while this interaction is antibonding from the Li_2 perspective, it enhances the bonding of C to Li_2. This picture of the tetrahedral $^1A_1$ is, of course, equivalent to the conventional model involving a substituted sp^3 carbon atom (except for the suggestion of a Li-Li bond).

When one forms the planar $^3B_1$ from the planar $^1A_1$

an electron is removed from the CH_2 p_π orbital ($1b_1$) and placed in the antibonding companion to the $4a_1$ bonding orbital.

$$5a_1 = a_1^* \approx p_\sigma - 2\sigma_g$$

This orbital adds a node between the C and Li_2 as observed in the increased C-Li_2 separation and the additional $2\sigma_g$ contributes to the decrease in the Li-Li separation. Detailed examination of the relevant orbitals (GVB orbital plots) indicate a significant amount of p_z orbital character (in the $2\sigma_g$ Li_2 orbital) has been added to the σ orbital hosting the unpaired electron ($5a_1$). Most of this electron seems to be confined to the region behind the Li_2 nuclei away from the CH_2 group. Due to the direction of the orbital extension, it is the single electron in this orbital that is, in large measure, responsible for the dramatic shift in the dipole moment in going from the $^1A_1$ planar (+4.32 debyes) to the $^3B_1$ planar (-1.34 debyes). This change in dipole moment is not due to a change in polarity ($H_2C^+Li_2^-$) since the overall electron distribution of both the singlet and triplet states show a net charge transfer from Li_2 to CH_2 corresponding to a $H_2C^-Li_2^+$ polarity.

If one forms the nonplanar $^3B_1$ by rotating the Li_2 group by 90° the σ bond remains intact (including the effect of the $5a_1$ orbital) and the p_π orbital on CH_2 interacts with the σ_u orbital on Li_2 as in the tetrahedral $^1A_1$ state. Due

to the effect of the $5a_1$ orbital in the σ system the C-Li_2 separation changes little upon rotation (planar to nonplanar), thus, the symmetry transformation that the b_1 orbital undergoes is essentially unnoticed.

After this work was completed we learned of a similar study by Bachrach and Streitweiser[18] in which they arrived at similar conclusions but with a far less reliable theoretical treatment. In addition we disagree on the usefulness of the population analysis as an interpretative tool.

LIST OF REFERENCES

LIST OF REFERENCES

1. T.H. Maugh II, Science, 194, 413 (1976).

2. H.F. Schaefer III, "The Electronic Structure of Atoms and Molecules", Addison-Wesley, Reading, Mass., 1972.

3. R. Hoffmann, R.G. Alder, and C.F. Wilcox, Jr., J. Am. Chem. Soc., 92, 4992 (1970).

4. J.B. Collins, J.D. Dill, E.D. Jemmis, Y. Apeloig, P.v.R. Schleyer, R. Seeger, and J.A. Pople, J. Am. Chem. Soc., 98, 5419 (1976).

5. A. Mavridis and J.F. Harrison, J. Am. Chem. Soc., 104, 3827 (1982).

6. W.D. Laidig and H.F. Schaefer III, J. Am. Chem. Soc., 100, 5972 (1978); Erratum: J. Am. Chem. Soc., 101, 3706 (1979).

7. R.T. Morrison and R.N. Boyd, "Organic Chemistry", 3rd edition, Allyn and Bacon, Inc., Boston, Mass., 1973, pg.840.

8. J.F. Harrison, R.C. Liedtke, and J.F. Liebman, J. Am. Chem. Soc., 101, 7162 (1979).

9. M.A. Vincent and H.F. Schaefer III, J. Chem. Phys., 77, 6103 (1982); E.W. Nilssen and A. Skancke, J. Org. Chem., 116, 251 (1976).

10. G.A. Henderson, W.T. Zemke and A.C. Wahe, J. Chem. Phys., 58, 2654 (1973).

11. F.W. Loomis and R.E. Nusbaum, Phys. Rev., 38, 1447 (1931).

12. K. Rudenberg, L.M. Cheung, and, S.T. Elbert, Int. J. Quantum Chem., 16, 1069 (1979).

13. F.B. Duijneveldt, "IBM Technical Research Report No.RJ-945", IBM Research Laboratory, San Jose, CA, 1971.

14. J.E. Williams, Jr. and A. Streitwieser, Jr., Chem. Phys. Lett., 25, 507 (1974).

15. S.J. Huzinaga, J. Chem. Phys., 42, 1293 (1965); T.H. Dunning, Jr., J. Chem. Phys., 53, 2823 (1970).

16. R.C. Raffenetti, J. Chem. Phys., 58, 4452 (1973).

17. For the tetrahedral $^1A_1$ and $^3B_1$ states, the SCF function has a $2b_1$ orbital occupied. In the singlet state, the doubly occupied $2b_1$ orbital electrons are correlated into $3b_1$ orbital (among the most important terms in the CI function).

18. S.M. Bachrach and A. Streitwieser, Jr., J. Am. Chem. Soc., 106, 5818 (1984).

CHAPTER III

THE ELECTRONIC AND GEOMETRIC STRUCTURE OF VARIOUS SMALL CATIONS CONTAINING SCANDIUM AND CHROMIUM

INTRODUCTION

Experimental studies of the gas-phase, bimolecular reactions of transition metal (TM) cations with alkanes[1,3,5] have prompted an interest in understanding the chemistry of these small systems. Such studies have immediate impact in organometallic chemistry, surface chemistry, and catalysis[2]. Reactions, where ions are involved, can be studied by use of state-of-the-art mass spectroscopic techniques, such as Ion Cyclotron Resonance[3,4] and Guided Ion Beam Mass Spectrometry[3,5], and the information collected from these studies has led to some understanding of the kinetic and thermochemical factors that allows a reaction to proceed. One of the advantages of the Guided Ion Beam experiment relative to the ICR experiment is being able to study endothermic, as well as exothermic, reactions[5]. These experiments address various questions: activation of C-H and C-C bonds, reactivity of different transition metal ions, reaction mechanisms, exothermic vs. endothermic reactions, bond energies, etc.

While the experiments to date provide information on bond energies and reaction mechanisms they say nothing about the electronic and geometric structure of these species. Mass spectrometers can only provide the mass ratios (m/z) of reactant and product ions[3]. Usually, proposed product structures are based on the structure of the reactants, subsequent reactivity information, and "plausible considerations" of the reaction process[3,6]. This can be difficult since structural possibilities increase with larger systems. For example, if the mass ratio of a product suggests a $TM\text{-}CH_3^+$ structure, other isomers ($H_2TM\text{-}CH^+$, $H\text{-}TM\text{-}CH_2^+$) should be considered. The necessary structural information, such as bond lengths, bond angles, bond energies, electron distributions, spin multiplicities, among others, can be obtained through the use of ab initio molecular structure techniques[7].

Theoretical studies of transition metal systems have lagged the experiments for several reasons. First-row transition metals and their ions are not well represented by the single determinent self consistent field (SCF) functions[8] which have been so useful in understanding the electronic structure of main group elements and compounds. In particular, the large number of closely spaced energy levels, the changing character of the 3s,3p orbitals (from semi-core to core) as one goes from Sc to Cu, and the as yet poorly understood relativistic effects raise the required level of theory significantly. Work to date[8,9] suggests

that a usefully accurate description of the electronic structure of a first row transition element or a small molecule containing such an element is possible if one starts with a multiconfiguration SCF (MCSCF) wavefunction which recognizes the differential electron correlation in the relevant low lying states of both the transition metal and organic fragment. Additional levels of theory (configuration interaction) can then be applied as the problem and goal warrant.

The electronic and geometric structure of various transition metal cations containing scandium and chromium, obtained by the use of ab initio MCSCF and CI techniques, will be discussed in this chapter. We are especially interested in the nature of the chemical bond between the transition metal cation and the ligand, and the effect of the low lying states of the fragments on the bonding structure of the overall ground state of the molecule. The systems of interest are divided into three sections: the bonding of Sc^+ and Cr^+ with the organic fragments CH_3, CH_2, and CH, as well as with H; the bonding in ScH_2^+; and the bonding in $CrCl^+$. In addition to this discussion we will consider the possible consequences of this study.

BASIS SETS AND MOLECULAR CODES

The basis set used for Sc and Cr consists of 14s,11p,6d functions constructed by augmenting Wachters'[10] 14s,9p,5d basis with two additional diffuse p functions[11] (to represent the 4p orbital) and an extra d function as recommended by Hay[12]. The exponents used for the two p functions are $\alpha=0.18975$ and $\alpha=0.03103$ for scandium, and $\alpha=0.1207$ and $\alpha=0.03861$ for chromium. The extra d function has an exponent of $\alpha=0.05880$ (Sc) and $\alpha=0.0912$ (Cr). This basis was contracted to 5s,4p,3d following Raffenetti's[13] contraction scheme. The basis for carbon was a 9s,5p,1d set consisting of Duijneveldt's[14] 9s,5p basis augmented by a d set with the exponent $\alpha=0.85$. The hydrogen basis was a 4s,1p set consisting of Huzinaga's[15] 4s basis augmented by a p set with an exponent of 1.0. The C and H basis sets were contracted to 3s,2p,1d and 2s,1p, respectively, as recommended by Raffenetti[13]. The basis for Cl was a 12s,10p,2d set consisting of Huzinaga's[16] 12s,9p basis augmented by a p set with exponent $\alpha=0.0436306$ and by 2 d sets with exponents of $\alpha=0.6$ and $\alpha=0.2$. The Cl functions were contracted to 4s,4p,2d as recommended by Raffenetti[13].

The contracted basis set described in the previous paragraph for Sc and H, [5s4p3d/2s1p], is referred to as **spd** in the text. A second set was formed by augmenting the **spd** set with a single f function ($\alpha= 1.0$) for Sc, contracting Huzinaga's 4s hydrogen set to three components, and by replacing the single p function on hydrogen with two p

functions (α= 1.73 and 0.43). This [5s4p3d1f/3s2p] contracted basis is referred to as **spdf** in the text.

All calculations were done on a Floating Point Systems FPS-164 computer, jointly supported by the Michigan State University Chemistry Department and the Office of the Provost, by using the Argonne National Laboratory collection of QUEST-164 codes. In particular, the integrals were calculated with the program ARGOS written by Pitzer[17]; the SCF and MCSCF calculations used the GVB164 program by Bair[18] and the UEXP program and related utility codes written by Shepard[19]. The configuration interaction calculations were done with the program UCI (and its related utility codes) written by Lischka, Shepard, Brown, and Shavitt[20]. The logical flow of the QUEST-164 system, as implemented at MSU, is shown in Figure 1.

SIZE CONSISTENCY

Every calculation reported is size consistent, i.e., the energy of the molecule when the fragments are far apart is also the sum of the energies of the individual fragments, not only at the MCSCF level but also at the MCSCF+1+2 level. This is an important characteristic of these calculations and suggests that the D_e's calculated from the MCSCF+1+2 wave functions are lower bounds.

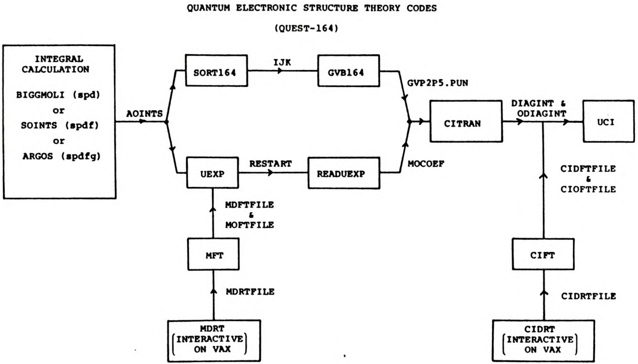
QUANTUM ELECTRONIC STRUCTURE THEORY CODES
(QUEST-164)
INTEGRAL CALCULATION
BIGGMOLI (spd)
or
SOINTS (spdf)
or
ARGOS (spdfg)
AOINTS
SORT164
IJK
GVB164
GVP2P5.PUN
UEXP
RESTART
READUEXP
MOCOEF
CITRAN
DIAGINT & ODIAGINT
UCI
MDFTFILE & MOFTFILE
MFT
MDRTFILE
MDRT (INTERACTIVE ON VAX)
CIDFTFILE & CIOFTFILE
CIFT
CIDRTFILE
CIDRT (INTERACTIVE ON VAX)

Figure 1. Flow chart for the QUEST-164 collection of codes as implemented in MSU. The names of the programs are found in the boxes and the transient files are out.

NATURE OF THE FRAGMENTS: TRANSITION METAL IONS

Before we discuss the bonding in the various transition metal-containing (cationic) molecular systems, it is useful to discuss the nature of the individual fragments. Since we are interested in bond energies, we must insure that the structure of the fragments, as well as the molecules, are properly represented. For now we will concentrate on the transition metal monopositive ions while the "companion ligands" will be discussed in subsequent sections.

In Figure 2 we observe the comparison of the experimental sd^N-d^{N+1} energy separation[21] with those calculated using SCF and MCSCF (d-d radial correlation) techniques. It is worth noting that an SCF wavefunction incorrectly predicts a (sd^3) ^5F ground state for V^+ rather than the experimentally observed ^5D ground state. This illustrates the need of a multiconfiguration wavefunction to better approximate the low lying states of transition metal ions[8].

We have choosen Sc^+ and Cr^+ as representatives of the first half of the first-row transition metal series for our studies of $[TM-R]^+$ systems (R = H, H_2, CH_3, CH_2, CH, and Cl). One of the advantages of studying monopositive TM ions is that s^2 correlations (mainly a near degeneracy effect $4s^2 \rightarrow 4p^2$)[8] of a $4s^2$ pair (low energy state in neutrals) will not be necessary since a state with a $4s^2$ pair is very high in energy. As in neutral atoms[8], we should include d^2 radial correlations,

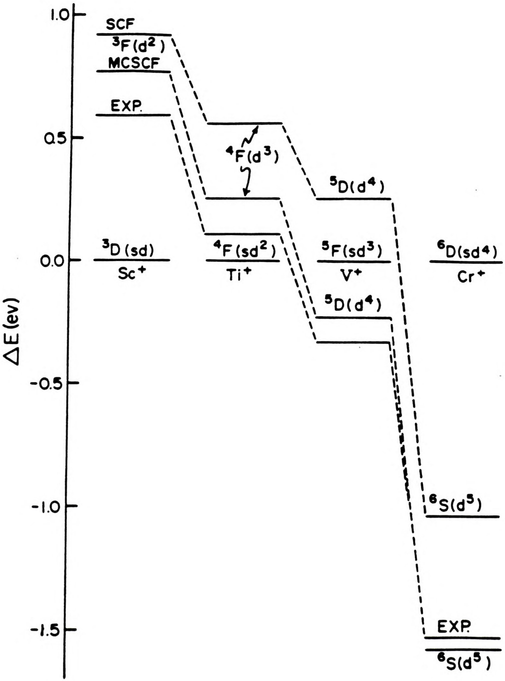

Figure 2. Comparison of experimental sd^N-d^{N+1} energy separation with SCF and MCSCF results.

$$| sd^N > = C_0 | sd^N >^{SCF} + C_1 | sd^{N-2}d^2 >$$

$$| d^{N+1} > = C_0 | d^{N+1} >^{SCF} + C_1 | d^{N-1}d^2 >$$

for improving the SCF model. Due to computational difficulties core-core and core-valence correlations are not included in our calculations.

The ground state[21] of Cr^+ is a ^6S state arising from a $3d^5$ configuration while the first excited configuration, $4s3d^4$, gives rise to a ^6D state. The Cr^+ (d^5-sd^4) splitting (expt = 35.1 kcal/mol)[21] is calculated to be 23.8 kcal/mol at the SCF level and 36.9 kcal/mol at the MCSCF (radially correlated) level. The ground state of Sc^+ is of ^3D symmetry and arises from the 4s3d configuration[21]. The companion ^1D state is 0.302 eV (6.96 kcal/mol) above the ^3D with the lowest state arising from the $3d^2$ configuration (^3F symmetry) being 0.596 eV (13.7 kcal/mol) above the ground state. The Sc^+ (sd-d^2) splitting (expt = 13.7 kcal/mol)[21] is calculated to be 21.2 kcal/mol at the SCF level and 17.3 kcal/mol at the SCF+1+2 (CI) level. The smaller energy difference between the relative sd^N and d^{N+1} states in the Sc^+ as compared to the Cr^+ ion will also be of concern when we observe the contribution of these atomic states to the molecular systems.

BONDING OF Sc^+ AND Cr^+ WITH H, CH_3, CH_2, AND CH

Recent experimental studies of gas-phase, bimolecular reactions of transition metal (TM) cations with organic molecules are providing significant insights[1,3,22] into the mechanism of important organometallic reactions. In addition, the thermochemical data extracted from the experiments[1] allows for the collection of an invaluable data base which will permit the systemization of the observed chemistry, prediction of possible new chemistries (which happens to be one of the major strengths of Organic Chemistry) and provide bench marks for theoretical studies

To date, these experiments have not been able to provide structural information on the various reaction products. The purpose of this study is to provide such structural information via a uniformly accurate theoretical study of the electronic and geometric structures of the titled molecules. We are interested in the nature of the chemical bond between transition metal monopositive cations, such as chromium and scandium, and various simple organic ligands (CH_3, CH_2, and CH), as well as, with H. In particular, we are concerned with the extent to which these fragments form single, double, and triple bonds. We have been motivated to investigate the possibility of CH forming a triple bond with Cr^+ by the recent theoretical prediction of Carter and Goddard[9] that the ground state of $CrCH_2{}^+$ has a double bond between CH_2 and Cr^+, and by the recent experimental work of Aristov and Armentrout[1e] suggesting that V^+ forms single, double, and triple bonds with CH_3, CH_2, and CH, respectively (Table 1). We anticipate that this study will result in our understanding the nature of the transition metal-main group element bond sufficiently well so as to permit a qualitatively correct prediction of the bonding in more complex transition metal-containing system.

The absolute energies, calculated and experimental bond energies for the various molecules to be discussed are collected in Tables 1-3.

TABLE 1. Experimental Bond Energies for Selected Scandium, Chromium, and Vanadium Cations[a].

	Sc^+-R		Cr^+-R		V^+-R
R	ref[1d]	ref[1g]	ref[1b]	ref[1g]	ref[1e]
H	54±4	55±2	35±4	27±2	50±2
CH_3	65±5	59±5	37±7	26±2	50.5±3
CH_2		97	65±7	<65	80±8
CH					115±5

[a] All values are in kcal/mol.

TABLE 2. Calculated Energies, Bond Strengths, and Geometric Parameters for Various Chromium Cations[a].

	MCSCF				(MCSCF+1+2)*				MCSCF+1+2			
molecule	R(Cr–R)/ θ(CH$_2$)	CSF's	E, au	D_e, kcal/ mol	R(Cr–R)/ θ(CH$_2$)	CSF's	E, au	D_e, kcal/ mol	R(Cr–R)/ θ(CH$_2$)	CSF's	E, au	D_e, kcal/ mol
CrH$^+$($^5\Sigma^+$)	1.67	7	−1043.6423		1.66	459	−1043.6547		1.63	5 513	−1043.6940	
	10.58	7	−1043.6128		10.58	459	−1043.6128		10.58	5 513	−1043.6539	
				18.5				26.2				25.1
CrCH$_3^+$($^5A_1$)	2.15/107.0	7	−1082.6960		2.12/108.2	2 599	−1082.7041		2.14/105.3	39 415	−1082.7467	
	10.58/120.0	7	−1082.6769		10.58/120.0	2 599	−1082.6769		10.58/120.0	39 415	−1082.7180	
				12.0				17.0				18.0
CrCH$_2^+$($^6B_1$)	2.10/115.8	7	−1082.0585		2.08/114.7	1 389	−1082.0689		2.06/117.3	25 395	−1082.1207	
	10.58/128.8	7	−1082.0397		10.58/128.8	1 389	−1082.0516		10.58/128.8	25 395	−1082.0871	
				11.8				10.8				21.0
CrCH$_2^+$($^4B_1$)	1.96/115.9	34	−1082.0818		1.96/115.1	18 636	−1082.1135		1.92/116.7	83 124	−1082.1490	
	10.58/128.8	34	−1082.0397		10.58/128.8	18 636	−1082.0516		10.58/128.8	83 124	−1082.0871	
				26.3				38.7				38.7
CrCH$^+$($^3\Sigma^-$)	1.76	126	−1081.4834		1.77	107 216	−1081.5425		?	249 208	?	
	10.58	126	−1081.3974		10.58	107 216	−1081.4293					
				36.7 ($^2\Pi$)				53.7 ($^2\Pi$)				
				53.8 (4Σ^-)				70.8 ($^4\Sigma^-$)				?

[a] The two values of "D_e" reported for CrCH$^+$ refer to the choice of either $^2\Pi$ or $^4\Sigma^-$ CH as the references. Bond lengths are in Å.

Table 3. Calculated Energies, Bond Strengths, and Geometric Parameters for Various Scandium Cations.[a]

	MCSCF				MCSCF+1+2			
Molecule	R(Sc-R)/ θ(CH_2)	CSF's	E, au	D_e, kcal/mol	R(Sc-R)/ θ(CH_2)	CSF's	E, au	D_e, kcal/mol
$ScH^+(^2\Delta)$	1.862	9	-760.09871		1.834	601	-760.10916	
	10.58	9	-760.02777		10.58	601	-760.02834	
				44.5				50.7
$ScCH_3^+(^2A'')$	2.270/109.2	4	-799.14581		2.246/108.9	3,153	-799.15661	
	10.58/120.0	4	-799.09196		10.58/120.0	3,153	-799.09253	
				33.7				40.1
$ScCH_2^+(^1A_1)$	2.004/112.0	10	-798.53932		1.997/112.0	3,660	-798.57014	
	10.53/128.8	10	-798.45467		10.58/128.8	3,660	-798.46181	
				53.1				68.0
$ScCH_2^+(^3A_1)$	2.286/112.36	7	-798.49988		2.263/111.36	4,683	-798.52915	
	10.58/128.8	7	-798.45467		10.58/128.8	4,683	-798.46181	
				28.4				42.3
$ScCH^+(^2\Pi)$	1.973	17	-797.91880		1.940	12,099	-797.98268	
	10.58	17	-797.81235		10.58	12,099	-797.82963	
				66.8[b]				96.0
$ScCH^+(^4\Pi)$	2.185	6	-797.88336		2.177	7,270	-797.93948	
	10.58	6	-797.81235		10.58	7,270	-797.82963	
				44.6[b]				68.9

[a] Bond lengths in Angstroms; [b] Values for D_e for $ScCH^+$ are relative to $^4\Sigma^-$ CH fragment

A. CrH^+ and $CrCH_3{}^+$

We may imagine a hydrogen atom bonding to a d_σ orbital in the ^6S state or to a 4s orbital in the m=0 component of the ^6D state of Cr^+. In both cases the symmetry of the resulting molecular state is $^5\Sigma^+$. Apart from the Cr^+ core the wavefunction would have the schematic (GVB)[23] form

$$(\sigma h + h\sigma)\ 3d^1_{\pi_x}\ 3d^1_{\pi_y}\ 3d^1_{\delta_+}\ 3d^1_{\delta_-}\ (\alpha\beta-\beta\alpha)\alpha\alpha\alpha\alpha$$

where at large distances σ is a $3d_\sigma$ orbital on Cr^+ and h is a hydrogen 1s function. A CrH^+ wavefunction of this form which dissociates to the correct Hartree-Fock products $[Cr^+(^6S) + H(^2S)]$ consists of seven configuration state functions (CSF's) and will be referred to as the MCSCF function. From the analysis described in Appendix A, one recognizes that this seven configuration MCSCF (SOGVB) function consists of a 2x2 MCSCF function (GVB) which properly dissociates the Cr-H bond, augmented by five spin eigenfunctions to completely describe six electrons being coupled into an overall quintet state. The energy of this wave function as a function of internuclear separation is shown in Figure 3. Also shown is the CI function formed by allowing all single and double excitations from the valence orbitals in this 7 CSF MCSCF reference space. In this and all subsequent CI calculations no excitations from the Ar

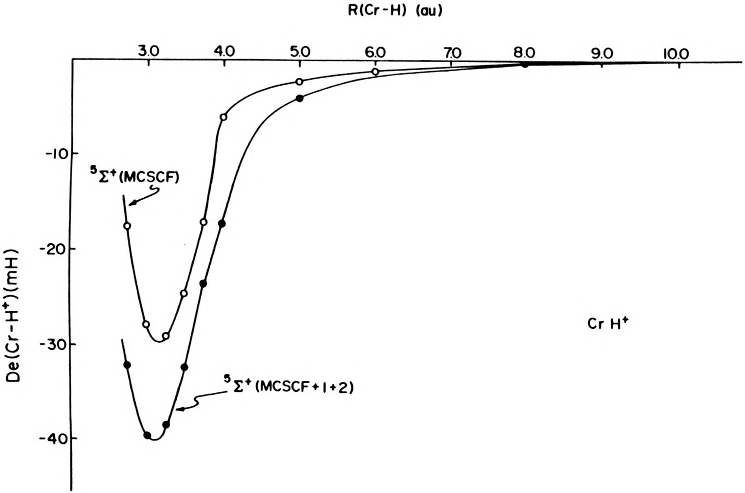

Figure 3. Potential energy curve for the lowest $^5\Sigma^+$ state of CrH^+.

core of Cr^+ were permitted; i.e., the core is determined variationally in the molecular environment and kept at that (SCF) level in the CI's. This CI function is referred to as the MCSCF+1+2 function and dissociates to the ^6S Cr^+ in which the d electrons are correlated essentially at the SCF+1+2 level. The binding energy predicted by this function is 25 kcal/mol, which is in excellent agreement with the more recent experimental value of 27 kcal/mol[1g] and is 71% of the earlier experimental value of 35 kcal/mol[1b].

As the CrH bond forms, the composition of the bonding orbitals (σ and h) evolve and we show in Figure 4 the contours of the GVB bond orbitals at equilibrium[24]. Clearly, a substantial amount of 4s character has mixed with the originally pure $3d_\sigma$ orbital. A striking representation of this mixing is shown in Figure 5 where we plot the occupation of the Cr^+ ($3d_\sigma$, $4p_\sigma$, and 4s) and h (1s) atomic orbitals as a function of internuclear distance. These occupations have been obtained from a Mulliken[25] analysis of the natural orbitals of the MCSCF calculation. As the H atom approaches Cr^+, there is a slight shift of electrons from H to the Cr $3d_\sigma$, and the originally empty $4p_\sigma$ and 4s orbitals until the nuclear separation reaches 4.00au at which time the d_σ occupancy plummets and the Cr 4s becomes the dominant Cr component of the bond orbital. Soon after, the occupancy of the Cr 4s orbital drops and that of the Cr $3d_\sigma$ increases until at equilibrium the Cr component of the bond is 61% sp and 39% d_σ. The bond is essentially covalent

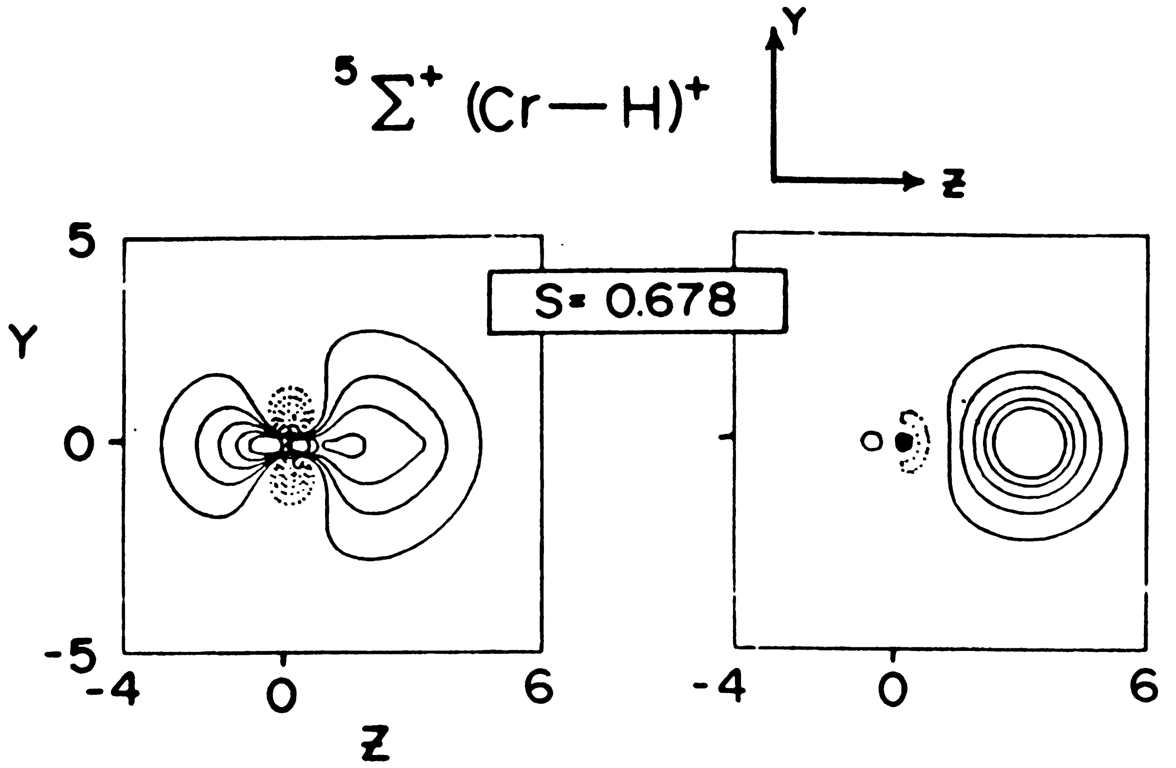

Figure 4. GVB orbitals for the Cr-H bond in $^5\Sigma^+$ CrH$^+$ at equilibrium geometry. The solid lines represent positive contours, the dotted lines negative contours. The smallest contour value is ±0.05au and the spacing is 0.05au. The same conventions are used for all plots.

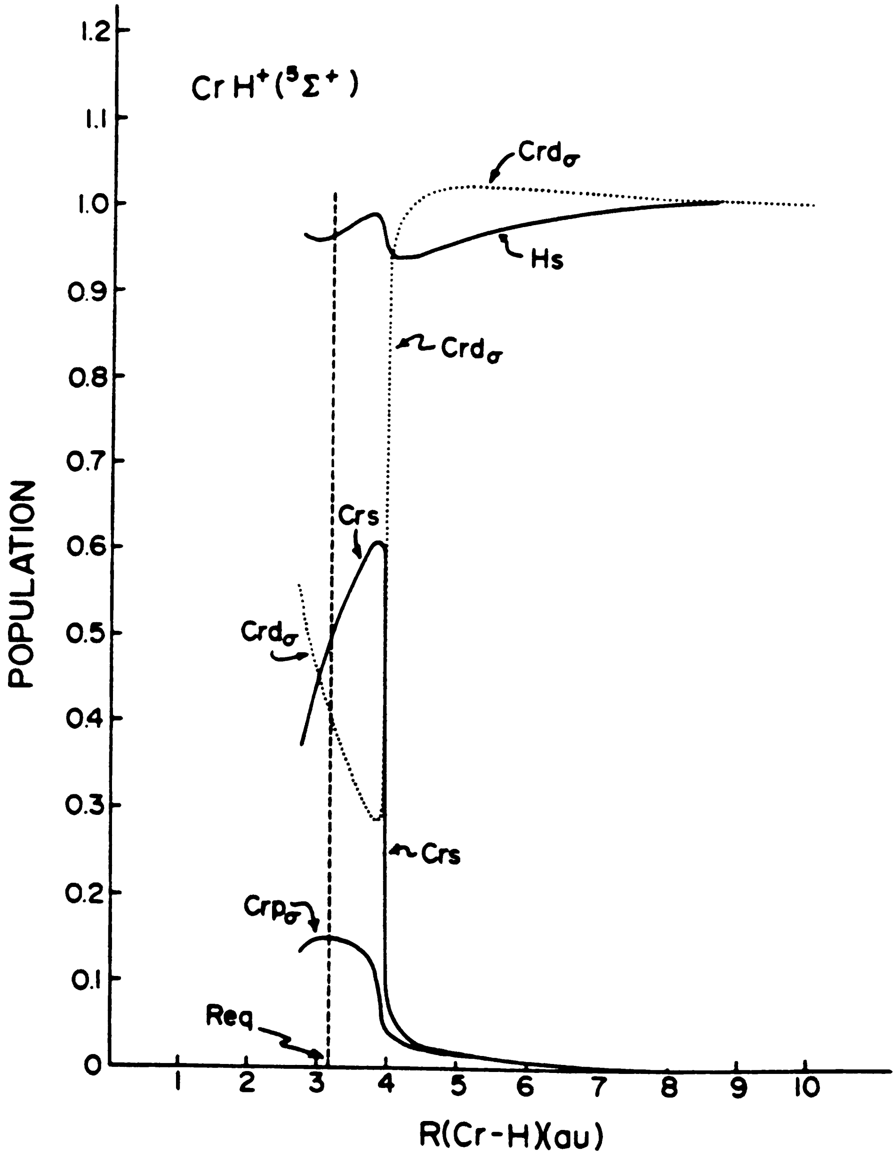

Figure 5. Electron population of selected atomic orbitals from the bonding natural orbitals of the 7 CSF MCSCF wavefunction of $^5\Sigma^+$ CrH$^+$. R_{eq} designates the calculated (equilibrium) bond length.

(48% H and 52% Cr). Also the Cr sp component of the bond is essentially all 4s. The abrupt change in the σ orbital from $3d_\sigma$ to a $3d_\sigma$,4s mixture is due to the $^5\Sigma^+$ root associated with the $4s3d^4$ configuration of Cr^+ crossing that with the $3d^5$ configuration (note the slight "kink" in the MCSCF potential energy curve).

When CH_3 approaches a Cr^+ ion it can bond via its singly occupied σ orbital

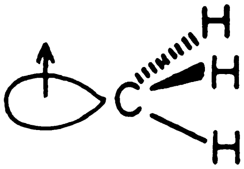

to the ^6D or ^6S state of Cr^+ to form a state of $^5A_1$ (C_{2v} if just considering the unpaired d electrons; $^5A'$ in C_s) symmetry. As in CrH^+ the dominant form of the wave function will be

$$(\sigma_{Cr}\sigma_{CH_3} + \sigma_{CH_3}\sigma_{Cr})\ 3d^1_{\pi_x}\ 3d^1_{\pi_y}\ 3d^1_{\delta_+}\ 3d^1_{\delta_-}\ (\alpha\beta - \beta\alpha)\alpha\alpha\alpha\alpha$$

and at very large Cr-C separations the σ_{Cr} orbital will be a $3d_\sigma$ and the σ_{CH_3} will be essentially a pure p orbital perpendicular to the CH_3 plane (assuming free CH_3 is planar[25]). Rather than optimizing the CH_3 geometry at each Cr-C separation we have constructed a potential curve with the CH_3 geometry constrained to be "tetrahedral" and then optimized the angles and Cr-C bond lengths around the resulting (approximate) equilibrium Cr-C separation. As with CrH^+ this MCSCF function consisted of seven CSF's and the subsequent CI calculation consisted of all single and double excitations from these seven CSF's with the constraint that there are no excitations from the Ar core, the 1s on carbon, and the three C-H bonds. The resulting potential energy curves are shown in Figure 6. The kink in these curves around R= 4.50au correlates precisely with the abrupt change in the occupancy of the Cr d_σ and the Cr 4s orbitals as shown in Figure 7. The MCSCF+1+2 optimized $CrCH_3{}^+$ geometry corresponds to a Cr-C separation of 2.14A and a HCH angle of 113.3° (at a fixed C-H distance of 1.070A). The MCSCF+1+2 bond energy was calculated directly relative to the energy of $CrCH_3{}^+$ at a Cr-C separation of 20au and with the CH_3 group planar. The resulting energy, 18.0 kcal/mol, is less than that calculated for CrH^+ and considerably less than either of the two experimental[1b,1g] values of 26 or 37 kcal/ mol. We believe that part of the error in our calculated D_e is a consequence of our CI function correlating only the CH_3 electrons participating in the σ bond with Cr^+. This leaves the six electrons in the C-H bonds at the SCF level with the consequence that the "in-situ" polarizability of CH_3 is not well represented. The Cr-C bond is essentially covalent (47% Cr, 53% C), and the detailed character is only slightly different from $Cr-H^+$, with the Cr contribution being 54% sp and 46% d_σ. Contours of the valence GVB[24] orbitals are shown in Figure 8.

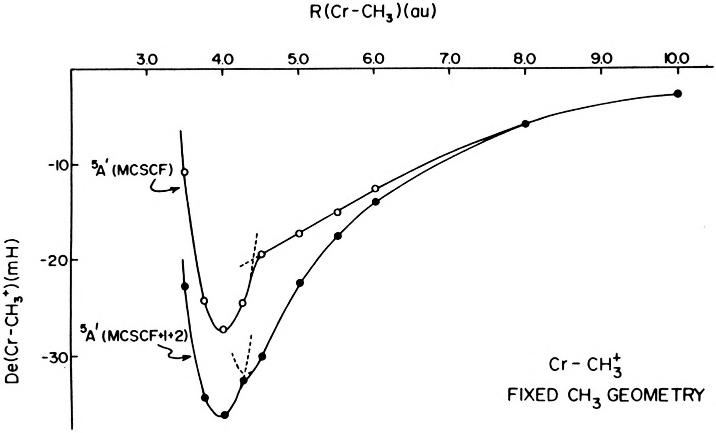

Figure 6. Potential energy curve for the lowest $^5A'$ state of $CrCH_3^+$. The CH_3 geometry is constrained to be tetrahedral with a C-H bond length of 1.070A. The energy units are millihartrees (mH) and one millihartree equals 0.6275 kcal/mol. These units are used for all potential energy curves.

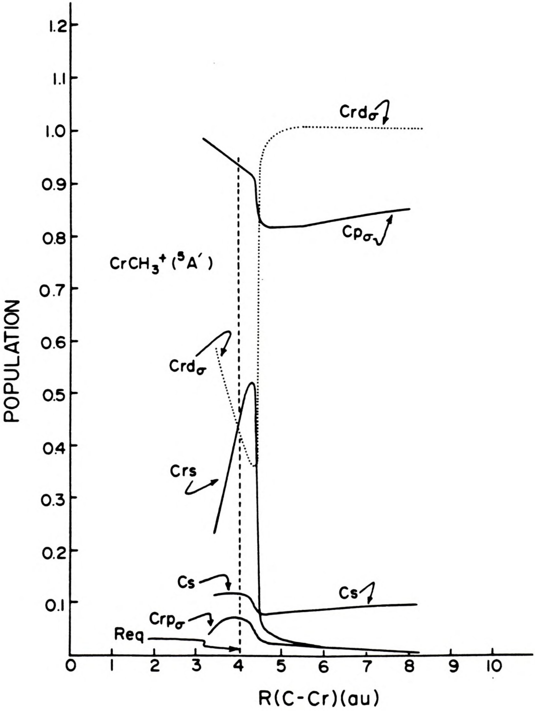

Figure 7. Electron population of selected atomic orbitals from the bonding natural orbitals of the 7 CSF MCSCF wavefunction of $^5A'$ $CrCH_3^+$.

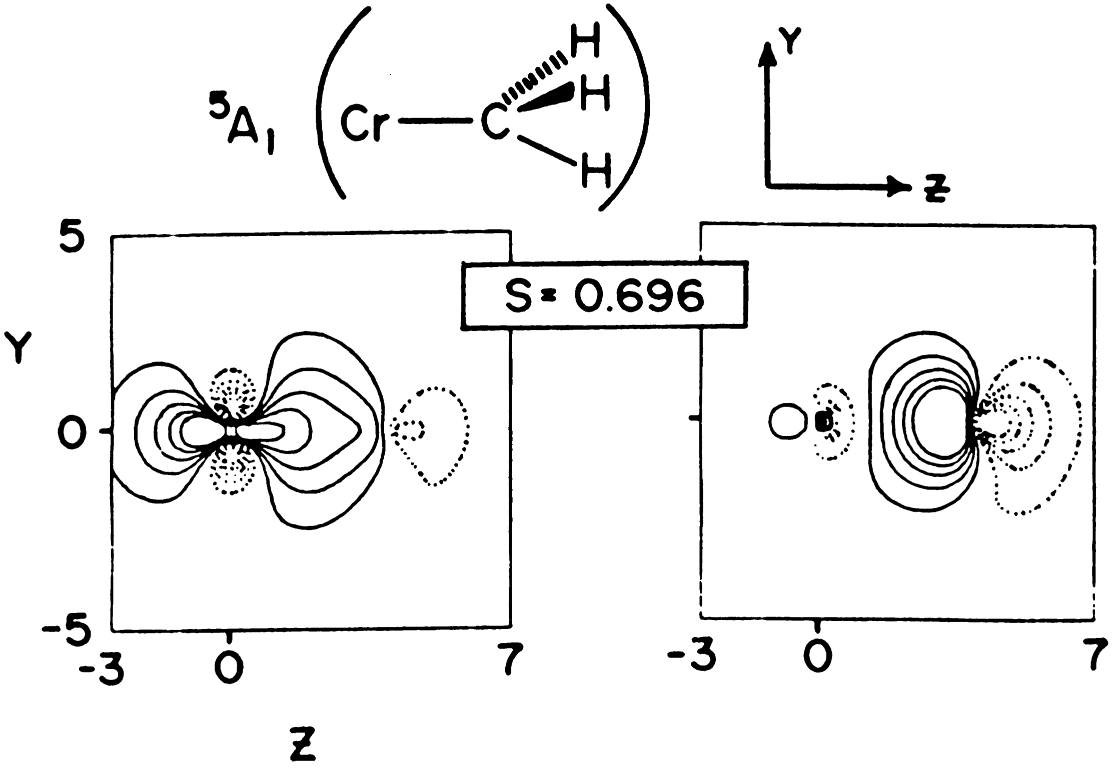

Figure 8. GVB orbitals for the Cr-C bond in $CrCH_3^+$ at its equilibrium geometry.

B. ScH^+ and $ScCH_3{}^+$

As a ^2S H atom approaches Sc^+ in the ^3D state, we may form doublet and quartet states of Σ^+, π and Δ symmetry. If the Sc^+ is in the ^3F state, the molecular states are of Σ^-, π, Δ and Φ symmetry. We anticipate the ground state will be a doublet of either Σ^+, Π, or Δ symmetry.

Consider first a $^2\Pi$ or $^2\Delta$ state of ScH^+. Suppressing the argon core, either state could be represented by a function of the form

$$(\sigma h+h\sigma)\ d_{\delta \text{ or } \pi}\ (\alpha\beta-\beta\alpha)\alpha$$

where at large separation, σ is a Sc^+ 4s orbital (or $3d_\sigma$ for the excited states of $^2\Pi$ and $^2\Delta$) and h is a hydrogen 1s function. The d orbital carries the angular momentum and is either d_δ or d_π. If one represents these states by an MCSCF function consisting of all CSF's of either Δ or Π symmetry arising from two valence orbitals of sigma symmetry and one of δ or π symmetry, one has, in C_{2v}, 9 CSF's. These functions separate to the correct SCF asymptotes. The binding energy of ScH^+ in the $^2\Delta$ state calculated with this ansatz, in both the spd and spdf basis, is shown as a function of R in Figure 9 and for the $^2\Pi$ state in Figure 10. Keeping the Ar core at the SCF level, we then allowed single and double excitations from the 9-configuration reference space. The bond energy vs. R calculated from these

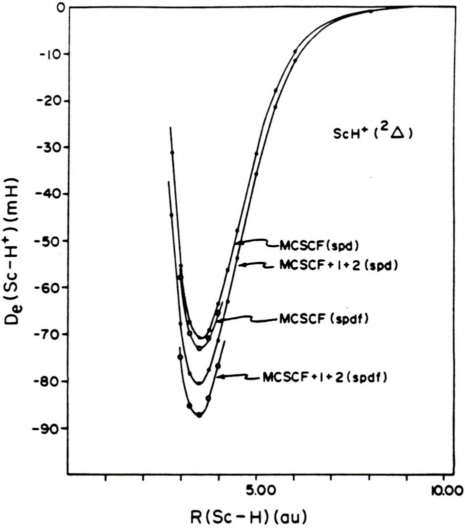

Figure 9. Binding energy of ScH^+ in the $^2\Delta$ state as a function of R for the **spd** and **spdf** basis sets in both the MCSCF and MCSCF+1+2 calculations.

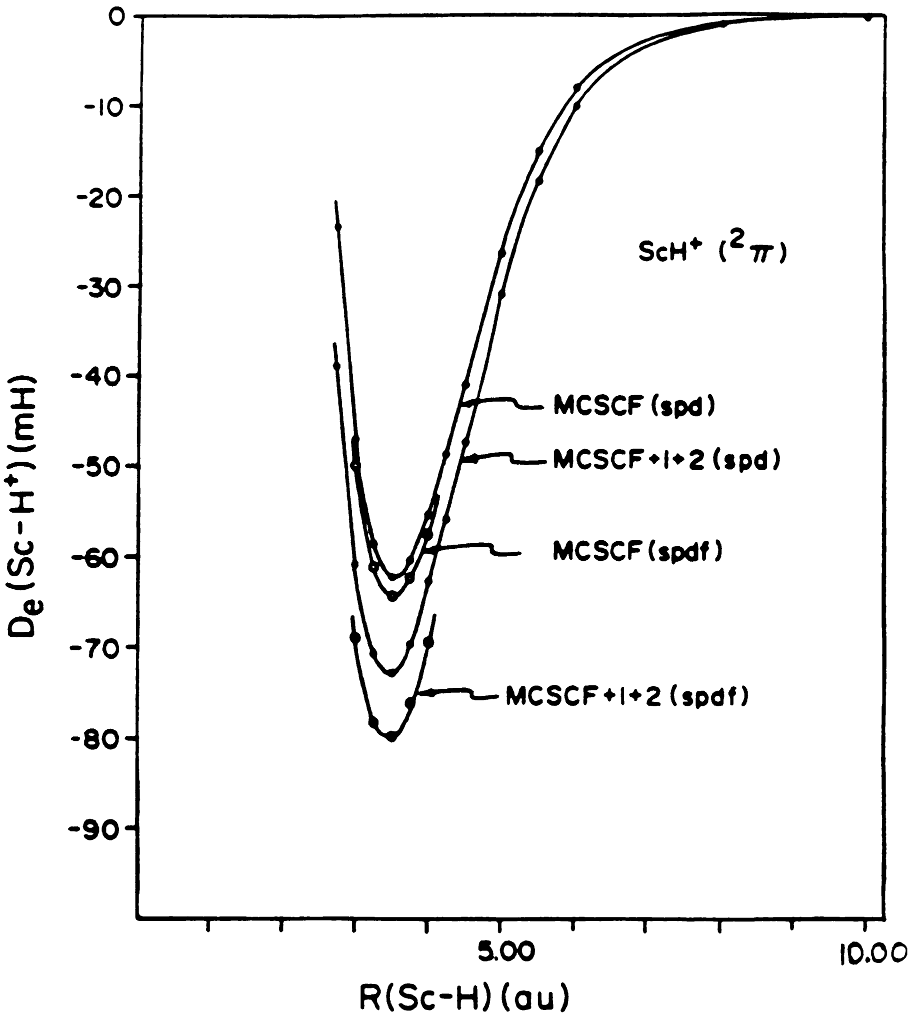

Figure 10. Binding energy of ScH^+ in the $^2\Pi$ state as a function of R for the spd and spdf basis sets in both the MCSCF and MCSCF+1+2 calculations.

MCSCF+1+2 (CI) functions is shown in Figures 9 and 10.

The $^2\Sigma^+$ state is unique in that the ^3F asymptote of Sc^+ does not contribute to this symmetry and the Sc^+ ion has the electronic configuration $4s3d_\sigma$, i.e., both the 4s and $3d_\sigma$ orbitals have the correct symmetry to bond to the incoming H atom. We could represent this state with the wave function

$$^2\Sigma^+ \sim (\ \sigma h + h\sigma\ )\ \sigma'\ (\ \alpha\beta - \beta\alpha\ )\alpha$$

where at large distances σ is a Sc^+ 4s orbital and σ' is the companion $3d_\sigma$. As Sc^+ and H approach each other we expect σ and σ' to become intimate mixtures of 4s and $3d_\sigma$. To allow for this mixing we represented this state with a MCSCF function which permitted all excitations and spin couplings among the three σ orbitals involved and which also separated to the correct SCF limit. The energy calculated with this function for both the spd and spdf basis is shown in Figure 11 along with the MCSCF+1+2 configuration interaction results.

The total energy, bond length, dissociation energy, and vibrational frequency calculated for each state of ScH^+ with both basis sets for the MCSCF and CI wave functions are collected in Table 4.

From Table 4 we conclude that the ground state of ScH^+ is of $^2\Delta$ symmetry with the $^2\Pi$ lying 4.8 kcal/mol higher and the $^2\Sigma^+$ being 1.1 kcal/mol above the $^2\Pi$. While these

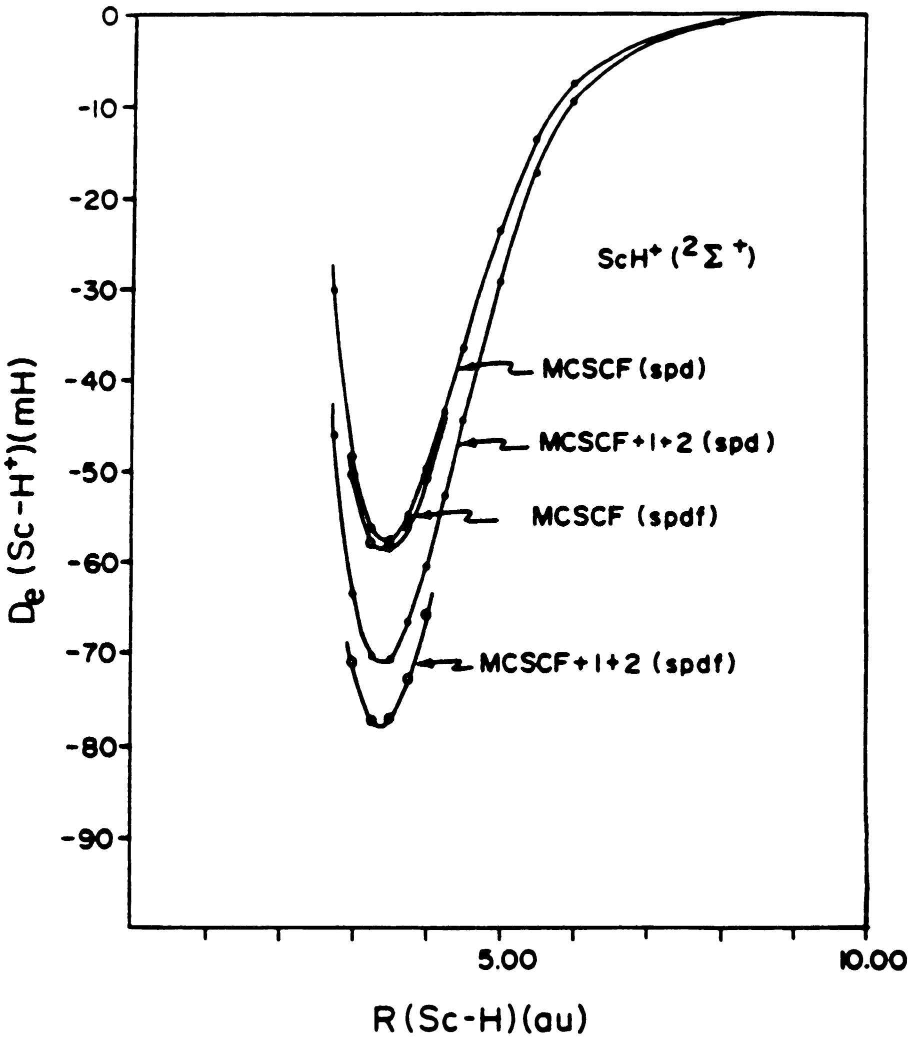

Figure 11. Binding energy of ScH$^+$ in the $^2\Sigma^+$ state as a function of R for the spd and spdf basis sets in both the MCSCF and MCSCF+1+2 calculations.

Table 4. Equilibrium Properties of ScH^+ in the $^2\Delta$, $^2\Pi$, and $^2\Sigma^+$ States Calculated with the **spd** and **spdf** Basis Sets Using the MCSCF and MCSCF+1+2 Functions.

	$^2\Delta$				$^2\Pi$				$^2\Sigma^+$			
	MCSCF		MCSCF+1+2		MCSCF		MCSCF+1+2		MCSCF		MCSCF+1+2	
	spd	spdf	spd	spdf	spd	spdf	spd	spdf	spd	spdf	spd	spdf
R_e, Å	1.862	1.856	1.834	1.822	1.866	1.859	1.832	1.816	1.820	1.810	1.790	1.776
D_e, kcal/mol	44.5	45.8	50.7	54.8	38.9	40.3	45.6	50.0	36.2	37.1	44.6	48.9
ω_e, cm^{-1}	1497	1501	1559	1595	1492	1457	1492	1560	1380	1385	1479	1532
E, au	-760.09871	-760.10165	-760.10916	-760.11768	-760.08974	-760.09290	-760.10102	-760.11012	-760.08574	-760.08809	-760.09964	-760.10842

energy separations are from the spdf-CI calculation the ordering and approximate separations are the same for either basis at either the MCSCF or CI level. Furthermore, since the vibrational frequencies are similar, the zero point energy will not introduce a differential effect and the D°'s will follow the same order. Correcting D_e for zero point energy results in a D° of 52.7 kcal/mol which is in good agreement with the Tolbert and Beauchamp[1d] value of 54±4 kcal/mol and the Armentrout et al.[1g] value of 55±2 kcal/mol. The bond lengths of the $^2\Delta$ and $^2\Pi$ states are comparable, but the bond length of the $^2\Sigma^+$ is substantially shorter. To determine the "atomic" orbital composition of the bonding orbitals we carried out a population analysis of the natural orbitals of the MCSCF (spd basis) wave function for each state as a function of internuclear separation. The results are shown in Figures 12-14.

Consider first the $^2\Delta$ results in Figure 12. At large separation (10au) we have one electron in both the H 1s orbital and the Sc^+ 4s orbital. As the distance between them decreases the Sc 4s character drops while the $3d_\sigma$ and $4p_\sigma$ occupations increase until, at equilibrium, we have 1.10 electrons "on" H with the remaining 0.9 valence σ electrons on Sc distributed as $4s^{0.45}$, $3d_\sigma{}^{0.29}$, and $4p_\sigma{}^{0.16}$. Schilling and Goddard[27] predicts a bond energy for the $^2\Delta$ state of 56 kcal/mol and a hybridization of the Sc bonding orbital of 41% 3d and 59% 4s and 4p. While our bond energy is in substantial agreement with this, our charge distri-

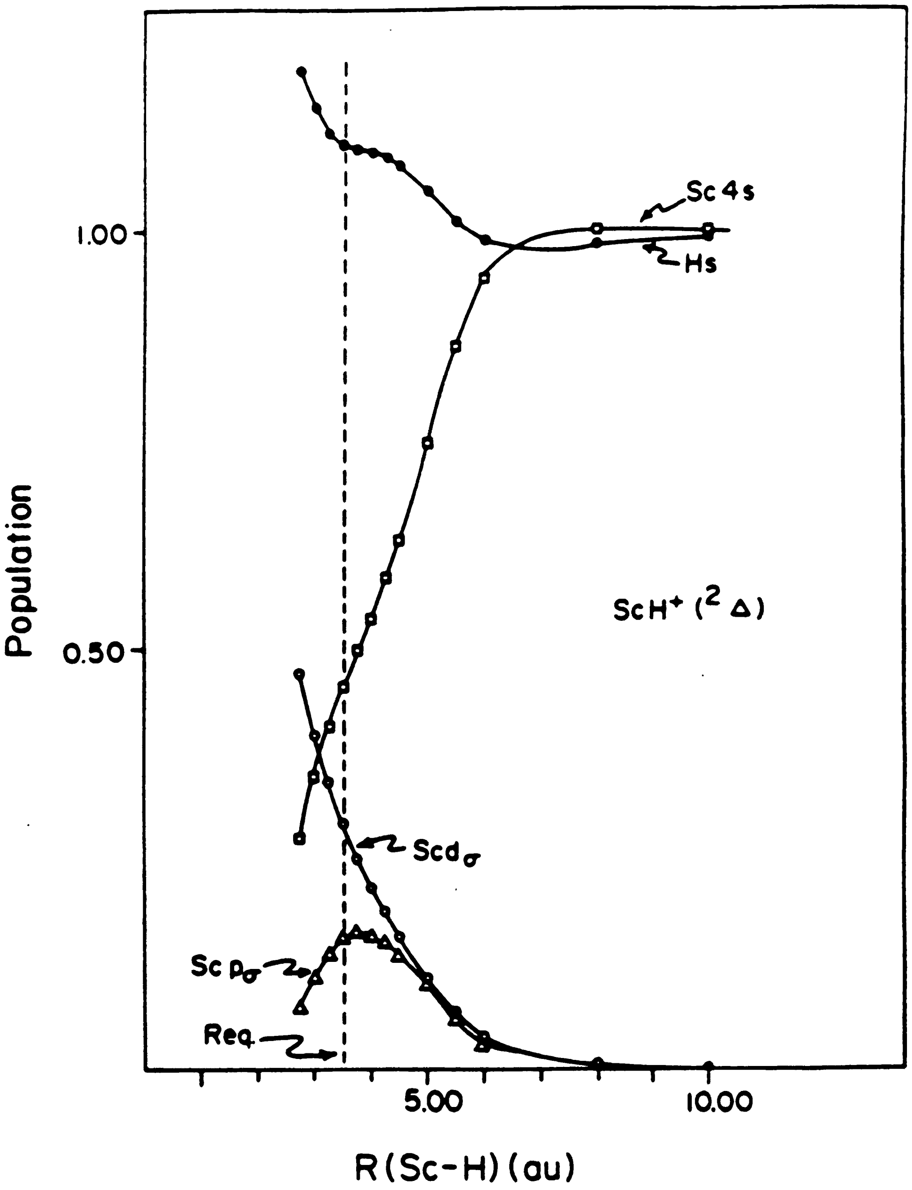

Figure 12. Electron population of selected atomic orbitals of σ symmetry from the bonding natural orbitals of the MCSCF wave function (spd basis) of $^2\Delta$ ScH^+.

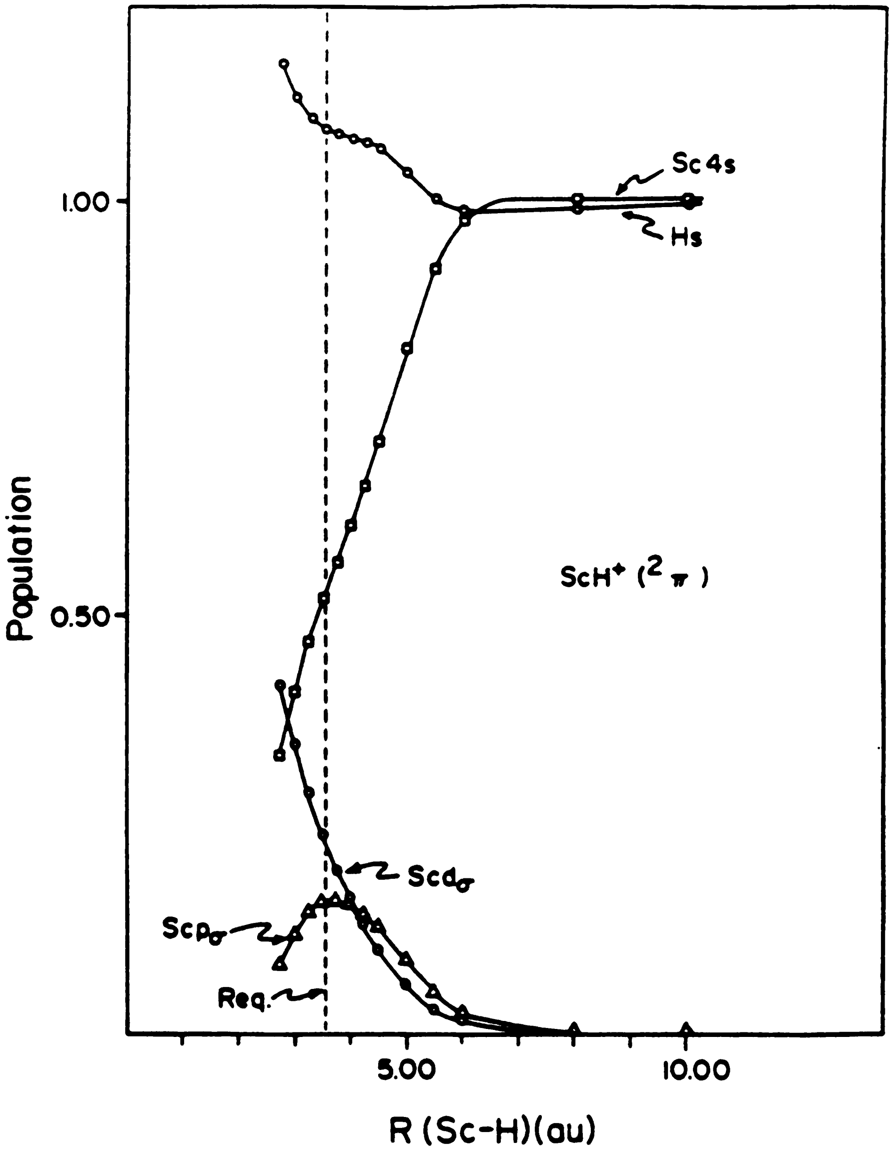

Figure 13. Electron population of selected atomic orbitals of σ symmetry from the bonding natural orbitals of the MCSCF wave function (spd basis) of $^2\Pi$ ScH^+.

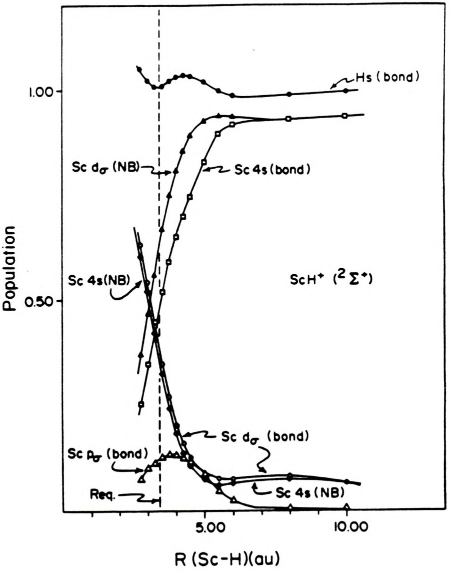

Figure 14. Electron population of selected atomic orbitals of σ symmetry from the bonding and nonbonding natural orbitals of the MCSCF wave functions (spd basis) of $^2\Sigma^+$ ScH^+.

bution suggests the bond is 32% $3d_\sigma$ and 68% sp. The population of the atomic orbitals in the $^2\Pi$ state have a similar distance dependence (as presented in Figure 13) and the equilibrium electron distribution is given by $4s^{0.52}$, $3d_\sigma^{0.24}$, and $4p_\sigma^{0.16}$ with 1.08 electrons on H. The $^2\Sigma^+$ results are shown in Figure 14. Since all of the valence electrons in this state are of σ symmetry, we have three electrons to keep track of. The two associated with the Sc-H bond are labeled "bond" while the remaining electron is "nonbonding" or "NB". The behavior of the bond populations is similar to those in $^2\Delta$ and $^2\Pi$ states and results in the equilibrium distribution $4s^{0.49}$, $3d_\sigma^{0.39}$, and $4p_\sigma^{0.12}$ with 1.00 electrons on H. The bond in this state is characterized by the largest $3d_\sigma$ population and the shortest bond length of the three studied. The "nonbonding" electron has the equilibrium distribution $4s^{0.35}$ and $3d_\sigma^{0.63}$.

Comparison between ScH^+ and ScH

Bauschlicher and Walch[28] showed that the ground state of ScH is of $^1\Sigma^+$ symmetry and is characterized by a bond with a large d_σ component. The bond in the low-lying excited states had considerably reduced d_σ character and seemed to be more sp hybridized and consequently resulted in larger bond lengths. Because Bauschlicher and Walch did not calculate D_e's or ω_e's we constructed wave functions for the six lowest states of ScH using the spd basis. Since for the neutral molecule one must be careful to take into account the near degeneracy[28] of the $4s^2$ pair on Sc, our MCSCF calculations included all excitations and spin couplings of the four valence electrons among the 4s,3d,4p, and H 1s orbitals. Our CI calculations were then single and double excitations from this MCSCF valence orbital reference space. The MCSCF+1+2 (CI) results are collected in Table 5. Also included are the first-order (FO) CI results from Bauschlicher and Walch[28]. The spd-CI results in Table 5 suggest that if one ionizes either the $^3\Delta$ or $^1\Delta$ states of ScH to form the $^2\Delta$ state of ScH^+, the bond length will decrease by ~0.01A, the vibrational frequency will increase by ~188cm^{-1}, and the bond energy will increase from 41.2($^3\Delta$) or 35.7($^1\Delta$) to 50.7 kcal/mol ($^2\Delta$). A similar pattern emerges if one ionizes $^3\Pi$ or $^1\Pi$ to form the $^2\Pi$ state, i.e., R_e decreases by ~0.01A, ω_e increases by 157 cm^{-1}, and the bond energy increases from 36.3 or 30.4 to 45.6 kcal/mol. Unlike the $^3\Delta,^1\Delta$ and $^3\Pi,^1\Pi$ pairs, the $^1\Sigma^+$ ($4s^23d$) and $^3\Sigma^+$ (4s3d4p)

Table 5. Equilibrium Properties of Neutral ScH in Several Low-Lying Electronic States Calculated with the spd Basis Set Using the MCSCF+1+2 Functions.

	$^1\Sigma^+$	$^3\Delta$	$^1\Pi$	$^1\Delta$	$^1\Sigma^+$	$^1\Pi$
R_e, Å	1.789	1.926	1.921	1.942	1.953	1.926
R_e,[a] Å	1.78	1.93	1.91		2.06	
D_e, kcal/mol	45.8	41.2	36.3	35.9	30.7	30.4
ω_e, cm^{-1}	1524	1376	1349	1366	1272	1321
E, au	-760.33206	-760.32552	-760.31763	-760.31680	-760.30809	-760.30833

[a] From ref 28.

states do not arise from the same configuration and since either could be ionized to form the $^2\Sigma^+$ state of ScH^+, each must be considered individually. The $^3\Sigma^+$ follows the above pattern but with larger changes: $\Delta R_e \sim 0.16Å$, $\Delta\omega_e \sim 207$ cm^{-1}, and an increase in the bond energy from 30.7 ($^3\Sigma^+$) to 44.6 ($^2\Sigma^+$). These changes are consistent with an increase in the number of d_σ electrons in the ScH^+ bond relative to the ScH bond. However, since the $^1\Sigma^+$ state of ScH is essentially a d bonded state there is a decrease in the d_σ character of the bond in going to ScH^+ and the bond length increases while the dissociation energy and vibrational frequency both decrease.

When CH_3 approaches Sc^+ it can bond via its singly occupied p_σ orbital and the resulting molecular state will have $^2A''$ (C_s) symmetry with the odd electron being hosted by the (essentially) d_{δ_-} orbital on Sc^+. An MCSCF function (similiar to the $^2\Delta$ ScH^+) was constructed as a function of the Sc-C separation and the resulting potential curve is shown in Figure 15 along with the MCSCF+1+2 result. As one would expect, the D_e for $ScCH_3{}^+$ (46 kcal/mol) is similar to that computed for ScH^+ (51 kcal/mol). The experimental values (Table 1) for D° are 65±5[1d] and 59±5[1g] kcal/mol suggesting that the CH_3 group is more strongly bound than H. Given the demonstrated sensitivity of D_e to basis set size and the probability that our basis set underestimates the

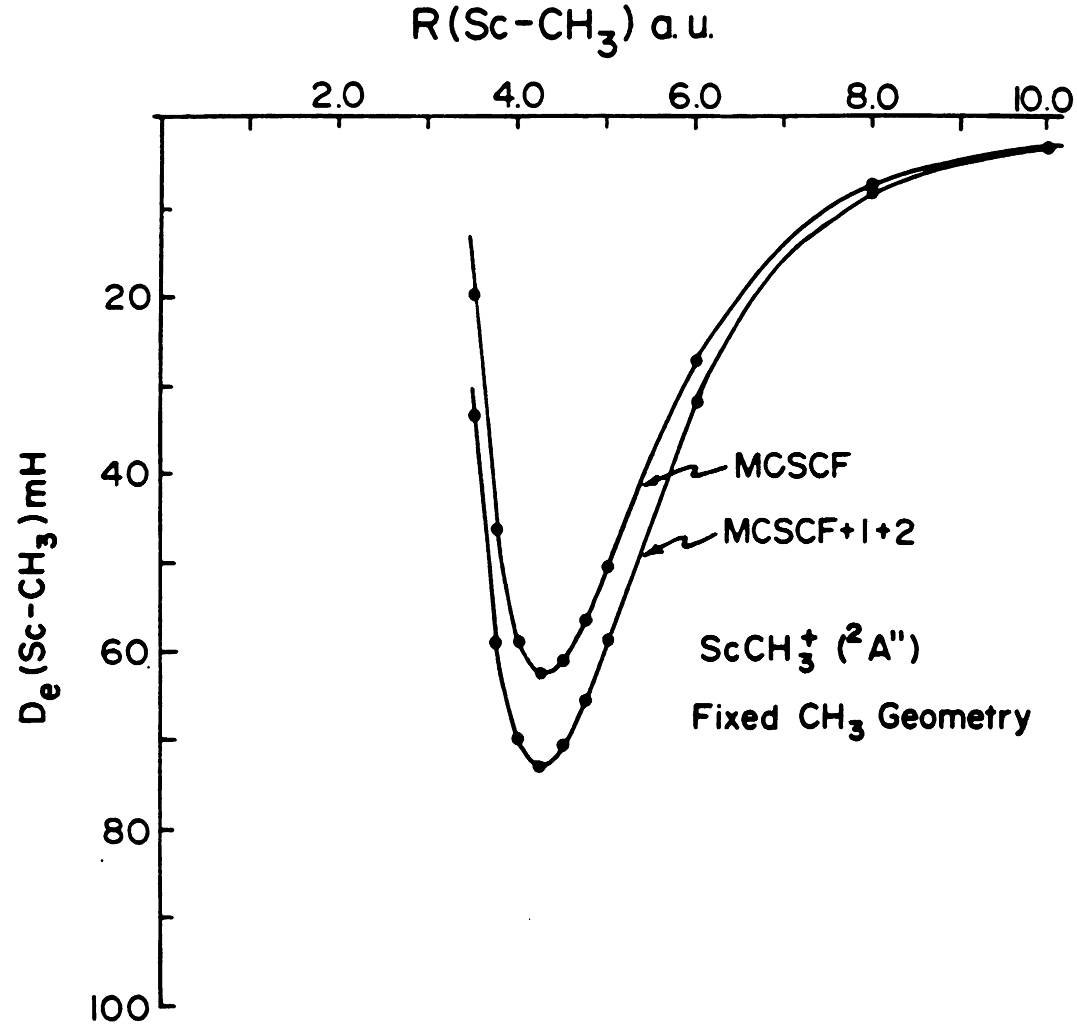

Figure 15. Potential energy curve for the lowest ${}^2A''$ state of $ScCH_3^+$. The CH_3 geometry is constrained to be tetrahedral with a C-H bond length of 1.070Å.

polarizability of CH_3, it is not unreasonable that we disagree with the experimental order. The MCSCF+1+2 optimized geometry for $ScCH_3^+$ corresponds to a Sc-C distance of 2.25A and a HCH angle of 108.9° (at a fixed C-H distance of 1.07A). The population of the various bonding orbitals as a function of the Sc-C bond length is presented in Figure 16. The Sc-C bond is slightly ionic with Sc hosting 0.8 electrons and CH_3 the remaining 1.2 electrons; the distribution of the 0.8 electrons on Sc is $4s^{0.42}$ $3d_\sigma^{0.28}$ $4p_\sigma^{0.08}$ and is remarkably similar to the distribution in ScH^+.

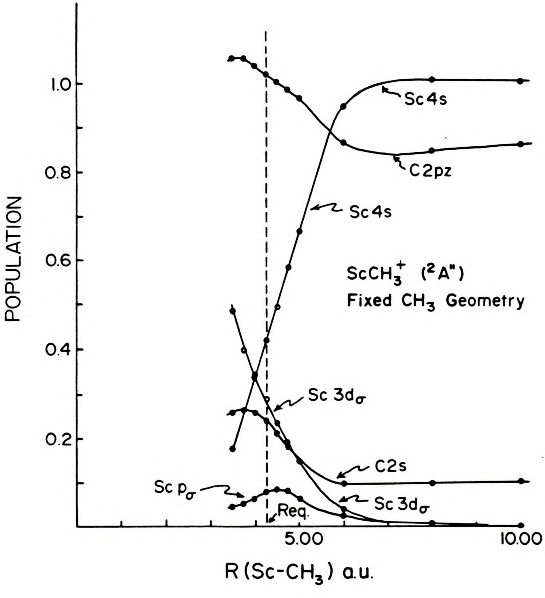

Figure 16. Electron population of selected atomic orbitals from the bonding natural orbitals of the 4 CSF MCSCF wavefunction of $^2A''$ $ScCH_3^+$.

C. $CrCH_2{}^+$

As CH_2 ($^3B_1$)

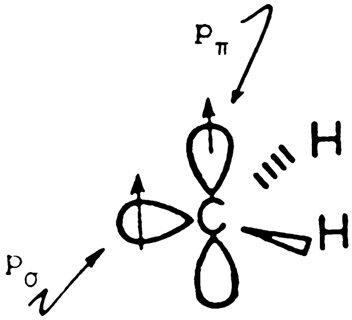

approaches Cr^+ it can use its p_σ orbital to form a bond to a Cr^+ σ orbital resulting in the $^6B_1$ state[9,29]

$$^6B_1 \sim (\ \sigma p_\sigma + p_\sigma \sigma\ )\ 3d^1_{\pi_x}\ 3d^1_{\pi_y}\ 3d^1_{\delta_+}\ 3d^1_{\delta_-}\ p^1_\pi\ (\ \alpha\beta-\beta\alpha\ )\alpha\alpha\alpha\alpha\alpha$$

Alternatively, we can use both the p_σ and p_π orbitals on CH_2 to form a double bond[9] to Cr^+ resulting in the $^4B_1$ state

$$^4B_1 \sim (\ \sigma p_\sigma + p_\sigma \sigma\ )\ (\ 3d_{\pi_x} p_{\pi_x} + p_{\pi_x} 3d_{\pi_x}\ )$$
$$3d^1_{\pi_y}\ 3^1_{\delta_+}\ 3d^1_{\delta_-}\ (\ \alpha\beta-\beta\alpha\ )\ (\ \alpha\beta-\beta\alpha\ )\ \alpha\alpha\alpha$$

MCSCF and MCSCF+1+2 functions were constructed for both these options as a function of Cr-C separation (the CH_2 geometry[30] was frozen at C-H R= 1.075A and a HCH angle of 128.8°). As usual, no excitations were permitted from the Ar core of Cr^+, the carbon 1s orbital, and the C-H bonding orbitals. The resulting potential energy curves shown in Figure 17 support the suggestion of Carter and Goddard[9] that the doubly bonded structure is more stable. The orbital occupancies in the bonding σ natural orbitals are plotted in Figures 18 and 19. In Figures 20 and 21 we compare the contours of the relevant GVB orbitals for the two states. From Figure 18 we see that the outer minimum in the MCSCF curve for the $^6B_1$ state corresponds to Cr using a $3d_\sigma$ orbital to bond the incoming methylene, while the inner minimum results from the Cr using a mixture of 4s and $3d_\sigma$. If one constructs the $^6B_1$ MCSCF solution as a function of R by converging the calculation at R= 20au (separated atoms) and uses this as an initial estimate for the subsequent $^6B_1$ calculations at smaller internuclear separations one traces the solid curve in Figure 17. If, however, one takes the converged solution at R= 4.25au and uses this as an initial estimate at R= 4.50au, one converges o a solution which has a character similar to that at R= 4.25au and has an energy which is higher than that obtained using the separated atoms (R= 20au) as an initial estimate. Other points obtained in this way (and the associated CI) are connected by a dashed line in Figure 17. If the molecule followed the "character-conserving" curve rather than the adiabatic curve it would separate to a Cr^+ in the $4s3d^4$ configuration. A slight kink is present in the $^4B_1$ state and Figure 19 shows the anticipated abrupt bond character change occurs between 4.5 and 4.25au. The frozen HCH angle used to construct Figure

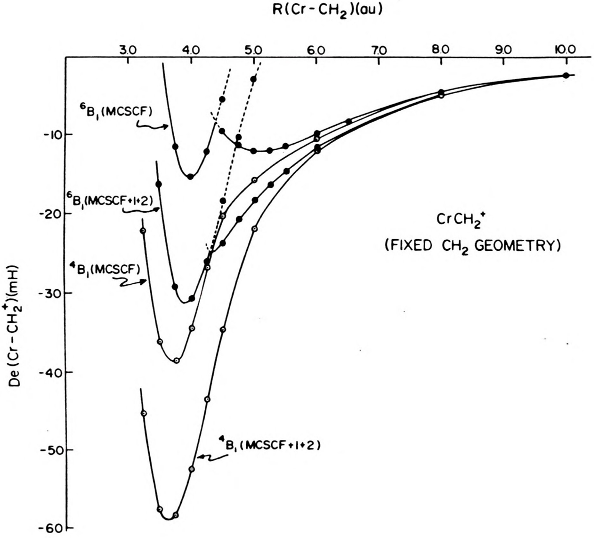

Figure 17. Potential energy curves for the $^6B_1$ (filled circles) and $^4B_1$ (open circles) states of $CrCH_2^+$. The CH_2 group is constrained to have a C-H bond length of 1.075A and an HCH angle of 128.8°.

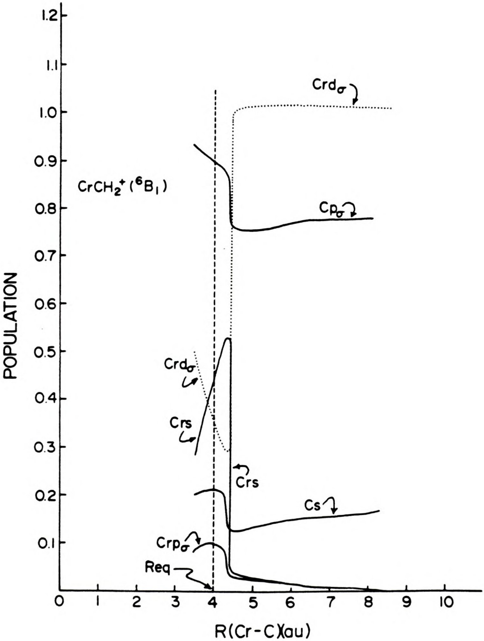

Figure 18. Electron population of selected atomic orbitals from the bonding sigma natural orbitals of the 7 CSF MCSCF wavefunction of $^6B_1$ $CrCH_2^+$.

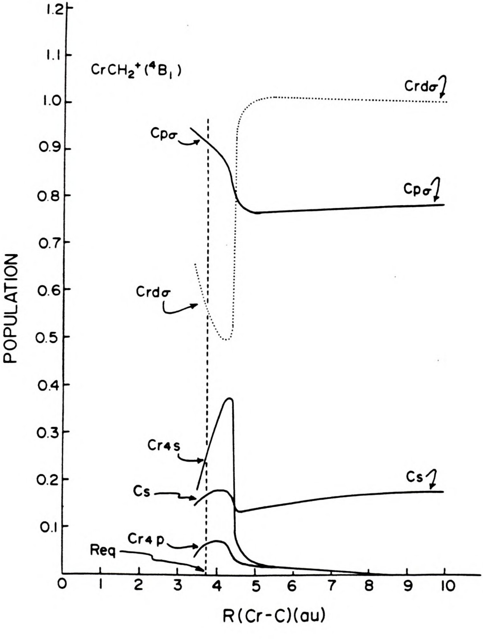

Figure 19. Electron population of selected atomic orbitals from the bonding sigma natural orbitals of the 34 CSF MCSCF wavefunction of $^4B_1$ $CrCH_2^+$.

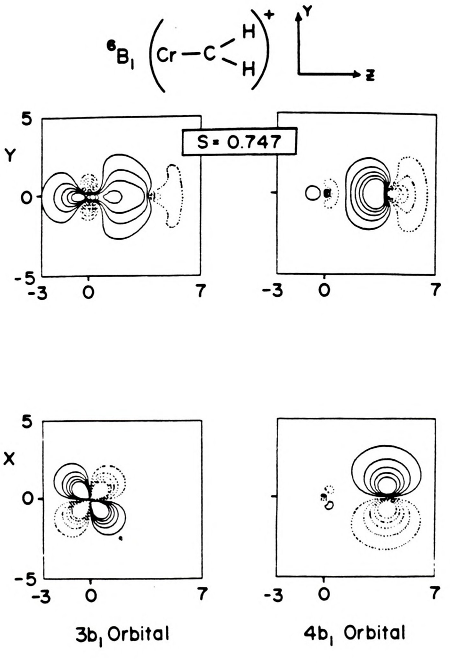
$^6B_1$ $(Cr-CH_2)^+$
H
H
Y
Z
S = 0.747
5
Y
0
-5
-3
0
7
-3
0
7
5
X
0
-5
-3
0
7
-3
0
7
3b₁ Orbital
4b₁ Orbital

Figure 20. GVB orbitals for the Cr-C σ bond and the singly occupied π orbitals of $^6B_1$ $CrCH_2^+$ at its equilibrium geometry.

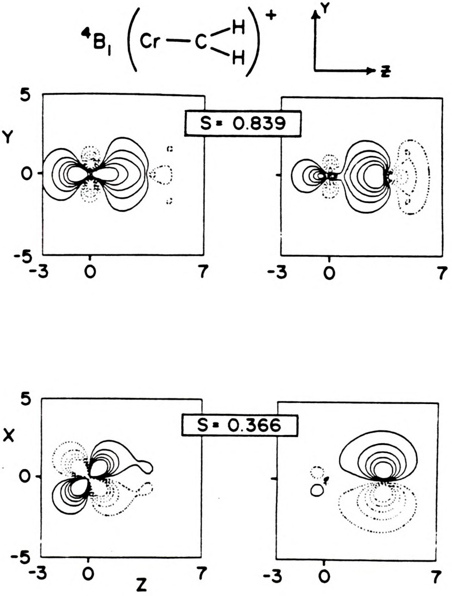
⁴B₁ (Cr—C H H)⁺
Y
z
5
Y
0
-5
-3
0
7
S= 0.839
-3
0
7
5
X
0
-5
-3
0
Z
7
S= 0.366
-3
0
7

Figure 21. GVB orbitals for the Cr-C σ and π bonds of $^4B_1$ $CrCH_2^+$ at its equilibrium geometry.

17 is essentially optimal for those points to the right of the Cr-C separation where the bond character changes but not for those to the left. It seems that when the Cr^+ contribution to the bond character changes from essentially pure $3d_\sigma$ to a strong mixture of $3d_\sigma$ and 4s, there is a significant shift of electrons from Cr into the CH_2 p_σ orbital reflecting the lower ionization potential of the 4s vs. the $3d_\sigma$ electron. This has the anticipated effect of reducing the HCH angle from the $^3B_1$ value to 116°, much closer to the $^1A_1$ value[30] of 103°, observed when the p_σ orbital is doubly occupied.

The σ bond in both molecules is essentially covalent being 57% C and 43% Cr for both the $^6B_1$ and $^4B_1$ states. In spite of this equal covalency, the character of the Cr contribution in the two states is significantly different, being 63% sp and 37% d_σ in the high spin state and, 36% sp and 64% d_σ in the low spin state. The higher d_σ composition of the σ bond in the low spin state correlates with the shorter bond length in this state. Optimizing the Cr-C distance and HCH angle (keeping the CH bond length at 1.075A) results in the MCSCF+1+2 values of 2.06A/117.3° for the $^6B_1$ state and 1.92A/116.7° for the $^4B_1$ state. These numbers are in excellent agreement with the Carter and Goddard[9] values of 2.07A/118.3° and 1.91A/117.6°, respectively. Using these optimized equilibrium geometries and the energies of the respective states at a Cr-C distance of 20au, we calculated the bond energies 21.0 ($^6B_1$) and 38.7

kcal/mol ($^4B_1$) which are consistent with the Carter and Goddard[9] values of 25.0 and 44.0 kcal/mol but which fall short of the experimental[1b] bond energy of 65±7 kcal/mol. The $^4B_1$-$^6B_1$ separation of Carter and Goddard is 19.0 kcal/mol while we calculated 17.7 kcal/mol.

The π bond between Cr^+ and CH_2 in the $^4B_1$ state is rather unusual. If one were to monitor the occupation of the natural orbitals (NO's) associated with the π bond in $H_2C=CH_2$ as a function of the separation between the triplet CH_2 groups one would find that when the groups are separated the two natural orbitals would both have unit occupation numbers. As the groups approached, the π-bonding NO would become more occupied than its antibonding companion until at equilibrium it would dominate and have an occupancy close to 2.0. The occupancy of the natural orbitals associated with the π bond in $CrCH_2^+$ are plotted in Figure 22. At the equilibrium separation of 1.92A the π NO's have occupation numbers of 1.48 and 0.52 which would characterize a very "long" bond between the main group elements. This observation, coupled with the small overlap (S= 0.366) of the GVB π orbitals in Figure 21 and the relatively small energy loss (17.7 kcal/mol) incurred in going from the $^4B_1$ to the $^6B_1$ states, suggests a relatively weak double bond. In addition, the atomic orbital occupations of the π natural orbitals associated with the bond, plotted in Figure 23, suggest that very little charge transfer has occurred through the π system.

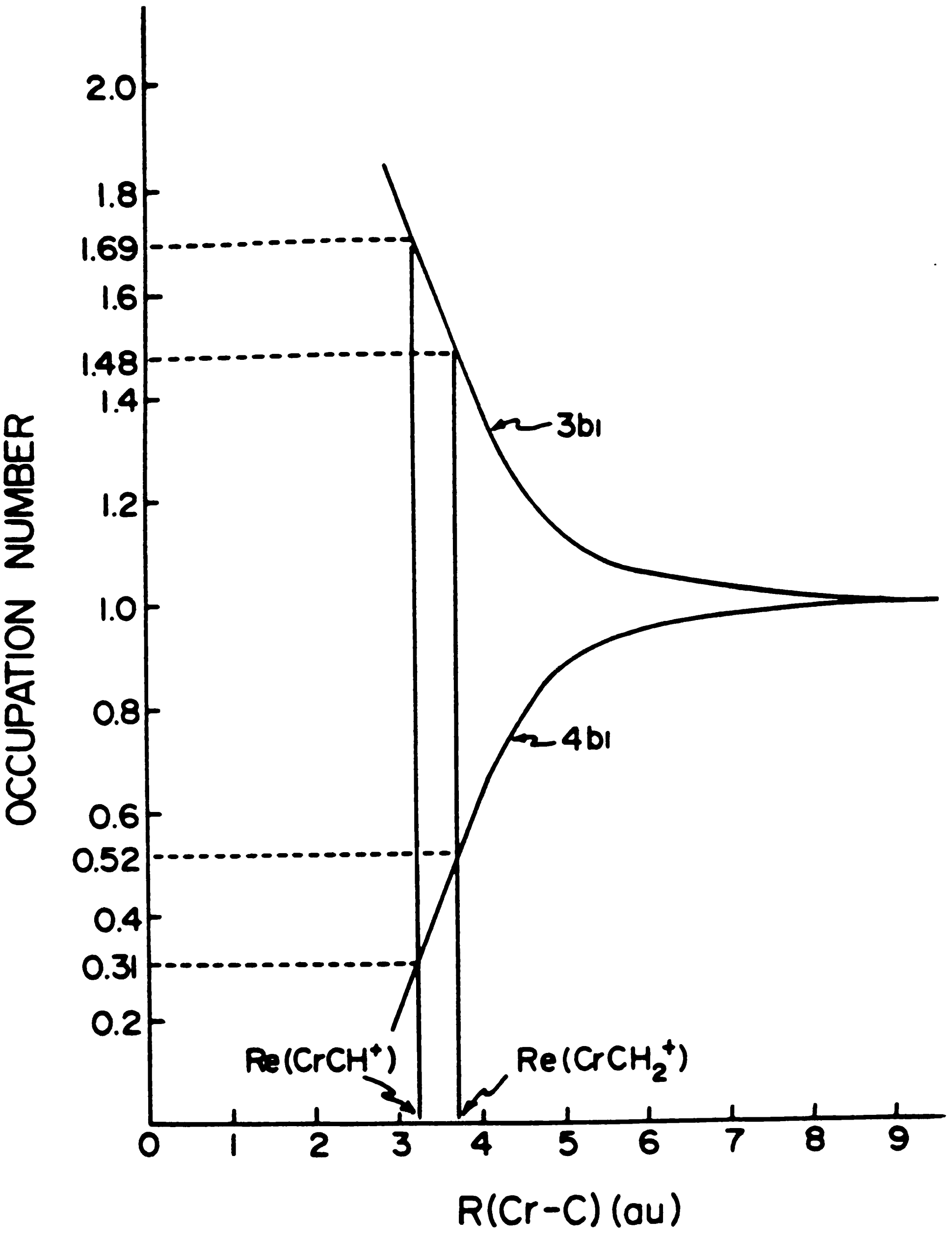

Figure 22. Natural orbital occupation numbers for the valence π orbitals of the MCSCF wavefunctions of $CrCH_2^+$ ($^4B_1$) and $CrCH^+$ ($^3\Sigma^-$).

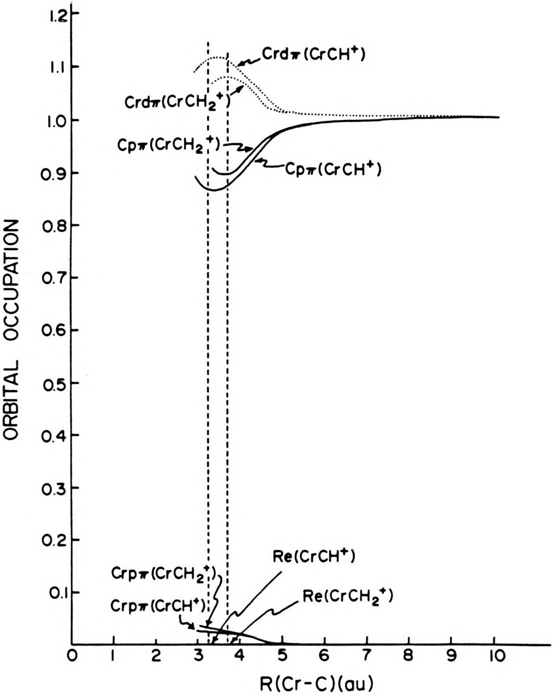

Figure 23. Electron population of selected atomic orbitals from the bonding π natural orbitals of the MCSCF wavefunctions for $CrCH_2^+$ ($^4B_1$) and $CrCH^+$ ($^3\Sigma^-$).

D. $ScCH_2^+$

The doubly bonded state of this molecule arises when the two valence electrons on Sc^+ (^3D) couple to the two valence electrons on $CH_2(^3B_1)$. The wave function has the schematic form

$$^1A_1 \sim [\ \sigma_{CH_2}\ \sigma_{Sc} + \sigma_{Sc}\ \sigma_{CH_2}\ ]\ [\ \pi_{CH_2}\pi_{Sc} + \pi_{Sc}\pi_{CH_2}\ ]$$
$$(\ \alpha\beta-\beta\alpha\ )\ (\ \alpha\beta-\beta\alpha\ )$$

where at large separation σ_{CH_2} and π_{CH_2} are the p_σ and p_π orbitals of free $CH_2(^3B_1)$ while σ_{Sc} and π_{Sc} are the 4s and $3d_\pi$ orbitals of $Sc(^3D)$. An MCSCF function which separates to the correct SCF products consists of 10 CSF's while the singles and doubles CI (MCSCF+1+2) from this reference space consists of 3,660 CSF's. The energy as a function of Sc-C separation is shown in Figure 24 for both wavefunctions. The Sc-C bond length changes from 2.004 A at the MCSCF to 1.998A at the CI level while the HCH angle remains at 112° in both calculations. The primary effect of the CI is to increase the calculated D_e by 15 kcal/mol to 68 kcal/mol. This is to be compared with the experimental value of 97 kcal/mol from Armentrout _et al_[1g]. There are no experimental data on the geometric parameters with which to compare.

The lowest triplet state which correlates to the ground state products maintains a bond in the σ system and triplet couples the π electrons. It is schematically

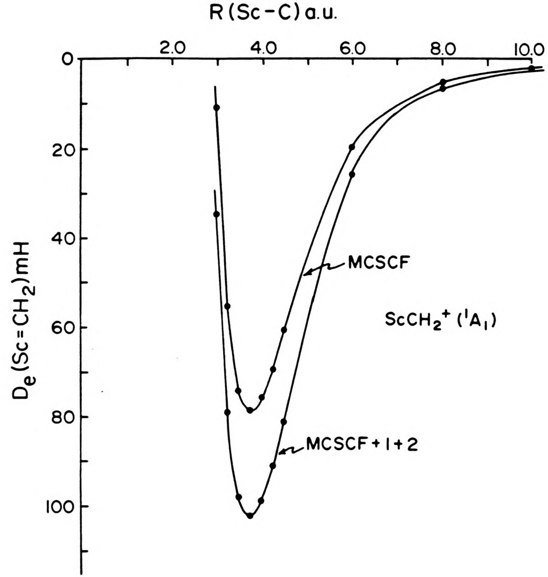

Figure 24. Potential energy curves for the lowest $^1A_1$ state of $ScCH_2^+$. The CH_2 group is constrained to have a C-H bond length of 1.075A and an HCH angle of 128.8°.

represented as

$$ {}^3A_1 \sim (\sigma_{CH_2}\sigma_{Sc} + \sigma_{Sc}\,\sigma_{CH_2}] \; \pi^1_{CH_2}\,\pi^1_{Sc} \; (\alpha\beta - \beta\alpha) \; \alpha\alpha $$

An MCSCF function of this form which separates to the SCF products consists of 7 CSF's while the corresponding singles and doubles CI from this reference space contains 4,683 CSF's. The energy of this ${}^3A_1$ state as a function of Sc-C separation is shown in Figure 25. The optimized Sc-C bond length changes from 2.287A at the MCSCF level to 2.264A at the CI level with the HCH angle going from 112.4° to 113.4°. The increased bond length of this state relative to the ${}^1A_1$ state is consistent with the loss of the π component of the ScC double bond. The calculated D_e for the ${}^3A_1$ state is 42 kcal/mol which is 26 kcal/mol less than the ${}^1A_1$ D_e reflecting the strength of the ScC π bond.

The electron distribution in selected valence orbitals is plotted as a function of internuclear separation in Figures 26 and 27. Although these plots correspond to the HCH angle of 128.8° they faithfully track the overall distance dependence of the orbital occupancies. At the optimal HCH angle the Sc orbitals have the occupancies $4s^{0.22}$ $4p_\sigma^{0.04}$ $3d_\sigma^{0.43}$ in the ${}^1A_1$ state and $4s^{0.38}$ $4p_\sigma^{0.11}$ $3d_\sigma^{0.21}$ in the ${}^3A_1$ state. The corresponding carbon occupancies are $2s^{0.31}$ $2p_\sigma^{0.96}$ and $2s^{0.42}$ $2p_\sigma^{0.89}$. Interestingly, the total Sc and carbon σ populations in both states are essentially identical although the electron

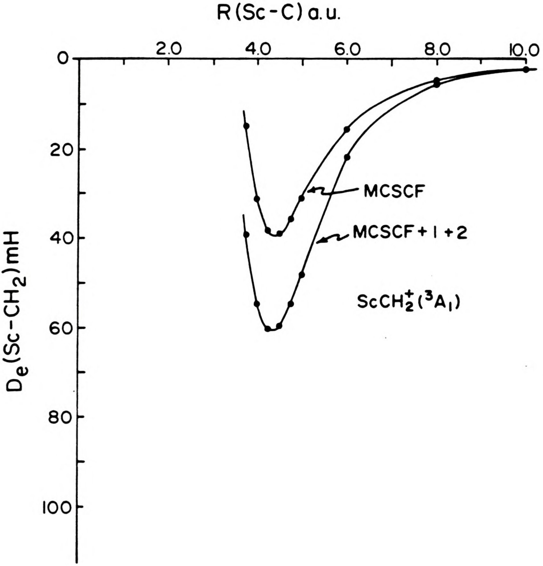

Figure 25. Potential energy curves for the lowest $^3A_1$ state of $ScCH_2^+$.

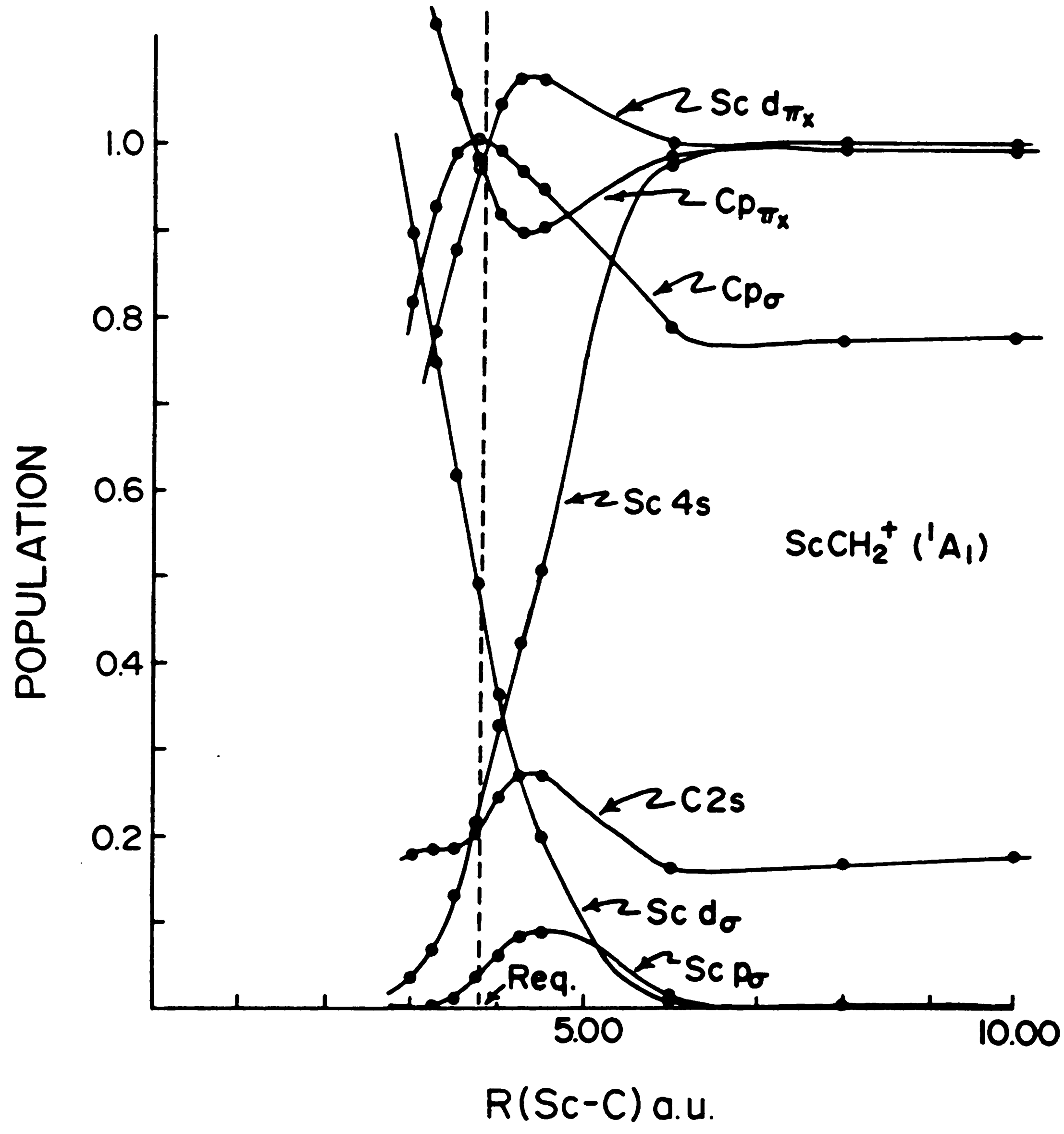

Figure 26. Electron population of selected atomic orbitals from the bonding σ and π natural orbitals of the 10 CSF MCSCF wavefunction of $^1A_1$ $ScCH_2^+$.

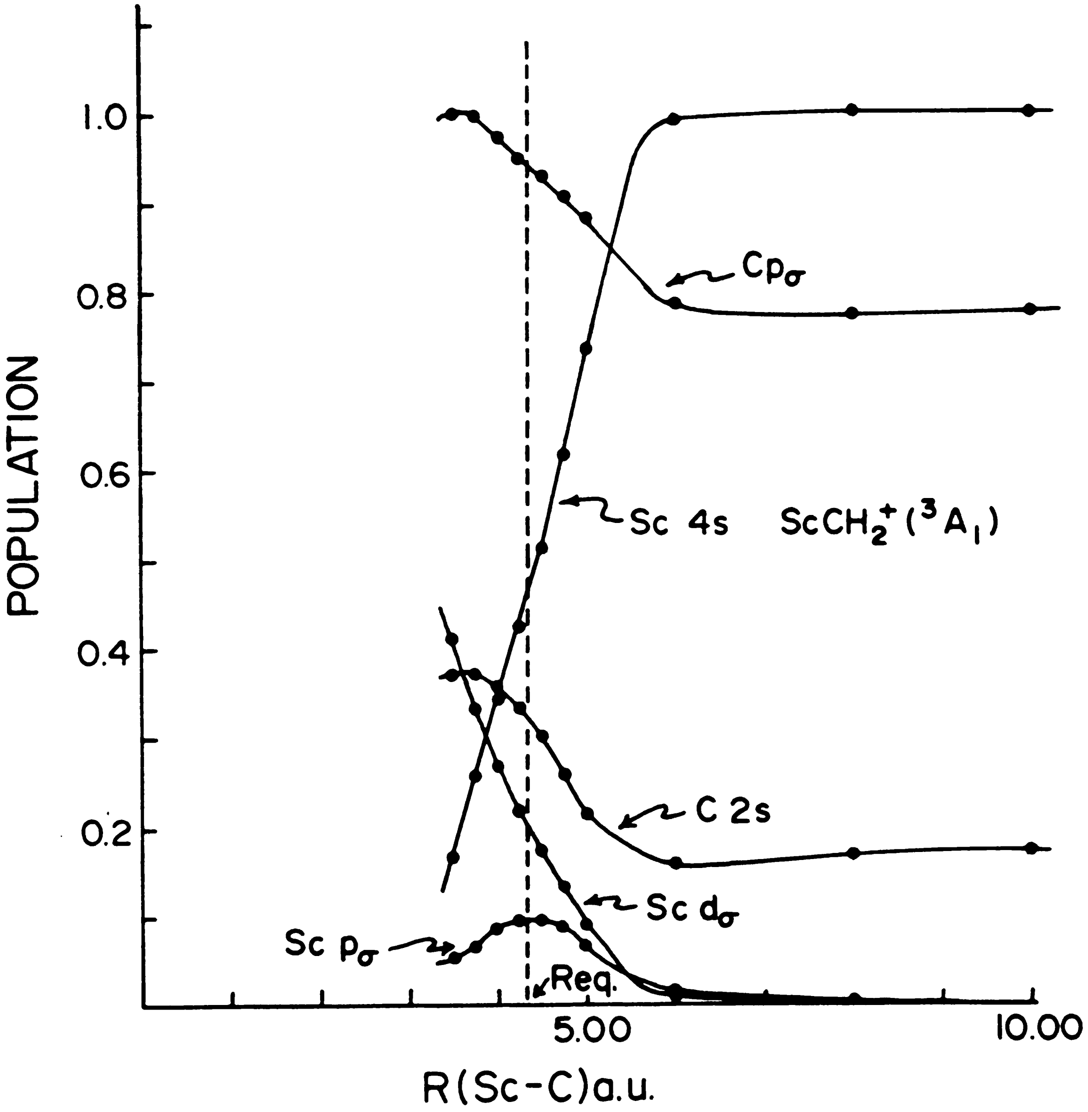

Figure 27. Electron population of selected atomic orbitals from the bonding sigma natural orbitals of the 7 CSF MCSCF wavefunction of $^3A_1$ $ScCH_2^+$.

distibutiton among the valence orbitals differs between the two states. Since the π distribution in both states has one electron on Sc and one on carbon, there has been a net loss of 0.3 electrons from Sc to carbon in both states. This transfer of electrons from Sc to the carbene p_σ orbital is consistent with the calculated in-situ HCH bond angle being less than free $^3B_1$ but greater than $CH_2(^1A_1)$.

E. $CrCH^+$

Given the predicted stability of the double bonded (low spin) $CrCH_2{}^+$ molecule, we restricted our $CrCH^+$ study to that function which could represent a triple bond between Cr^+ and CH. Since this required three unpaired electrons on CH, our asymptote for this fragment is the $^4\Sigma^-$ state, schematically represented by

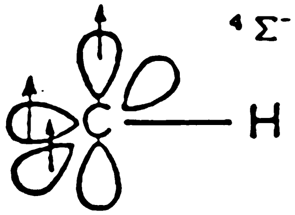

An appropriate function for the $^3\Sigma^-$ state of $CrCH^+$ would be

$$^3\Sigma^- \sim (\sigma p_\sigma + p_\sigma \sigma)(d_{\pi_x} p_{\pi_x} + p_{\pi_x} d_{\pi_x})(d_{\pi_y} p_{\pi_y} + p_{\pi_y} d_{\pi_y})$$
$$3d^1_{\delta_+}\, 3d^1_{\delta_-}\, (\alpha\beta-\beta\alpha)(\alpha\beta-\beta\alpha)(\alpha\beta-\beta\alpha)\,\alpha\alpha$$

The MCSCF function of this form which separates to the SCF products (^6S + $^4\Sigma^-$) consists of 126 CSF's (in C_{2v} symmetry) and was constructed as a function of the Cr-C separation (at a fixed C-H distance[31] of 1.082A). The MCSCF+1+2 (no excitations from the Ar core of Cr^+, the C 1s orbital, and the C-H bond) calculation from the 126 CSF valence orbital reference space consists of 249,208 configurations and was too large for our computational facilities. The computation can be brought within more manageable limits by restricting the MCSCF+1+2 configurations to always have the two triplet coupled d electrons singly occupied. This, in effect, correlates the six electrons involved in the "triple bond" and keeps the two singly occupied d orbitals at the SCF level. The resulting number of configurations is then reduced to 107,216. This "bond only" CI is designated by $(\mathrm{MCSCF+1+2})^*$ in the various figures and Table 2. The resulting potential energy curves are shown in Figure 28, the atomic population of the σ NO's in Figure 29, the π NO occupation numbers in Figure 22, and the atomic population of the π NO's in Figure 23. The CI calculations predict a Cr-C separation of 1.77Å and a bond energy of 70.8 kcal/mol making $\mathrm{Cr{\equiv}CH^+}$ the most strongly bound of the Cr molecules in this study. Since the $^3\Sigma^-$ state of $\mathrm{CrCH^+}$ separates to $\mathrm{Cr^+}$ in the ground ^6S state and CH in the excited $^4\Sigma^-$ state, we must reduce the calculated D_e by the $^2\Pi$-$^4\Sigma^-$ excitation energy (17.1 kcal/mol) before comparing to experimental data obtained via thermochemically interpreted experiments. This results in a calculated bond energy of 53.7 kcal/mol for $\mathrm{CrCH^+}$.

The atomic populations shown in Figure 29 suggest that this Cr-C σ bond is also the most polar of those studied, being 64% C and 36% Cr. In addition, the Cr σ contribution is 70% d and 30% sp, reflecting the short Cr-C

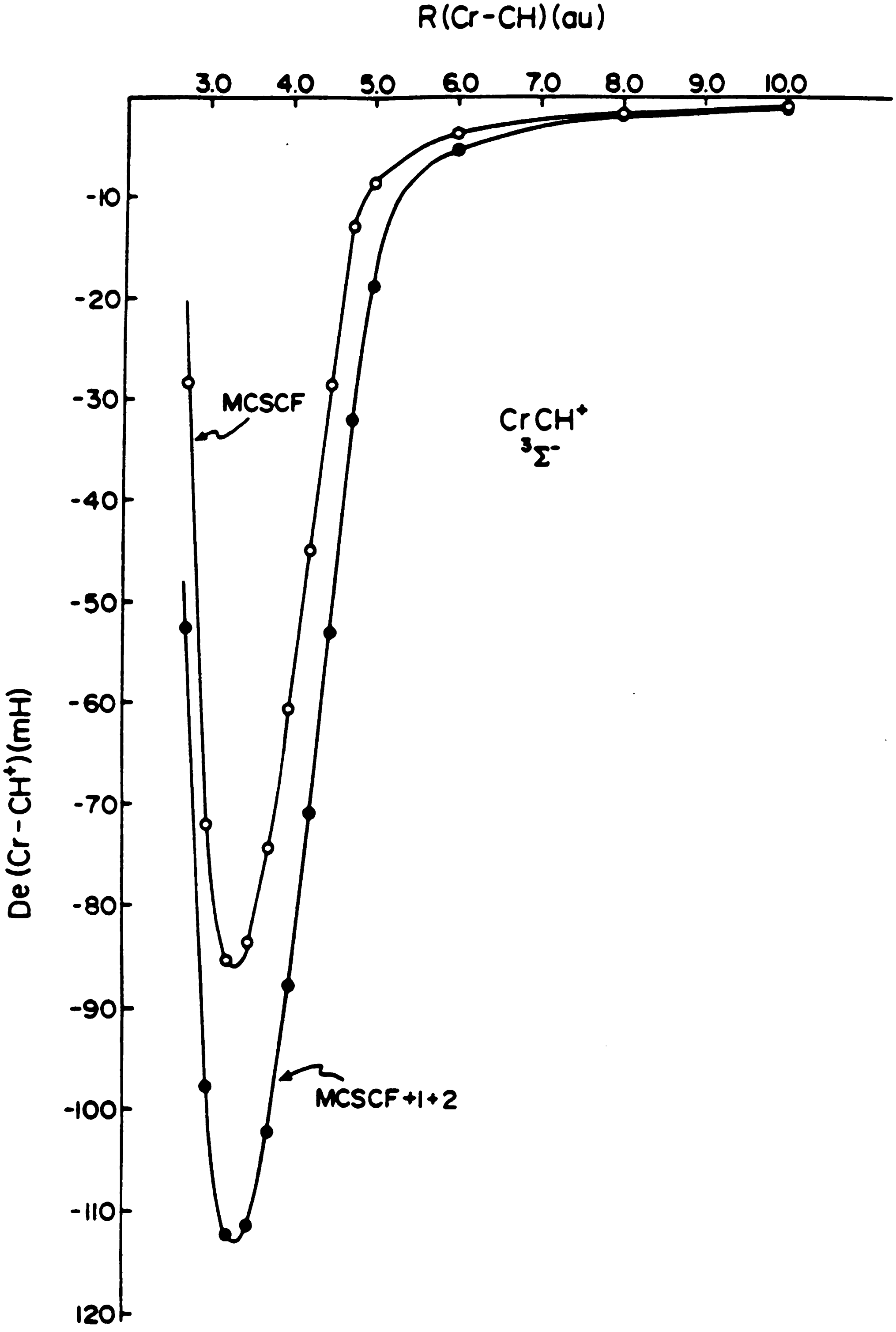

Figure 28. Potential energy curves for the lowest $^3\Sigma^-$ states of $CrCH^+$. The CH distance is taken as 1.082A.

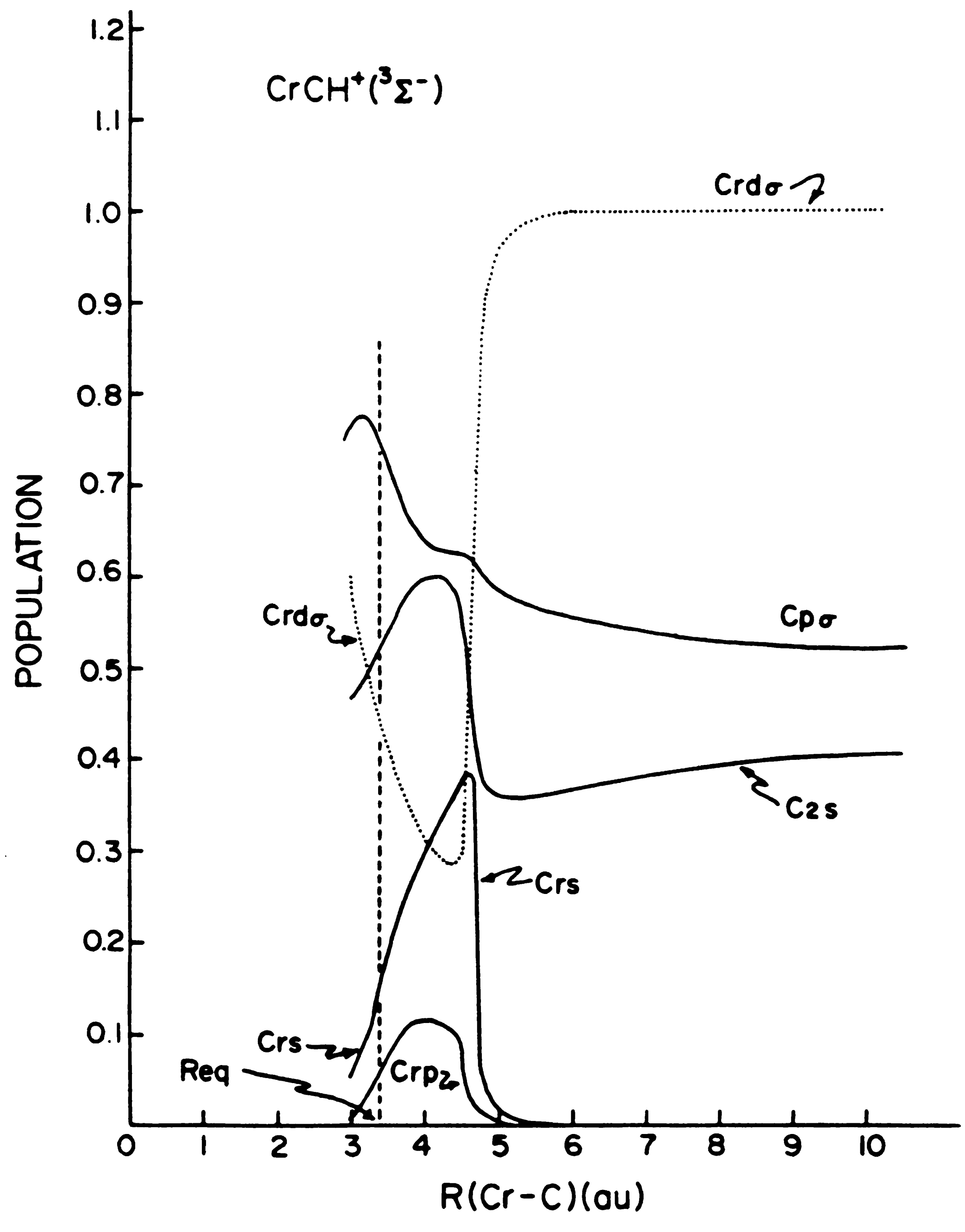

Figure 29. Electron population of selected atomic orbitals from the bonding σ natural orbitals of the 126 CSF MCSCF wavefunction of $^3\Sigma^-$ $CrCH^+$.

bond. This d_σ dominance is evident in contours of the GVB bonding orbitals shown in Figure 30 where the σ bond overlap (S= 0.850) is greater than the σ bond overlap (S= 0.747) in $CrCH_2^+$. The π_x and π_y bonds are similar to that found in $Cr{=}CH_2^+$; the π NO occupation numbers (Figure 22) are both significant and the total charge transfer in the π system is small. More remarkably, on the scale of Figure 22, the distance dependence of the occupation numbers for the π orbitals in the $^4B_1$ state of $CrCH_2^+$ and the $^3\Sigma^-$ state of $CrCH^+$ is indistinguishable.

From Figure 29 we see that when the CH group is separated from Cr^+ the singly occupied σ bonding orbital is 52% C p_σ, 41% C 2s, and 7% H (not shown). As this (essentially) sp-hybridized orbital approaches Cr^+, the 2s character initially decreases, the $2p_\sigma$ character increases, and the Cr d_σ orbital remains singly occupied. This situation continues until the Cr-C separation is less than 5au, at which point there is an abrupt transfer of electrons in the σ system from Cr^+ to CH. This charge transfer is associated with a sharp drop in the potential energy curve (Figure 28). At a Cr-C separation of 4.00au the electron distribution in the carbon orbitals has increased to 1.24 (0.60 in the C 2s and 0.64 in the C $2p_\sigma$), while the electron distribution in the Cr σ valence orbitals has dropped to 0.70 (0.30 in both the Cr $3d_\sigma$ and 4s orbitals and 0.10 in the Cr $4p_\sigma$). As the molecule approaches the equilibrium Cr-C separation the occupancy of the chromium 4s,4p and the

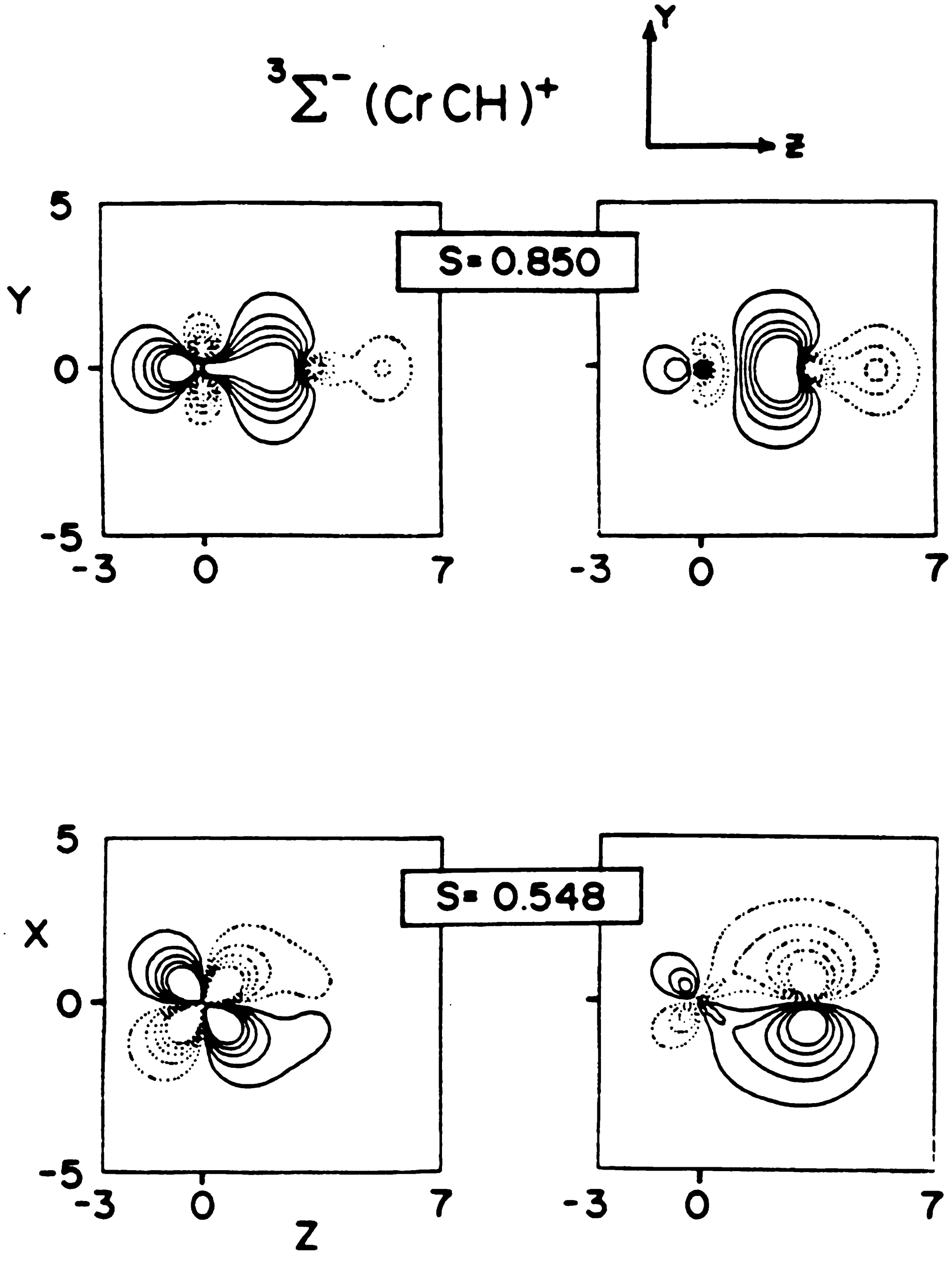

Figure 30. GVB orbitals for the Cr-C σ and π bonds of $^3\Sigma^-$ $CrCH^+$.

carbon 2s orbitals drop while the chromium $3d_\sigma$ and carbon $2p_\sigma$ occupation increases. This behavior suggests that the Cr 4s orbital attracts the CH group and "pulls it in" to a distance where the Cr $3d_\sigma$ and $3d_\pi$ orbitals can form a bond. A similar interpretation can be obtained for the interaction of Cr^+ with CH_2 and CH_3.

F. $ScCH^+$

If the $Sc^+(^3D)$ forms a double bond with the CH group, we anticipate the unpaired electron will be in a π orbital localized primarily on carbon

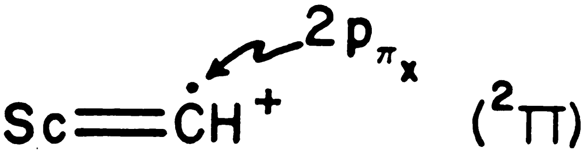

$$\overset{2p_{\pi_x}}{Sc{=}\dot{C}H^+} \qquad (^2\Pi)$$

Suppressing the Ar core on Sc, the carbon 1s orbital and the CH bond orbital, the primary component of the wavefunction would have the form

$$^2\Pi_x \sim [\ \sigma_{CH}\ \sigma_{Sc} + \sigma_{Sc}\ \sigma_{CH}\ ]\ [\ \pi_{y_{CH}}\pi_{y_{Sc}} + \pi_{y_{Sc}}\pi_{y_{CH}}]$$
$$\pi_{x_{CH}}\quad (\ \alpha\beta-\beta\alpha\ )\ (\ \alpha\beta-\beta\alpha\ )\ \alpha$$

Asymptotically, the σ_{Sc} would be a 4s orbital, the $\pi_y(Sc)$ a $3d_{yz}$ orbital, σ_{CH} a p_σ (sp hybrid on C) and $\pi_x(CH)$ a p_π orbital on C. The MCSCF function which separates to the SCF products (^3D + $^4\Sigma^-$) consists of 17 CSF's while the corresponding CI (MCSCF+1+2) contains 12099 CSF's. The distance dependence of energy of the $^2\Pi$ state of $ScCH^+$ is shown for both functions in Figure 31 while the electron population of various orbitals is shown in Figure 32. The calculated dissociation energy is 96.3 kcal/mol and the bond length is 1.940A. If we reference this D_e to the ground $^2\Pi$

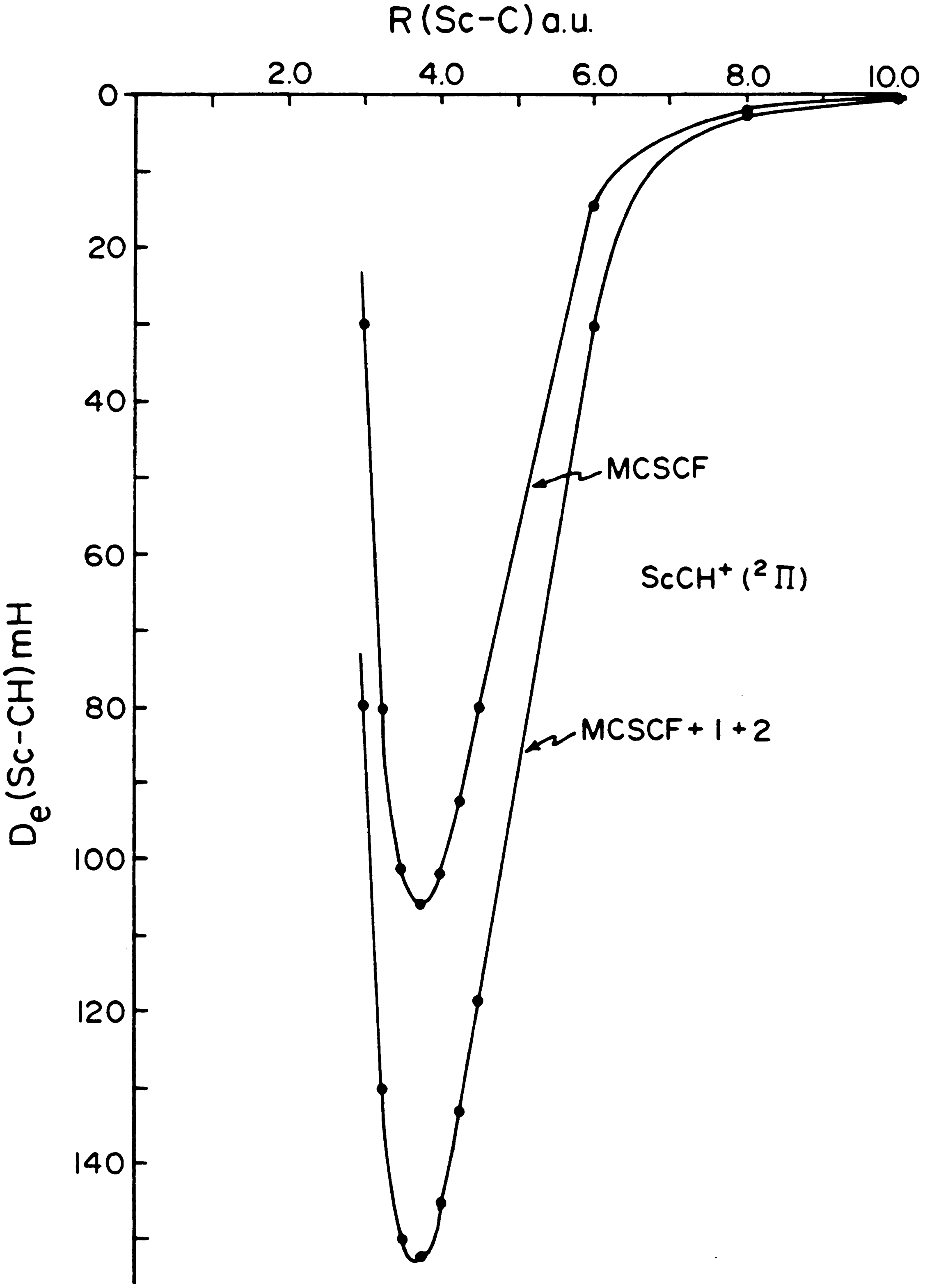

Figure 31. Potential energy curves for the lowest $^2\Pi$ state of ScCH$^+$. The CH distance is taken as 1.082Å.

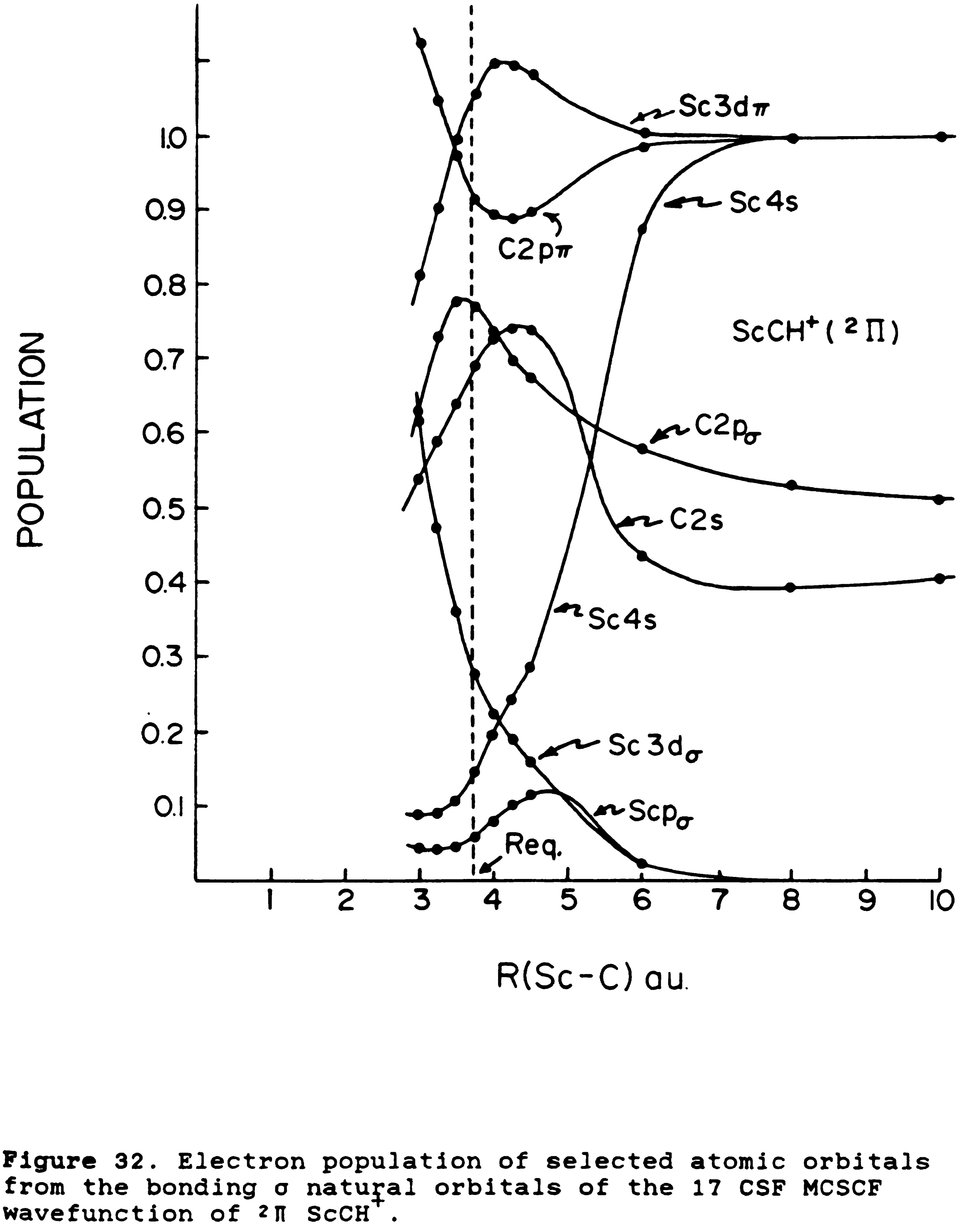

Figure 32. Electron population of selected atomic orbitals from the bonding σ natural orbitals of the 17 CSF MCSCF wavefunction of $^2\Pi$ $ScCH^+$.

state of CH using our calculated $^2\Pi$ - $^4\Sigma^-$ separation of 10 kcal/mol, we predict a D_e of 86 kcal/mol. This double bond is substantially stronger and somewhat shorter than that in $ScCH_2^+(^1A_1)$ (68 kcal/mol and 1.998A).

If one breaks the π bond in this $^2\Pi$ state by triplet coupling the π electrons

$$^4\Pi \sim [\ \sigma_{CH}\sigma_{Sc} + \sigma_{Sc}\sigma_{CH}]\ \pi_{y_{CH}}\pi_{y_{Sc}}\pi_{x_{CH}}\quad (\ \alpha\beta-\beta\alpha\ )\ \alpha\alpha\alpha$$

the resulting state is bound by 69.4 kcal/mol and has a bond length of 2.177A. Breaking the π bond costs 27 kcal/mol and increases the bond length by 0.24A. Recall that breaking the π bond in $ScCH_2^+$ costs 26 kcal/mol and increases the bond length by 0.17 A. The larger bond energy in the carbyne relative to the carbene is therefore due to the σ bond. Looking at the electron distribution in Figures 26 and 32, we see that the carbyne p_σ orbital hosts ~1.5 electrons and is essentially 50% 2s while the carbene p_σ orbital contains ~1.3 electrons and is 25% 2s. The stronger bond is the more ionic and the one in which the carbon bonding orbital is essentially an sp hybrid.

There are several other low lying states associated with the ^3D + $^4\Sigma^-$ asymptote. For example, if we keep the σ bond intact but singlet couple the Sc $3d_\delta$ orbital to the carbyne p_π orbital we have a $^2\Delta$ state. Alternatively, we may singlet couple the Sc $3d_\sigma$ electron to the carbyne p_π orbital and obtain a $^2\Sigma^-$ state. We optimized the geometry

for these states and the corresponding quartets and the results are summarized in Figure 33. When we go from a $^2\Pi$ to a $^4\Pi$ the energy increases but in going from a $^2\Delta$ to a $^4\Delta$ or a $^2\Sigma^-$ to a $^4\Sigma^-$ the energy decreases. This is because the higher multiplicity in the Π state can be achieved only at the expense of a chemical bond between orbitals of the same symmetry (there is also a substantial increase in the bond length). In the Δ and Σ^- cases the higher multiplicity is lower in energy because the bond is between orbitals of different symmetry (and, therefore, very weak) and one recovers an exchange interaction which more than compensates for the lost bond energy. Consistent with this, we note that the bond lengths in the Δ and Σ^- symmetries are considerably less sensitive, than the Π, to the multiplicity.

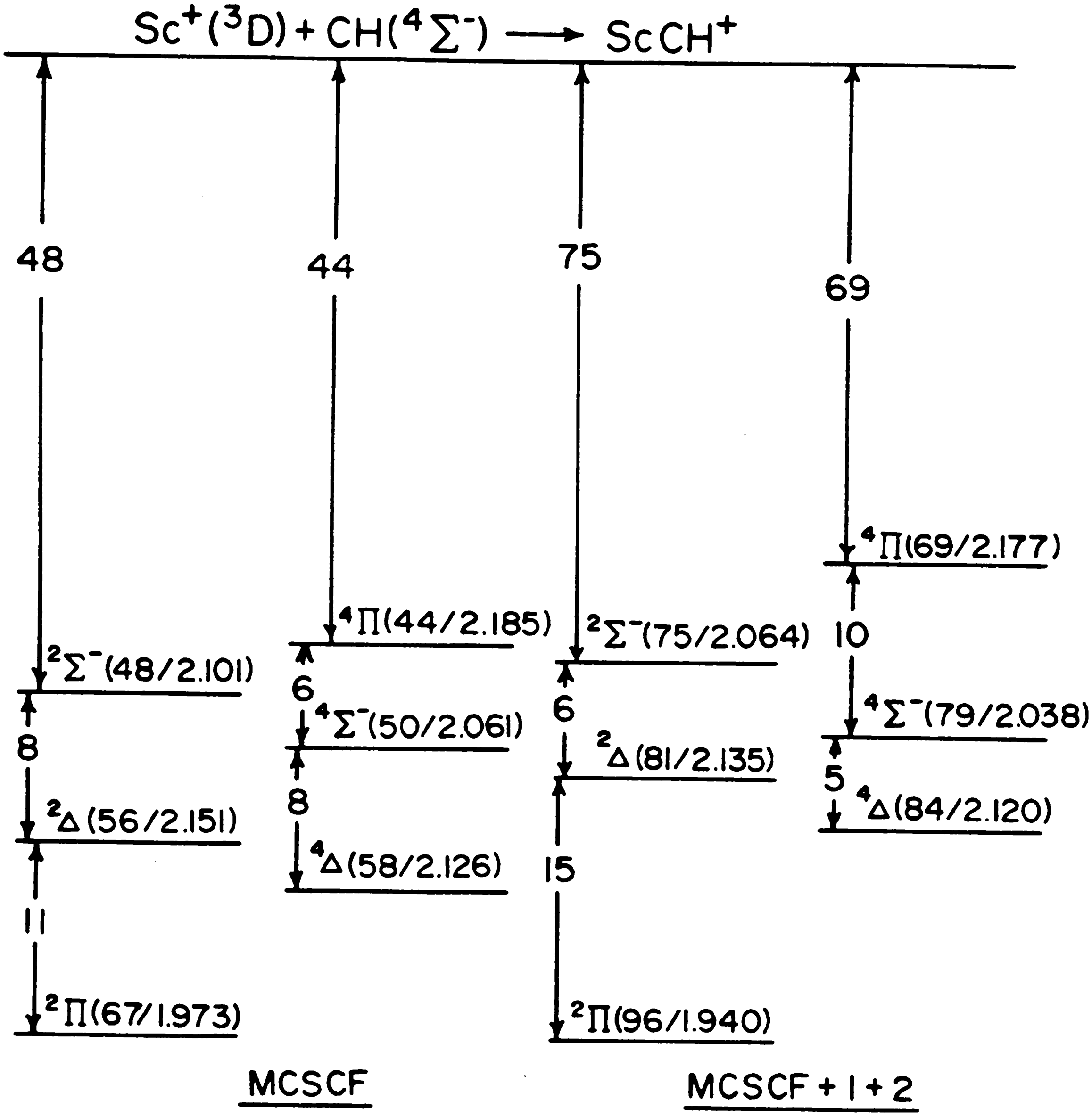
$Sc^+(^3D) + CH(^4\Sigma^-) \longrightarrow ScCH^+$
48
44
75
69
$^4\Pi(69/2.177)$
10
$^4\Pi(44/2.185)$
$^2\Sigma^-(75/2.064)$
$^2\Sigma^-(48/2.101)$
6
6
$^4\Sigma^-(79/2.038)$
$^4\Sigma^-(50/2.061)$
8
$^2\Delta(81/2.135)$
5
8
$^4\Delta(84/2.120)$
$^2\Delta(56/2.151)$
$^4\Delta(58/2.126)$
15
11
$^2\Pi(67/1.973)$
$^2\Pi(96/1.940)$
MCSCF
MCSCF + 1 + 2

Figure 33. Bond energy and Sc-C bond lengths of various states of $ScCH^+$ which dissociate to $Sc(^3D) + CH(^4\Sigma^-)$.

Comparison between Cr-C and C-C bonds

The structural predictions resulting from the various calculations on the different Cr-C bonded molecules, described in this study, are summarized in Table 2. We have included the results of the "bond only" CI calculation, $(MCSCF+1+2)^*$ for CrH^+, $CrCH_3{}^+$, and $CrCH_2{}^+$ to calibrate the effect of not correlating the triplet coupled electrons in $CrCH^+$. The data suggest that this omission results in the Cr-C bond being longer than the "fully" correlated calculation would predict. Figure 34 shows the calculated Cr-C bond lengths plotted vs. standard C-C single, double, and triple bond lengths. It seems likely that this remarkable correlation is somewhat fortuitous since we anticipate a slight reduction in the Cr-C bond length for $CrCH^+$ when the two open shell electrons are correlated at the same level as the bonding electrons. Nevertheless, the data support the characterizaton of $CrCH_3{}^+$, $CrCH_2{}^+$ $(^4B_1)$, and $CrCH^+$ $(^3\Sigma^-)$ as having a single, double, and triple bond between the metal and the carbon atoms. It is interesting and consistent that $CrCH_2{}^+$ $(^6B_1)$ has a metal-carbon bond length less than the sp^3 single bond in $CrCH_3{}^+$ but greater than the sp^2 double bond in $CrCH_2{}^+$ $(^4B_1)$. This sp^2 single bond should correlate with the bond length in the $(\pi-\pi^*)^3$ state of CH_2CH_2.

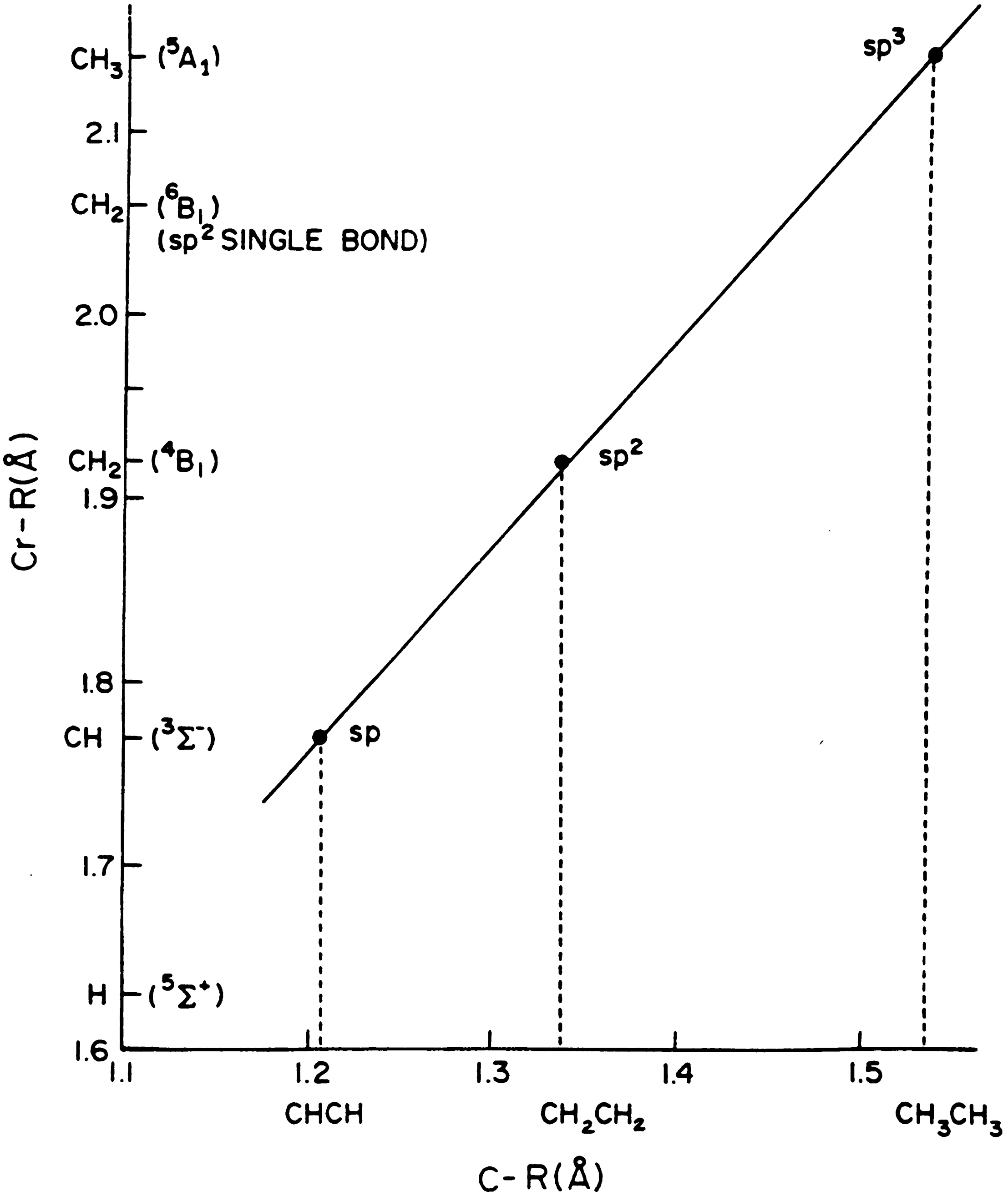

Figure 34. Correlation of predicted $(Cr-R)^+$ bond lengths with standard R-R bond lengths.

BONDING OF Sc^+ WITH H_2

Recently, the results of guided ion beam experiments have provided estimates of the ScH^+ bond energies (D°) of 54±2[1d] and 55±2[1g] kcal/mol and estimated that the D° for the process

$$ScH_2^+\ (^1A_1) \rightarrow ScH^+\ (^2\Delta) + H\ (^2S)$$

is either ≥50 kcal/mol[1d] or equal to 64±5 kcal/mol[1g]. Both experiments suggest that the second ScH bond is comparable in strength to the first and because the sum is greater than 104 kcal/mol predict that the reductive elimination of H_2 from ScH_2^+ will be endothermic.

We are especially interested in these results since a study of the electronic and geometric structure of ScH_2^+ would be a logical extension to our study of ScH^+, discussed in the previous section. Understanding the nature of the bonding structure in ScH_2^+ would allow us to gain some insight into multiple ligands bonded to one transition metal center and, thus, into the structure of possible isomers which could play a role in the chemistry of transition metal ions. The reported experimental results can be used as basis for comparison.

Results and Discussion

ScH_2^+ has four valence electrons and, if both hydrogens are independently bonded to Sc^+ (two ScH bonds as

opposed to a Sc-H_2 bond), the molecule must be a closed shell singlet. If we constrain ScH_2^+ to have C_{2v} symmetry and put it in the YZ plane with Sc at the origin and the Y axis as the C_2 axis, then the Ar core has the following representation

$$(\text{core})^2 = 1a_1^2\ 2a_1^2\ 3a_1^2\ 4a_1^2\ 5a_1^2\ 1b_2^2\ 2b_2^2\ 1b_1^2\ 2b_1^2$$

and the SCF configuration would be

$$|\ ^1A_1 > \sim (\text{core})^2\ 6a_1^2\ 3b_2^2\ \alpha\beta\alpha\beta$$

We represent the $^1A_1$ state of ScH_2^+ with an MCSCF function consisting of all $^1A_1$ CSF's which can be formed from the four valence electrons and four orbitals $6a_1$, $7a_1$, $3b_2$, and $4b_2$; thus, building in the ability to separate smoothly to the $[Sc^+(^1D) + H_2(^1\Sigma_g^+)]$ or $[ScH^+(^2\Sigma^+) + H(^2S)]$ products. We optimized the geometry of ScH_2^+ at this MCSCF level in both the spd and spdf basis sets. These results are collected in Table 6 along with our estimates of the harmonic vibrational frequencies. The harmonic frequencies were obtained by using force constants extracted from a least-squares fit of the ScH_2^+ energy to the bond length and bond angle. The grid was sparce, consisting of nine points encompassing the minimum with a ΔR and $\Delta\theta$ of 0.1au and 5°. We believe that the ScH_2^+ frequencies are high, perhaps by 10%.

A population analysis of the MCSCF wave function at

Table 6. Equilibrium Properties of ScH_2^+ in the Ground $^1A_1$ State Calculated with the **spd** and **spdf** Basis Sets Using the MCSCF and MCSCF+1+2 Functions.

	$ScH_2^+(^1A_1)$			
	MCSCF		MCSCF+1+2	
	spd	spdf	spd	spdf
E, au	−760.65948	−760.66406	−760.68426	−760.69935
R_e, Å	1.780	1.768	1.757	1.746
θ, deg	103.4	104.8	103.6	106.7
$\tilde{\nu}_{bend}$, cm^{-1}	478	491	460	489
$\tilde{\nu}_S$, cm^{-1}	1561	1712	1714	1734
$\tilde{\nu}_A$, cm^{-1}	1568	1722	1723	1745

the calculated equilibrium geometry allocates the four valence electrons as follows:

$$4s^{0.47}\ 4p_y^{0.05}\ 3d_{\sigma/\delta_+}^{0.23}\ 4p_z^{0.15}\ 3d_{yz}^{0.79}\ h_1^{1.15}\ h_2^{1.15}$$

Given the known deficiencies of the Mulliken population analysis[25] one should not make too much of the quantitative details of this distribution. The qualitative message, however, is clear. The bonding in ScH_2^+ is primarily due to the Sc 4s and $3d_{yz}$ orbitals hybridizing as

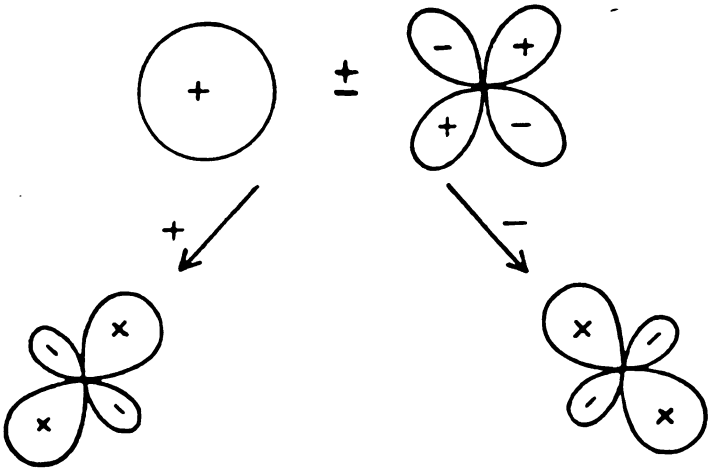

and then bonding to the incoming hydrogen atoms. This picture is consistent with the calculated valence angle of 106.7° and the large "d character" in the bond (a total of 1.02 3d electrons or 0.51 3d electron/bond) is consistent with the bond length in ScH_2^+ (1.745A) being shorter than any in the calculated states of ScH^+. The sdpf-CI function

predicts that ScH_2^+ is bound (D_e) by 106.4 kcal/mol relative to Sc^+ (^3D) and 2H (^2S). Since the ScH^+ ($^2\Delta$) D_e was calculated to be 54.7 kcal/mol, we conclude the D_e for the process

$$ScH_2^+\ (^1A_1) \rightarrow ScH^+\ (^2\Delta) + H\ (^2S)$$

is 51.7 kcal/mol. Using the calculated vibrational frequencies of ScH_2^+ and ScH^+, this D_e translates into a D° of 48.3 kcal/mol. Even if our calculated vibrational frequencies for ScH_2^+ were too high by 10% this D° would be increased by only 0.5 kcal/mol. There are two experimental values available for this dissociation energy: Tolbert and Beauchamp[1d] report $D° \geq 50$ kcal/mol while Armentrout et al.[1g] measure $D° = 64 \pm 5$ kcal/mol. In light of our success with the ScH^+ bond energy, the large discrepancy (~25%) between the calculated value of 48.3 kcal/mol and the measured value of 64 kcal/mol is disappointing.

In an attempt to understand the source of this discrepancy we carried out several additional calculations at the predicted equilibrium geometry. In particular we increased the number of active orbitals in the MCSCF (we used $6a_1$, $7a_1$, $8a_1$, $3b_2$, $4b_2$, $3b_1$, $1a_2$) to allow for correlation perpendicular to the molecular plane and increased flexibility in the "σ" system. While the resulting MCSCF energy was lowered by 6 milihartrees the MCSCF+1+2 was essentially unchanged from that reported in

Table 6.

From the summary of the calculated energetics shown in Figure 35 we anticipate that the reductive elimination of H_2 from ScH_2^+ will be endothermic. While the calculated endothermicity is only 2 kcal/mol we do expect our differential correlation error to favor the $^1A_1$ state of ScH_2^+, and thus, increase this calculated endothermicity. Since this calculated endothermicity is with respect to the spin forbidden process

$$ScH_2^+ \ (^1A_1) \rightarrow Sc^+ \ (^3D) + H_2 \ (^1\Sigma_g^+)$$

the spin-allowed process (in which Sc^+ is in the ^1D state)would be endothermic by at least 9 kcal/mol.

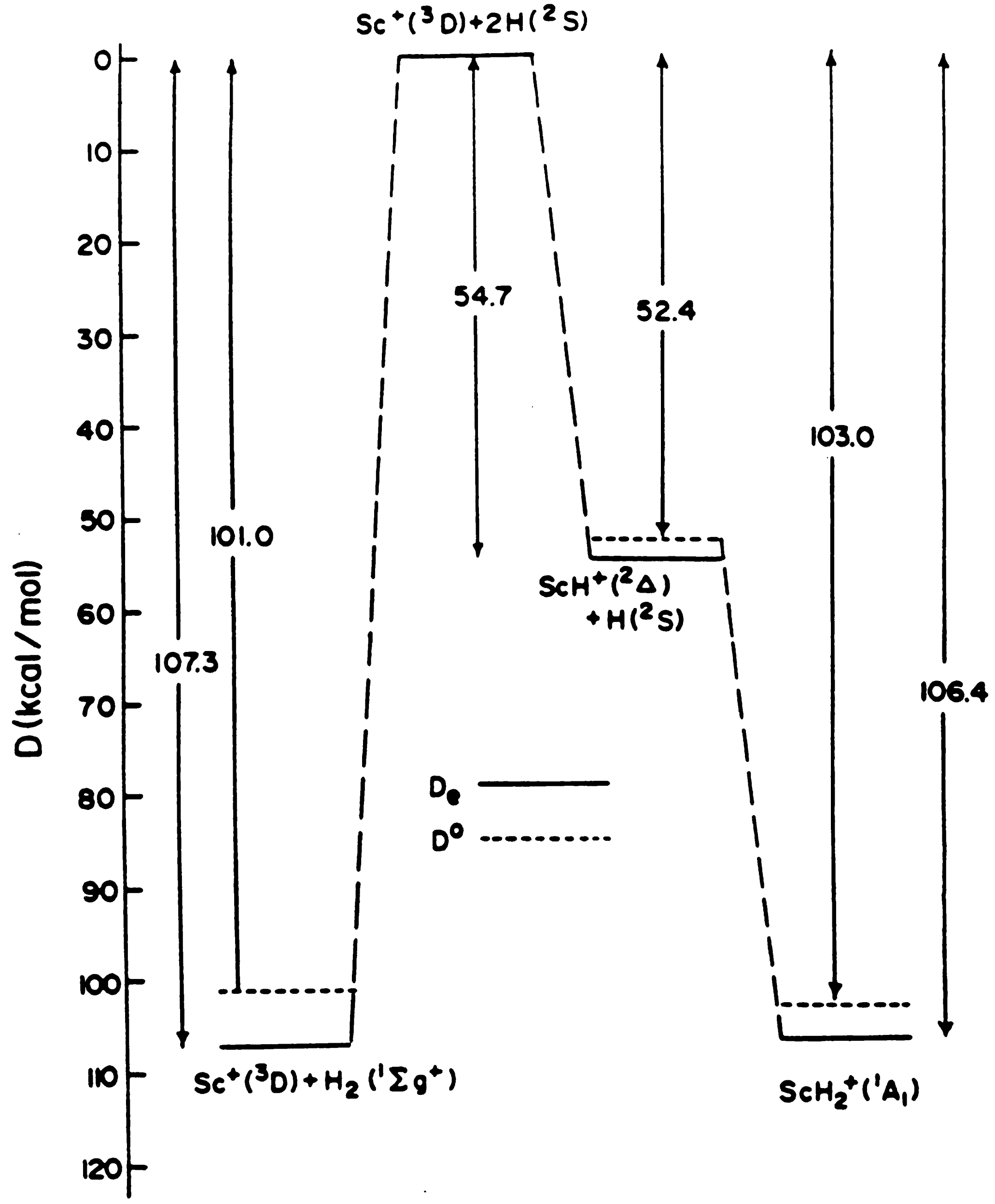
Sc⁺(³D)+2H(²S)
0
10
20
30
40
50
60
70
80
90
100
110
120
D(kcal/mol)
107.3
101.0
54.7
52.4
103.0
106.4
ScH⁺(²Δ)
+H(²S)
Dₑ
D⁰
Sc⁺(³D)+H₂(¹Σg⁺)
ScH₂⁺(¹A₁)

Figure 35. Computed dissociation energies of various combinations of Sc^+ and two H atoms relative to the separated ground state atoms. The dotted horizontal lines (D°) are the D_e's corrected for zero-point vibrational energy.

BONDING OF Cr^+ WITH Cl.

It has been shown that various first-row transition metal cations react exothermically with small alkanes while others do not. For example, Cr^+ does not react exothermically with small alkanes but Fe^+ does[3,32]. Recently, reactions of chloro-substituted Cr^+ with small hydrocarbons were found to be exothermic[32].

$$\mathrm{CrCl^+} \quad + \quad /\backslash/ \text{--->} \quad \mathrm{ClCrC_4H_8^+} \quad + \quad \mathrm{H_2}$$

This is an example of the chemical activation of an unreactive transition metal ion[32,33]. Another interesting aspect of these reactions is the fact that Cl remains "adhered" to Cr^+ throughout the reaction leading to the thought that Cl plays an active role in the overall exothermicity of this reaction.

In this study we are interested in the electronic and geometric structure of the low lying states of $CrCl^+$. Through the analysis of the molecular wavefunction we wish to develop a qualitative understanding of the nature of the chemical bond and gain insight into the role Cl plays in activating Cr^+.

A. Wavefunctions and Computational Details

Cl in the ^2P ground state has only one unpaired electron. If this electron approaches either a d_σ orbital in the ^6S state or a 4s orbital in the m=0 component of the ^6D state of Cr^+ then the resulting molecular state is a $^5\Sigma^+$.

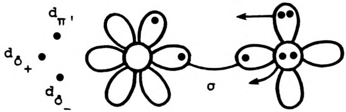

This is analogous to the bonding involved in CrH^+.

Suppressing the argon core of Cr and all but the 3p electrons on Cl, the $^5\Sigma^+$ state of $CrCl^+$ can be represented by the schematic (GVB)^{23} functional form

$$[\ \sigma\ p_\sigma + p_\sigma\ \sigma\ ]\ \ p_{\pi_x}^2\ p_{\pi_y}^2\ d_{\pi_x}^1\ d_{\pi_y}^1\ d_{\delta_+}^1\ d_{\delta_-}^1$$

where at large separation σ is a d_σ orbital from the ^6S state of Cr^+ and p_σ is a $3p_z$ orbital from Cl. All singly occupied d orbitals have α spin and the two electrons in the σ, p_σ orbital pair, as well as the doubly occupied p_π orbitals, are singlet coupled. A $CrCl^+$ wave function of this form, which dissociates to the correct Hartree-Fock products $[Cr^+(^6S) + Cl(^2P)]$, consists of 7 configuration state functions (CSF's)^{20} and will be referred to as MCSCF(7). The CI wave function, consisting of all single and double excitations from the 7 CSF reference space, contains 92,256 CSF's. This wave function is referred to as MCSCF(7)+1+2.

If instead a doubly occupied p orbital from Cl approached either a d_σ or a 4s orbital on Cr^+ then the resulting molecular state is a $^5\Pi$. This leaves the unpaired electron perpendicular to the "sigma" system available for pi-bonding with Cr^+.

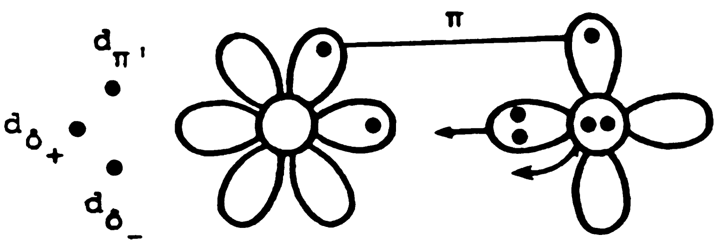

Whether this state is bound or not will depend to a large extent on the interaction of the three electrons in the sigma system and the extent of overlap of the pi "bonding" orbitals.

The wave function for the $^5\Pi$ state of $CrCl^+$ has the asymptotic functional form

$$[\, d_{\pi_y} \, p_{\pi_y} + p_{\pi_y} \, d_{\pi_y} \,] \; p_\sigma^2 \; p_{\pi_x}^2 \; d_\sigma^1 \; d_{\pi_x}^1 \; d_{\delta_+}^1 \; d_{\delta_-}^1$$

in which all singly occupied d orbitals have α spin and the two electrons in the $d_{\pi y}, p_{\pi y}$ orbital pair, as well as the doubly occupied $p_{\sigma,\pi}$ orbitals, are singlet coupled. In addition to all of the obvious spin couplings, all distributions of 3 electrons among both p_σ and d_σ orbitals are also included. The resulting wave function for the $^5\Pi$

state contains 14 CSF's (MCSCF(14)) and dissociates to the correct [$Cr^+(^6S)$ + $Cl(^2P)$] Hartree-Fock products. The corresponding CI wave function, MCSCF(14)+1+2, consists of 139,579 CSF's.

B. Energetics and Geometric Structure

The calculated dissociation energies and other geometric parameters obtained from the MCSCF and MCSCF+1+2 functions of the $^5\Sigma^+$ and $^5\Pi$ states of $CrCl^+$ are collected in Table 7. At equilibrium, the difference in energy between the $^5\Sigma^+$ and the $^5\Pi$ states of $CrCl^+$ is 8.2 kcal/mol at the MCSCF level and 5.4 kcal/mol at the MCSCF+1+2 level. The bond lengths of both states are essentially identical; in comparing with CrH^+, the bond length of CrH^+ is shorter by ~0.6Å while the bond in $CrCl^+$ is almost twice as strong.

C. Potential Energy Curves and Charge Distribution.

An analysis of the interaction of Cr^+ with Cl is necessary for the interpretation of the overall chemistry of the two low lying states of $CrCl^+$. The calculated potential energy curves for the $^5\Sigma^+$ and $^5\Pi$ states at the MCSCF and MCSCF+1+2 levels are shown in Figure 36. In Figures 37 and 38, we show the electron distribution of the valence orbitals more involved in bonding, as a function of internuclear distance for both states of $CrCl^+$. The occupations of

TABLE 7. Equilibrium Properties of $CrCl^+$ in the $^5\Sigma^+$ and the $^5\Pi$ States calculated using the MCSCF and MCSCF+1+2 Functions.

	$^5\Sigma^+$		$^5\Pi$	
	MCSCF	MCSCF+1+2	MCSCF	MCSCF+1+2
R_e, Å	2.21	2.19	2.20	2.17
D_e, kcal/mol	34.4	47.3	26.2	41.9
ω_e, cm^{-1}	456	475	463	481
CSF's	7	92,256	14	139,579
E, au	-1502.64287	-1502.78949	-1502.63015	-1502.78082

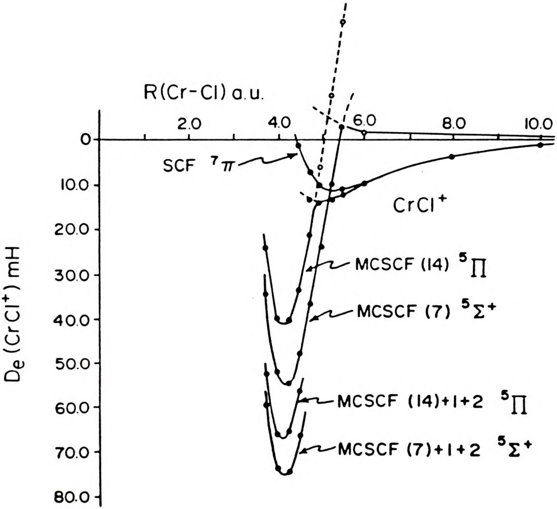

Figure 36. Potential energy curves for the lowest $^5\Sigma^+$, $^5\Pi$, and $^7\Pi$ states of $CrCl^+$.

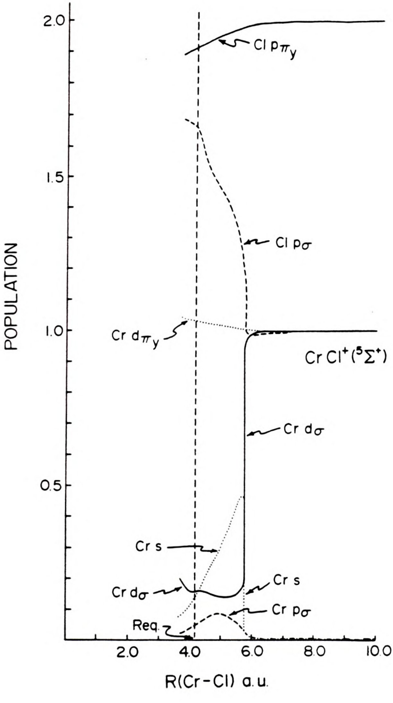

Figure 37. Electron population of selected atomic orbitals from the bonding natural orbitals of the 7 CSF MCSCF wavefunction of $^5\Sigma^+$ $CrCl^+$.

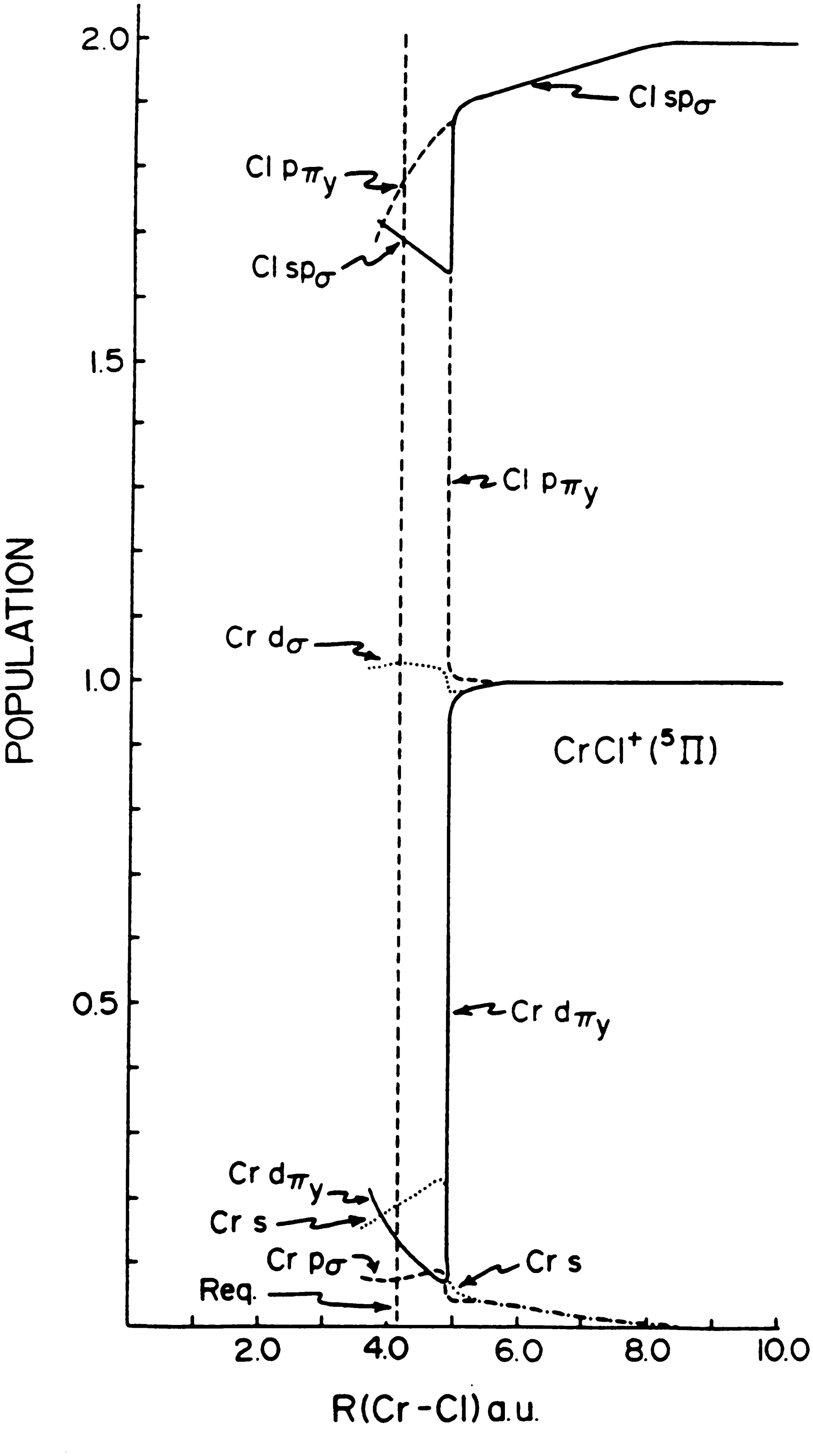

Figure 38. Electron population of selected atomic orbitals from the bonding natural orbitals of the 14 CSF MCSCF wavefunction of $^5\Pi$ CrCl$^+$.

the valence orbitals were obtained from a Mulliken analysis[25] of the natural orbitals of the MCSCF calculations.

By comparing Figures 36 and 3 (CrH^+), we can observe that for the $^5\Sigma^+$ state of $CrCl^+$, the interaction of the atomic fragments is initially repulsive but at around 6.00 au the energy drops, resulting in a D_e of 34.4/47.3 kcal/mol (MCSCF/MCSCF+1+2) relative to the asymptotic products. On the other hand, the initial interaction of Cr^+ and H is attractive but at ~4.00 au, the drop in energy is also abrupt leading to a dissociation energy of 18.5/25.1 kcal/mol (MCSCF/MCSCF+1+2).

The character of these potential energy curves can be understood by following the occupation of the valence orbitals found in Figures 37 and 5 for the $^5\Sigma^+$ states of $CrCl^+$ and CrH^+. At large internuclear separation, the d_σ orbital from Cr^+ and the p_σ orbital from Cl are singly occupied, and the $p_{\pi y}$ from Cl is doubly occupied. At less than 6.00 au, there is an abrupt change in the occupancy of the d_σ and 4s orbitals on Cr^+. This sudden exchange of "occupancy" (sharp decrease in d_σ and increase in 4s) is observed in CrH^+ and is due to the mixing of the ^6S and the ^6D states of Cr^+. This d_σ/4s exchange represents the initial reason for the observed discontinuity in the potential energy curves. In CrH^+ the d_σ occupancy proceeds to increase again while the 4s decreases until an almost 50-50 mixture of d_σ/4s at equilibrium. In $CrCl^+$, however, after the initial 4s,d_σ occupation exchange, the 4s occupancy drops, the d_σ remains essentially constant while p_σ on Cl increases from the asymptotic occupancy of 1.0 to the equilibrium value of 1.55. This is the main difference between $CrCl^+$ and CrH^+ ——the charge transfer from the Cr^+ 4s orbital to Cl. In the $CrCl^+$ case, this charge transfer also contributes to the discontinuity observed. From the population analysis, we infer that this charge transfer is a consequence of a higher $^5\Sigma^+$ state with the asymptotic products [$Cr^{++}(^5D) + Cl^-(^1S)$] intersecting the ground $^5\Sigma^+$ state with the lower energy asymptotic products [$Cr^+(^6S)$ + $Cl(^2P)$]. There is also an indication of "backbonding" (Cl → Cr) through the π orbitals. Therefore, at equilibrium, the overall charge distribution in the $^5\Sigma^+$ state is as follows:

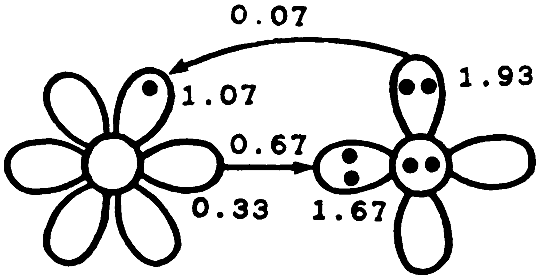

where the net charge transfer from Cr^+ to Cl is ~0.5 electrons.

In the $^5\Pi$ state of $CrCl^+$, as Cr^+ and Cl approach each other (Figure 36) the interaction is initially attractive. However, as in the $^5\Sigma^+$ case, this initial curve (solid curve) undergoes a sharp change in slope at ~5.00 au

resulting in a minimum of 26.2/41.9 kcal/mol (MCSCF/ MCSCF+1+2). The solid curve represents the minimum energy solution for the $^5\Pi$ state where the converged calculation at R=20.0 au is used as an initial estimate for subsequent calculations at smaller internuclear distances.

However, if one takes the converged solution of the $^5\Pi$ state at R=4.75 au as an initial estimate for R=5.00 au, one converges to a solution (dashed line with opened circles in Figure 37) leading to the asymptotic products [$Cr^{++}(^5D)$ + $Cl^-(^1S)$]. This interpretation is based on the population analysis shown in Figure 38.

In Figure 38, we can see that, at ~5.00 au, there is an abrupt transfer of 0.88 electrons from Cr^+ to Cl through the π orbitals (Cr $d_{\pi y}$ and Cl $p_{\pi y}$) giving the molecule considerable Cr^{++},Cl^- character at this point. Subsequently, there is a shift of electrons back to Cr through the π system ($\approx$0.1) and through the σ system. In the σ system there is a larger amount of backbonding (compared to $^5\Sigma^+$) from the "sp_σ" orbital in Cl to the 4s orbital in Cr^+ with little participation from the d_σ in Cr^+, i.e., very little 4s/d_σ mixing through the same mechanism seen in the $^5\Sigma^+$. Another way of thinking about this is that, in this case, the 4s has an alternate source of electrons other than d_σ and the three electrons in the "σ system" are distributed to avoid a greater repulsive interaction. Therefore, at equilibrium, the overall charge distribution in the $^5\Pi$ state is as follows:

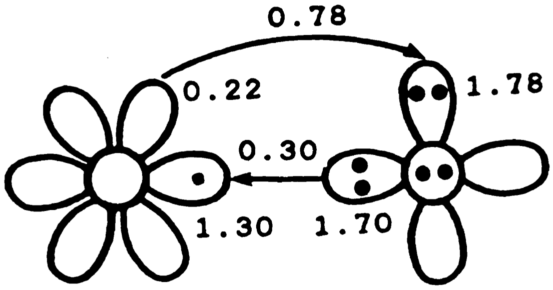

where the net charge transfer (Cr → Cl) for the lower energy minimum is ~0.5 electrons.

In order to form Cl^- in the $^5\Pi$ state of $CrCl^+$, we must have electron transfer from the d_π orbital of Cr^+ to the Cl p_π orbital. If the two electrons in the d,p-π_y orbitals of the $^5\Pi$ state were instead triplet coupled, we would then have the $^7\Pi$ state of $CrCl^+$. An SCF calculation was done for this state and its corresponding potential energy curve appears in Figure 37. The dissociation energy of this state is only 8.2 kcal/mol relative to the [$Cr^+(^6S)$ + $Cl(^2P)$] fragments. This much reduced D_e, relative to the $^5\Pi$ state, is a measure of the importance of the charge transfer in the $^5\Pi$ state which is now prohibited in the $^7\Pi$ state by the Pauli Principle. It is worth noting the similarities of this potential energy curve with that of the $^5\Pi$ state at distances greater than 5.00 au where no charge transfer has taken place in either state.

The large Cr^{++},Cl^- character in both the $^5\Sigma^+$ and $^5\Pi$ states suggests that the relative energies of these states may be interpreted with a ligand field model. Since the

Cr^{++} ion is a d^4 configuration and, therefore, a ^5D state we would expect the three components of the ^5D ($^5\Sigma^+$, $^5\Pi$, and $^5\Delta$) state to be split by the ligand field of Cl^- in the order $^5\Sigma^+ < {}^5\Pi < {}^5\Delta$ which is as observed for the $^5\Sigma^+$ and $^5\Pi$ states of $CrCl^+$. We have not calculated the $^5\Delta$ state of $CrCl^+$ but anticipate it will be somewhat higher in energy than the $^5\Pi$ state.

D. Long Range Interactions.

Both the $^5\Sigma^+$ and $^5\Pi$ states of $CrCl^+$ dissociate to the [$Cr^+(^6S) + Cl(^2P)$] products but, as Cr^+ approaches Cl, the interaction is quite different at long range. At very large distances, Cl views Cr^+ as a point charge. The energy of interaction was calculated for Cl in two ways. One, we will call the "Σ System" where the singly occupied valence orbital of Cl lies on the internuclear axis pointing towards the point charge.

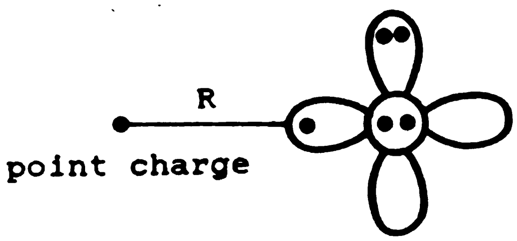

The other system is the "Π System" where a doubly occupied orbital is now in the direction of the point charge while

the singly occupied orbital is perpendicular to this.

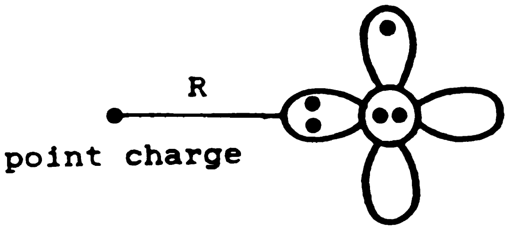

In general, the energy of interaction of an atom with a point charge can be express[34] as

$$E = E^{o} - \frac{1}{2} \alpha_{\alpha\beta} F_{\alpha} F_{\beta} - \frac{1}{3} \theta_{\alpha\beta} F'_{\alpha\beta}$$

where $\alpha_{\alpha\beta}$ is the polarizability tensor, $\theta_{\alpha\beta}$ is the quadrupole moment tensor of the system, and F_{α}, F_{β} and $F'_{\alpha\beta}$ are the electric field and the electric field gradient components generated by the point charge[34]. Considering the symmetry of the chlorine atom approaching a point charge, the energy expression is then

$$\Delta E_{\Sigma \text{ or } \Pi} = E(Cl,R) - E(Cl,0) = - \frac{\alpha_{zz}^{\Sigma \text{ or } \Pi}}{2R^4} + \frac{\theta_{zz}^{\Sigma \text{ or } \Pi}}{R^3}$$

where the first term on the far right is the charge-induced dipole interaction and the second term is the charge-quadrupole interaction.

The polarizability of the Σ system was calculated

to be α_{zz}^{Σ}=10.7 a.u. and the quadrupole moment as θ_{zz}^{Σ}=1.78 a.u. For the Π system, α_{zz}^{Π}=10.9 a.u. and θ_{zz}^{Π}=-0.89 a.u. The results for the charge-induced dipole interaction energy, the charge-quadrupole interaction energy, the combined interaction energy (ΔE_{Σ} and ΔE_{Π}) and the calculated ab initio large distance energies (for $CrCl^+$) are assembled in Table 8.

The $\Delta E_{\Sigma \text{ or } \Pi}$ values are comparable to the calculated ΔE values for the $^5\Sigma^+$ and the $^5\Pi$ states of $CrCl^+$ at large distances, with a 7-12% deviation at ~R=6.0 bohrs. As the chlorine atom approaches the point charge from large separations, the interaction energy becomes slightly repulsive for the "Σ System" (as in the $^5\Sigma^+$ state of $CrCl^+$) while the "Π System" is quite attractive (as in the $^5\Pi$ state of $CrCl^+$). This is a consequence of the change in sign of the quadrupole moment of Cl in the "Π System".

TABLE 8. Long Range Interaction Energies of a Chlorine Atom approaching a Point Charge.

"Σ"-System:

R, au	$-\alpha/2R^4$, mH	Θ/R^3, mH	ΔE_{Σ}, mH	ΔE_{calc}, mH
10.0	-0.54	1.78	1.24	1.24
8.0	-1.30	3.47	2.17	2.14
6.0	-4.13	8.23	4.10	3.65
"Π"-System:				
10.0	-0.54	-0.89	-1.43	-1.46
8.0	-1.33	-1.74	-3.07	-3.17
6.0	-4.21	-4.11	-8.32	-8.94

CONCLUSIONS:

COMPARISON BETWEEN THE Sc AND Cr COMPOUNDS

A. Transition Metal-Single Ligand Bonds

1. Bond Lengths and Orbital Composition

The preceding discussion suggests that CH_3, CH_2, and CH form single, double, and triple bonds, respectively, with Cr^+, and single, double, and double bonds with Sc^+. The calculated Cr-C and Sc-C bond lengths are consistent with this observation. The Sc^+ ion has only two valence electrons available for bonding, which explains the inability of $ScCH^+$ to host a triple bond. The correlation of the Cr-C bond lengths with the standard C-C bond lengths (Figure 34) is also consistent with the molecules containing a single, double, and triple bonds. In Figure 39, we summarize the structural and energetic results discussed for both Sc and Cr sets of compounds. The Sc-ligand bond lengths and bond energies are always larger than the corresponding Cr compounds. The large Sc-ligand bond length is a reflection of the larger ionic radius of Sc^+. Of course, the metal-CH bond is longer in $ScCH^+$ than in $CrCH^+$ because the former is a double bond while the latter is a triple bond.

Throughout our study of Cr^+ and Sc^+ compounds, we note the importance of the $4s,d_\sigma$ mixture in characterizing the electronic structure of transition metal-single ligand bonds. The ground state of the Cr^+ ion has a $3d^5$ electronic configuration while the ground state of Sc^+ has a 4s3d configuration. The Cr^+ $4s3d^4$ excited state is ~ 35

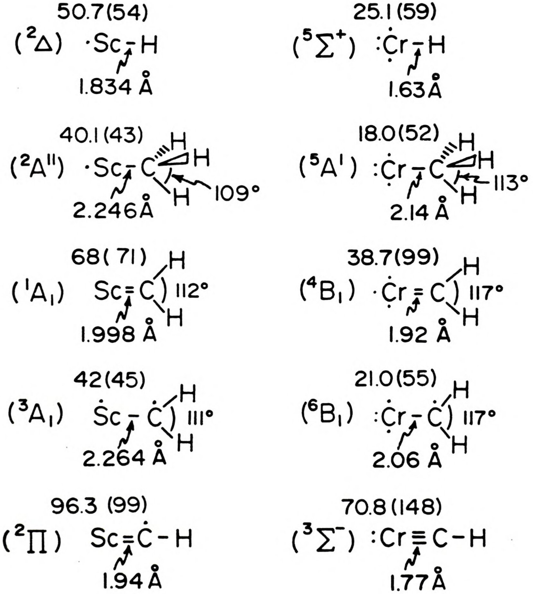
50.7(54)
(²Δ) ·Sc–H
1.834 Å
25.1(59)
(⁵Σ⁺) :Cr–H
1.63Å
40.1(43)
(²A'') ·Sc–C H H H
109°
2.246Å
18.0(52)
(⁵A') :Cr–C H H H
113°
2.14 Å
68(71)
(¹A₁) Sc=C H H
112°
1.998 Å
38.7(99)
(⁴B₁) ·Cr=C H H
117°
1.92 Å
42(45)
(³A₁) Sc–C H H
111°
2.264 Å
21.0(55)
(⁶B₁) :Cr–C H H
117°
2.06 Å
96.3 (99)
(²Π) Sc=C–H
1.94 Å
70.8(148)
(³Σ⁻) :Cr≡C–H
1.77Å

Figure 39. Comparison of the calculated bond energies and geometric parameters for various Sc and Cr compounds. Bond energies adjusted by the exchange energy loss in forming the TM-R bonds are in parenthesis.

kcal/mol[21] above the d^5 ground state and the Sc^+ $3d^2$ excited state is ~14 kcal/mol[21] above the sd ground state. At large internuclear separations from the incoming ligands, the σ electron in Cr^+ is essentially a pure d_σ orbital and, in Sc^+, a 4s orbital. As the metal approaches the ligand, we observed (by use of the potential energy curves and the population plots) how a higher root of the same molecular symmetry becomes lower in energy, to the point which, at equilibrium, a mixture of the "asymptotic" ground and excited molecular states is preferred. The effect of this interplay of low lying states differs for the two metals since Sc^+ has $3d_\sigma$ being mixed in with the 4s orbital and Cr^+ has the 4s mixed "into" the $3d_\sigma$, but we can see that these mixtures are more "gradual" when the ligand approaches Sc^+ than approaching Cr^+. The 4s orbital has a larger spatial extension than the 3d orbitals and, thus, is the first to feel the presence of the substituent. A mixture of the 4s, $3d_\sigma$, and $4p_\sigma$ orbitals allows for proper polarization of the localized molecular orbital on the metal towards the ligand.

In Table 9 we summarize, for both Sc^+ and Cr^+, the percentage of metal contribution to the σ bond and the percentage of 4s and $3d_\sigma$ character for comparison with the calculated bond lengths of the $TM{-}H^+$, $TM{-}CH_3{}^+$, $TM{-}CH_2{}^+$, and $TM{-}CH^+$ sequence. The percentage of the Cr d_σ orbital in the σ bond increases, the 4s character decreases, and the Cr-C bonds become more ionic as the bond order increases. Also, as the d_σ character increases the bond length becomes

TABLE 9. Comparison of the Transition Metal (TM) Contribution to the σ Bond, the Percentage of 4s and $3d_\sigma$ Orbital Character, and the Bond Lengths in Each of the Sc^+-C and Cr^+-C Bonds.

TM^+	Sc^+				Cr^+			
	% TM	% d_σ	% 4s	R_{TM-C}, Å	% TM	% d_σ	% 4s	R_{TM-C}, Å
TM^+-CH_3	38	36	54	2.25	47	46	48	2.14
TM^+-CH_2	35	62	32	2.00	43	64	29	1.92
TM^+-CH	25	57	30	1.94	36	70	23	1.77

shorter. A similar pattern emerges for the Sc analogs, but when the ligand changes from CH_2 to CH, the bond order does not increase but the extent of charge transfer does and the proportionalities of the 4s/d_σ mixture is adjusted accordingly. $ScCH^+$ is more ionic than $CrCH^+$ since the extra π backbonding is not possible.

The mechanism in which the excited sd^4 state of Cr^+ comes into play is, first, a previously pure d_σ orbital becomes an approximate 50/50 mixture of 4s and d_σ and, second, as the bond order increases, the Cr 4s decreases not only by a transfer "back" to the d_σ orbital but, also, by a (charge) transfer to the substituent (extent of which also increases as the bond order increases) making the relative %d_σ larger. This mechanism is not obvious from the electron distribution diagrams directly since the 4s,d_σ mixture occurs simultaneously with the charge transfer through the σ and π system.

From the discussion of the energetics and the population analysis of the low lying $^5\Sigma^+$ and $^5\Pi$ states of $CrCl^+$, the bonding in both states has large ionic character due to the charge transfer from Cr^+ to Cl. Also in both states, there are varying degrees of backbonding leading to an overall charge transfer of ~0.5 electrons. The $^5\Sigma^+$ and $^5\Pi$ roots, with the asymptotic products of [Cr^{++} (d^4) + Cl^- (^1S)], are low in energy (more so than any associated with [Cr^{++} + C^-]) and we are able to observe a more direct influence of these roots on the nature of the bond. These "ionic" excited states seem to be in strong competition with the $^5\Sigma^+$ and $^5\Pi$ states stemming from the excited state of Cr^+ (^6D,sd^4), as well as the states from the ground state products. In all TM^+-C systems discussed, we observed the usual 4s/d_σ mixture but, even during charge transfer, there is a decrease in the amount of 4s and an increase in d_σ (extent of which varied). In the $^5\Sigma^+$ state of $CrCl^+$, we can see an increase in 4s and a decrease in d_σ (Cr^+ sd^4 state mixing in) followed by a decrease in 4s while the $3d_\sigma$ remains constant (not observed in Cr^+-C or Sc^+-C). The $^5\Sigma^+$ "ionic" root took over the readjustment of the 4s/d_σ mixture. There is a charge transfer from the 4s orbital on Cr to Cl until the 4s occupancy reached the same as that of $3d_\sigma$. In this case, the 4s/d_σ becomes about 50/50, but the total number of electrons (in the σ bond) is much less than that of the Cr-C bonds. The total charge transfer is a combination of σ-donation (Cr→Cl) and π-backbonding (Cl→Cr).

In the $^5\Pi$ state of $CrCl^+$, the incoming p_σ orbital on Cl is already doubly occupied, therefore, charge transfer will not occur from Cr→Cl through the σ but through the π system. As for 4s/d_σ, the amount of 4s contributing to the σ bond is about the same as in the $^5\Sigma^+$ state but the "source of electrons" is not the d_σ electrons, rather, the p_σ orbital from Cl. The d_σ occupancy remains constant during this (Cl→Cr backbonding) charge transfer (as in the $^5\Sigma^+$ state).

The previous analysis was possible by the use of

electron distribution diagrams (population plots) where the the atomic orbital components of the σ (and π) molecular orbitals are monitored as a function of internuclear distance (from large to around equilibrium separations). Besides the disadvantages of not relying on the quantitative details[25] (exact values) of the occupations, an excellent qualitative picture is possible by examining the changes involved in the formation of the molecular system. Further comments on the $4s/d_\sigma$ mixture will be made by use of the exchange energy loss concept.

2. Exchange Energy Loss

It is interesting that although the Cr compounds have the shorter bonds they have the smaller bond energies. This is quite different from the familiar structure/energy systematics of molecules composed entirely of main group elements and reflects the importance of the Exchange Energy Loss concept in transition metal systems.

The exchange energy associated with the d electrons in the free Cr^+ ion (d^5 configuration) is given by

$$K\ (^6S) = \sum_{i>j}^{5} K_{ij}$$

i.e., the sum of 10 interactions between the five singly occupied d orbitals (d_σ, $d_{\pi x}$, $d_{\pi y}$, $d_{\delta+}$, and $d_{\delta-}$). If we estimate a Cr^+ d-d exchange integral as 17 kcal/mol, the exchange energy loss in forming one, two or three bonds is approximately 34, 60 and 77 kcal/mol. This is interpreted as the amount of energy Cr^+ must use to randomize the spins of its high spin coupled electrons in anticipation of forming one, two or three bonds using only d orbitals. The Sc^+ ion in the ^3D state requires 3 kcal/mol to prepare for either a single or double bond.

When the calculated D_e's are augmented by the estimated exchange energy loss, the numbers in parenthesis in Figure 39 are obtained. These very simple "corrections" result in "derived" bond energies which are more in line with conventional bond length/bond strength expectations. In particular, the $Cr{\equiv}CH^+$ derived bond strength is ~3 times as large as that of $Cr{-}CH_3{}^+$ and suitably larger than that of $Sc{=}CH^+$. While this simple model brings some order to the calculated bond strengths, it must be emphasized that the calculated, and not the "derived" bond energies, should be compared with experiments. Furthermore, the model is based on SCF concepts and presumes that the ground electronic configuration of the transition metal ion is dominant not only asymptotically, but also at R_e. This, clearly, is not the case as the various population analysis plots demonstrate. Nonetheless, we believe the model accounts in large measure for why the positive ions of the early transition series elements have such different D_e's for the same ligand[35].

An extension to the exchange energy model was presented by Carter and Goddard[9] to explain the relative amount of the 4s/d_σ mixture in the σ bond of $CrCH_2^+$ ($^4B_1$). We previously estimated the exchange energy loss in forming a double bond, is approximately 60 kcal/mol, if we only consider the Cr^+ (d^5) ion. If the exchange energy loss were calculated for the Cr^+ (sd^4) ion, it would take ~37 kcal/mol to form a double bond. The Cr^+ (sd^4) ion appears to be 23 kcal/mol more favorable towards forming a double bond, but the Cr^+ (sd^4) ion is approximately 24 kcal/mol (SCF) higher in energy than the ground state ion, thus, explaining the near 50/50 mixture of 4s,d_σ in the σ bond. A similar analysis can be performed for the triple bond, as well as the single bond. The exchange energy loss, incremented by the d^5-sd^4 excitation energy, needed in forming one, two, and three bonds is approximately 34, 61, and 79 kcal/mol. Under these terms, the Cr^+ (sd^4) ion is 0, 1, and 2 kcal/mol higher in energy than the Cr^+ (d^5) ion. For completion, one should include the relative Cr^{++} (d^4/sd^3) "excitation energies", keeping in mind that the actual amount of Cr^{++} character depends on the electronegativity of the substituent.

B. Transition Metal-Double Ligand Bonds

One of the motives that led us to study ScH_2^+ was to calculate the differential energy of removing one -H bond from ScH_2^+ and compare with our calculated values for ScH^+. We calculate that the second bond in ScH_2^+ is almost as strong as the first (a D_e of 51.7 vs. 54.7 kcal/mol) though not as strong as experiment suggests ($D° \geq 50^{1d}$ or equal to 65^{1g} kcal/mol). The equilibrium structure of the ground $^1A_1$ state of ScH_2^+ is nonlinear ($\theta = 106.7°$) with a bond length of 1.75A. This bond length is shorter than in any of the three ScH^+ states studied and reflects the larger d character in the ScH_2^+ bonds. Sc contributes to the bonds in ScH_2^+ via the $4s \pm 3d_{yz}$ hybrids which is consistent with the optimized H-Sc-H bond angle.

Through our analysis of the calculated energies we anticipate that the reductive elimination of H_2 from ScH_2^+ will be endothermic by ~9 kcal/mol. Preliminary results on the $^4B_2$ state of CrH_2^+ at the MCSCF level show that the bond strength of the second bond is ~7 kcal/mol, about 12.5 kcal/mol (MCSCF) weaker than the first CrH^+ bond. Therefore, the reductive elimination of H_2 from CrH_2^+ would exothermic by ~75 kcal/mol.

Further studies are necessary to show the effect of multiple ligands on the bond strengths of the individual bonds. We have shown the case of two ligands of the same kind. An interesting system to pursue would be the bonds in $CrClH^+$ and $CrClH_2^+$. As mentioned before, Cr^+ does not react exothermically with small alkanes* but $CrCl^+$ does*. If we were to compare (theoretically) the reactions of Cr^+ and $CrCl^+$ reacting with H_2 or CH_4, we would need to study the bond strengths of multiple-ligand systems in order to understand the effect Cl has on Cr^+ and/or its participation in the reaction mechanism so that the reaction would proceed exothermically.

LIST OF REFERENCES

LIST OF REFERENCES

1. a) R.R. Corderman and J.L. Beauchamp, J. Am. Chem. Soc., 98, 3998 (1976)

   b) P.B. Armentrout, L.F. Halle, and J.L. Beauchamp, J. Am. Chem. Soc., 103, 6501 (1981)

   c) L.F. Halle, P.B. Armentrout, and J.L. Beauchamp, J. Am. Chem. Soc., 103, 962 (1981)

   d) M.A. Tolbert and J.L. Beauchamp, J. Am. Chem. Soc., 106, 8117 (1984)

   e) N. Aristov and P.B. Armentrout, J. Am. Chem. Soc., 106, 4065 (1984)

   f) S.K. Huang and J. Allison, Organometallics, 2, 883 (1983)

   g) J.L. Elkind, N. Aristov, R. Georgiadis, L. Sunderlin, and P.B. Armentrout, private communication.

2. a) H.F. Schaefer III, Acc. Chem. Res., 10, 287 (1977) and references therein

   b) G.A. Somorjai, Chemical Society Reviews, 13, 321 (1984)

   c) G.C. Bond, "Catalysis by Metals", Academic Press, New York, 1962

   d) J. Sinfelt, Advan. Catalysis, 23, 91 (1973); Prog. in Solid State Chem., 10, 55 (1975)

   e) P. Biloen and W.M.H. Sachtler, Adv. in Catalysis, 30, 165 (1981)

   f) E. Murad, W. Swinder, S.W. Benson, Nature (London), 289, 273 (1981); E. Murad, J. Geophys. Res., 83, 5525 (1978)

3. J. Allison, "The Gas Phase Chemistry of Transition Metal Ions with Organic Molecules", to appear in Progress in Inorganic Chemistry, Vol. 34, 1984 and references therein

4. T.A. Lehman and M.M. Bursey, "Ion Cyclotron Resonance

Spectroscopy", John Wiley and Sons, Inc., New York, 1976

5. a) P.B. Armentrout, and J.L. Beauchamp, J. Am. Chem. Soc., 102, 1936 (1980)

   b) P.B. Armentrout, L.F. Halle, and J.L. Beauchamp, J. Chem. Phys., 76, 2449 (1982)

   c) R.V. Hodges, P.B. Armentrout, and J.L. Beauchamp, Int. J. Mass Spectrom. Ion Phys., 29, 375 (1979)

6. J. Muller, Angew. Chemie, 11, 653 (1972)

7. See Appendix A and references therein.

8. B.H. Botch, T.H. Dunning, Jr., and J.F. Harrison, J. Chem. Phys., 75, 3466 (1981); S.P. Walch and C.W. Bauschlicher, Jr., J. Chem. Phys., 78, 4597 (1983)

9. E.A. Carter and W.A. Goddard III, J. Phys. Chem., 88, 1485 (1984)

10. A.J.H. Wachters, J. Chem. Phys., 52, 1033 (1970)

11. T.H. Dunning, Jr., private communication.

12. P.J. Hay, J. Chem. Phys., 66, 4377 (1977)

13. R.C. Raffenetti, J. Chem. Phys., 58, 4452 (1973)

14. F.B. Duijneveldt, IBM Research Laboratory, San Jose, CA, 1971, IBM Technical Research Report No. RJ-945.

15. S. Huzinaga, J. Chem. Phys., 42, 1293 (1965)

16. S. Huzinaga, "Approximate Atomic Functions II", Research Report, Division of Theoretical Chemistry, Department of Chemistry, The University of Alberta, 1971

17. The ARGOS integral program was developed by R.M. Pitzer (Ohio State University).

18. The GVB164 program was written by R. Bair (Argonne National Laboratory).

19. A description of the UEXP program is given in: R. Shepard, J. Simons, I. Shavitt, J. Chem. Phys., 76, 543 (1982)

20. H. Lischka, R. Shepard, F.B. Brown, and I. Shavitt, Int. J. Quant. Chem. Symp., 15, 91 (1981)

21. C.E. Moore, Natl. Stand. Ref. Data Ser., Natl. Bur. Stand. No. 35.

22. J. Allison and D.P. Ridge, J. Am. Chem. Soc., 98, 7445 (1976)

23. a) W.A. Goddard,III, T.H. Dunning, Jr., W.J Hunt, P.J. Hay, Acc. Chem. Res., 6, 368 (1973)

b) W.A. Goddard,III and L.B. Harding, Annu. Rev. Phys. Chem., 29, 363 (1978)

24. The GVB bond orbitals were extracted from the MCSCF calculation by truncating the MCSCF expansion to the perfect pairing configurations, renormalizing, and using the MCSCF orbitals.

25. R.S. Mulliken, J. Chem. Phys., 23, 1833, 1841, 2338, and 2343 (1955). For a critique, see J.O. Noell, Inorg. Chem., 21, 11 (1982)

26. J. Pacansky, J. Phys. Chem., 86, 485 (1982)

27. B.J. Schilling, W.A. Goddard III, and J.L. Beauchamp, J. Am. Chem. Soc., 108, 582 (1986)

28. C.W. Bauschlicher, Jr., and S.P. Walch, J. Chem. Phys., 76, 4560 (1982)

29. M.A. Vincent, Y. Yoshioka, and H.F. Schaefer III, J. Phys. Chem., 86, 3905 (1982)

30. C.W. Bauschlicher, Jr., H.F. Schaefer III, and P.S. Bagus, J. Am. Chem. Soc., 99, 7106 (1977). This CH_2 ($^3B_1$) geometry is not optimal (see, for example, C.W. Bauschlicher, Jr., Chem. Phys. Lett., 74, 273 (1980)) but the energetic consequences of its use in constructing the $CrCH_2^+$ potential energy curves is negligible.

31. This CH distance was obtained by optimizing the energy of the $^4\Sigma^-$ state at the SCF level by using the C and H basis set used in the $CrCH^+$ calculation.

32. M.L. Mandich, M.L. Steigerwald and W.D. Reents, private communication.

33. J. Allison, private communication.

34. a) J.F. Harrison, "Chemistry 991 Lecture Notes", Department of Chemistry, Michigan State University
b) A.D. Buckingham, Adv. Chem. Phys., 12, 107 (1967)

35. This analysis was also used for the transition metal cation series which included Ti^+ and V^+ bonding to CH. See Appendix B.

APPENDIX A

APPENDIX A

ELECTRONIC STRUCTURE THEORY:
TECHNIQUES

INTRODUCTION

This appendix will include a general discussion of the techniques used to characterize the electronic structure of the various molecular systems described in this dissertation. Special emphasis will be given to the development of wavefunctions used in the calculations.

To study the electronic structure of molecules is to study the interaction of atoms brought close enough together to form a lower energy system, resulting in changes in the electron distribution (compared to that of separated atoms) due to the proximity of the nuclei in a molecule. To date, the fundamental equation that describes a system of this type is the time-independent Schroedinger equation,

$$H\Psi = E\Psi$$

where H is the Hamiltonian operator (in atomic units),

$$H = -\sum_{i=1}^{N}\frac{1}{2}\nabla_i^2 - \sum_{A=1}^{M}\frac{1}{2M_A}\nabla_A^2 - \sum_{i=1}^{N}\sum_{A=1}^{M}\frac{Z_A}{r_{iA}} + \sum_{i=1}^{N}\sum_{j>i}^{N}\frac{1}{r_{ij}} + \sum_{A=1}^{M}\sum_{B>A}^{M}\frac{Z_A Z_B}{R_{AB}}$$

(M_A is the mass ratio between nucleus A and an electron), Ψ is the wavefunction, and E is the total energy of the system. The solution to this equation has only been found exactly for atomic and molecular ensembles containing one electron. Therefore, one must rely on approximate solutions.

First of all, in the case of molecular systems, the Born-Oppenheimer approximation[1,2] allows the wavefunction, Ψ, to be separated into its nuclear and electronic components. This is based on the idea that nuclei are much heavier than electrons, so they move more slowly. At fixed nuclear positions one can then solve for the electronic Schroedinger equation,

$$H_e\Psi_e = E_e\Psi_e ,$$

where the electronic Hamiltonian is

$$H_e = -\sum_{i=1}^{N}\frac{1}{2}\nabla_i^2 - \sum_{i=1}^{N}\sum_{A=1}^{M}\frac{Z_A}{r_{iA}} + \sum_{i=1}^{N}\sum_{j>i}^{N}\frac{1}{r_{ij}} \qquad (1)$$

Ψ_e is the electronic wavefunction which describes the motion of the electrons but is dependent of the position of the

nuclei, as well as, those of the electrons. E_e is the electronic energy (also dependent on the position of the nuclei). What this means is that Ψ_e and E_e are different functions and values, respectively, at different spatial arrangements of the nuclei[1].

The total energy of the system, where the nuclear coordinates are fixed, is

$$E = E_e + \sum_{A=1}^{M} \sum_{B>A}^{M} \frac{Z_A Z_B}{R_{AB}} \qquad (2)$$

which includes the electronic energy and a constant nuclear repulsion. Since the total energy, E, is a function of R_{AB}, this function can define a potential surface as shown below:

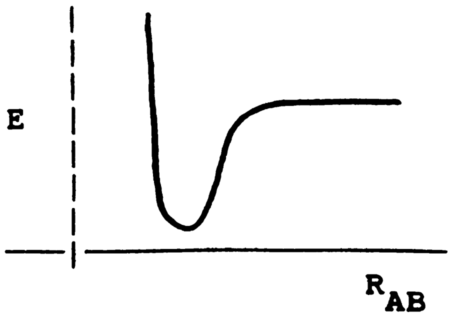

As mentioned before, one can now concentrate on the solution to the electronic Schroedinger equation, i.e, Ψ_e for a given H_e. The electronic Hamiltonian in Eq.(1) depends only on the spatial coordinates of the electrons and not on its spin. Therefore, we are using a non-relativistic Hamiltonian. Even though spin variables are not included in the Hamiltonian, the electronic wavefunction must meet the following requirement:

> "A many-electron wavefunction must be antisymmetric with respect to interchange of the coordinate x (both space and spin) of any two electrons,
>
> $$\Psi(x_1,\ldots\ldots,x_i,\ldots\ldots,x_j,\ldots\ldots,x_N) = -\Psi(x_1,\ldots\ldots,x_j,\ldots\ldots,x_i,\ldots\ldots,x_N)."$$ [1]

This is known as the Pauli Exclusion Principle. The subcript "e" is to be implied when discussing the electronic wavefunction.

There has been intense theoretical research in the construction of electronic wavefunctions to describe the energetic and spatial distribution of electrons in atoms and molecules. The most reliable techniques of approximation are the non-empirical or ab initio methods[1-7], i.e., empirical data is not used in the calculation. Most of these techniques are based on the Variational Principle:

> "Given a normalized wavefunction $|\Psi\rangle$ that satifies the appropriate boundary conditions (usually $\Psi(\infty)=0$), then the expectation value of the Hamiltonian is an upper bound to the exact ground state energy, i.e.,
>
> $$\langle\Psi|H|\Psi\rangle \geq E_0 \quad ."$$ [1]

The reliability of the solution depends on the choices made in the construction of Ψ which should not be oversimplified.

DEVELOPMENT OF WAVEFUNCTIONS

An arbitrary function can be expanded in terms of known functions that form a complete set. For example, the wavefunction Ψ for a one electron system can be expanded in a linear combination of the one-electron functions, Φ_i :

$$\Psi(\underset{\sim}{q}) = \sum_{i=1}^{\infty} \Phi_i(\underset{\sim}{q})\ C_i$$

(weighed by the coefficients C_i) where these Φ_i's form a complete set: $\{\Phi_i\}_{i=1}^{\infty}$, and are linearly independent.

For a many-electron function,

$$\Psi(\underset{\sim}{q}_1,\underset{\sim}{q}_2,\ldots,\underset{\sim}{q}_N) =$$

$$\sum_{i=1}^{\infty} \sum_{j=1}^{\infty} \ldots \sum_{n=1}^{\infty} C_i C_j \ldots C_n\ \Phi_i(\underset{\sim}{q}_1)\ \Phi_j(\underset{\sim}{q}_2)\ \ldots \Phi_n(\underset{\sim}{q}_N)$$

where for each term we have a product of one-electron functions. This function must satisfy the Pauli Principle. To see this, let us consider the two-electron case:

$$\Psi(\underset{\sim}{q}_1,\underset{\sim}{q}_2) = \sum_{i,j} C_i C_j\ \Phi_i(\underset{\sim}{q}_1)\ \Phi_j(\underset{\sim}{q}_2)$$

Since the wavefunction is antisymmetric with respect to electron interchange, we may write:

$$\Psi(\underset{\sim}{q}_1,\underset{\sim}{q}_2) = \sum_{i,j} 2^{-1/2}\, B_i B_j \left[\!\left[\Phi_i(\underset{\sim}{q}_1)\, \Phi_j(\underset{\sim}{q}_2) - \Phi_i(\underset{\sim}{q}_2)\, \Phi_j(\underset{\sim}{q}_1) \right]\!\right]$$

This can be rewritten as a determinant:

$$\Psi(\underset{\sim}{q}_1,\underset{\sim}{q}_2) = \sum_{i,j} 2^{-1/2}\, B_i B_j \begin{vmatrix} \Phi_i(\underset{\sim}{q}_1) & \Phi_j(\underset{\sim}{q}_1) \\ \Phi_i(\underset{\sim}{q}_2) & \Phi_j(\underset{\sim}{q}_2) \end{vmatrix}$$

$$= \sum_{i,j} B_i B_j\, \mathcal{A} \left[\Phi_i(\underset{\sim}{q}_1)\, \Phi_j(\underset{\sim}{q}_2) \right]$$

where $\mathcal{A}$ is an antisymmetrization operator[2] which insures that the one-electron function product in the brackets, "[]", will be expressed in a Slater determinant (as the one shown previously) which in turn insures that the overall wavefunction, Ψ, will be antisymmetric with respect to electron interchange. This analysis is easily extended to N-electron systems.

In the Hartree-Fock (HF) approximation for a molecular system, the wavefunction Ψ is expressed as

$$\Psi(\underset{\sim}{q}_1,\underset{\sim}{q}_2,\ldots,\underset{\sim}{q}_N) = \mathcal{A} \left[\Phi_1(\underset{\sim}{q}_1)\Phi_2(\underset{\sim}{q}_2)\cdots\Phi_N(\underset{\sim}{q}_N) \right] \qquad (3)$$

where Φ_i's are molecular (spin-) orbitals occupied by the i^{th} electron. There are no sums in this expression, i.e., this wavefunction is based on one configuration (one "product" arrangement of one orbital per electron). This is called a Hartree product. When a configuration (single determinent) is expressed in brackets, only those orbitals that are occupied will be included; the rest of the orbitals, Φ_j, in the complete set will be excluded (these are then known as virtual orbitals).

Before we get into the choices of Φ_i's which will be a part of the configuration, we should realize that an orbital is a wavefunction that describes a single particle; in this case, an electron. Since an electron has an intrinsic spin, the wavefunction to describe the electron must include a component that will take the spin into account. This would give us a spinorbital:

$$\Phi(\underset{\sim}{g}) = \begin{cases} \Phi(\underset{\sim}{r})\ \alpha(\omega) \\ \quad \text{or} \\ \Phi(\underset{\sim}{r})\ \beta(\omega) \end{cases}$$

where $\underset{\sim}{r}$ are the spatial coordinates and, $\alpha(\omega)$ and $\beta(\omega)$ are two orthogonal spin functions, i.e., spin up or spin down. When we are concerned with molecular orbitals, the nature of the functions $\Phi(\underset{\sim}{r})$ is dependent on the molecular environment. A general technique in constructing molecular orbitals is to expand them in terms of known basis functions which are characteristic of the atoms in the molecule:

$$\Phi_i(\underset{\sim}{r}) = \sum_{\mu=1}^{\infty} C_{\mu i}\chi_\mu(\underset{\sim}{r})$$

For the equality to hold, these known basis functions, χ_μ, should form a complete set. To avoid computational difficulties, Gaussian Basis Sets[3] are generally used in calculations of molecular systems. This technique (using atomic basis functions) is the Linear Combination of Atomic Orbitals (LCAO). In summary, the electrons in a molecule occupy the molecular orbitals which are composed of combinations of atomic orbitals.

Returning to the Hartree-Fock approximation, the Hartree-Fock wavefunction, Ψ_{HF}, is the best single determinent wave function composed of orbitals, Φ_i, in Eq. (3), which gives the lowest possible value for the expectation value of the energy (Variational Principle)[2]. This energy is the Hartree-Fock energy, E_{HF}. It is unlikely that the orbital functions, Φ_i, can be practically expressed by a complete set of basis functions. By use of a finite set of basis functions, the best single determinant wavefunction (where the coefficients $C_{\mu i}$'s are optimally determined) is the Self-Consistent-Field (SCF) wavefunction[2]. As the expansion length reaches infinity (complete set), the SCF energy and wavefunction approaches the Hartree-Fock limit.

To further understand how an SCF wave function is obtined, let us reacquaint ourselves with the Variational Principle. The spin orbitals in a Slater determinent are usually taken to be orthogonal to each other,

$$\langle \phi_i | \phi_j \rangle = \delta_{ij} = \begin{matrix} 0 & \text{if } i \neq j \\ 1 & \text{if } i = j \end{matrix}$$

since this allows the energy expression of a single determinent (1-D) wavefunction to be written in the following simple way:

$$E_{1-D} = \langle \Psi_{1-D} | \ H \ | \Psi_{1-D} \rangle = \sum_{i=1}^{N} \langle \phi_i | \ - \frac{1}{2} \nabla_i^2 - \sum_{A=1}^{M} \frac{Z_A}{r_{iA}} \ | \phi_i \rangle$$

$$+ \sum_{i<1}^{N} \left[\!\left[\langle \phi_i \phi_j | \ \frac{1}{r_{ij}} \ | \phi_i \phi_j \rangle - \langle \phi_i \phi_j | \ \frac{1}{r_{ij}} \ | \phi_j \phi_i \rangle \right]\!\right]$$

by use of the non-relativistic Hamiltonian described in Eq. (1). The integrals, < | | >, are divided into one-electron integrals and two-electron integrals. The two-electron integrals have implied a specific electron, ( ), order:

$$\langle \phi_i \phi_j | \ \ldots \ | \phi_i \phi_j \rangle \rightarrow \langle \phi_i(1) \phi_j(2) | \ \ldots \ | \phi_i(1) \phi_j(2) \rangle$$

$$\langle \phi_i \phi_j | \ \ldots \ | \phi_j \phi_i \rangle \rightarrow \langle \phi_i(1) \phi_j(2) | \ \ldots \ | \phi_j(1) \phi_i(2) \rangle$$

Through this convention only the orbital indices are needed and the electron order is understood. The following is a simplified notation of the previous energy equation:

$$E = \sum_{i} \langle \ i \ | \ i \ \rangle + \sum_{i<j} \left[\!\left[\langle \ ij \ | \ ij \ \rangle - \langle \ ij \ | \ ji \ \rangle \right]\!\right]$$

The first two-electron integral is known as a Coulomb integral, < ij | ij >. The second is an Exchange integral, < ij | ji >, because this integral shows the effect of the

interchange of two electrons in orbitals Φ_i and Φ_j (a consequence of the wave function satisfying the Pauli Principle).

To obtain a Self-Consistent-Field (SCF) wave function, a single determinant of 1-electron orbitals is optimized so as to minimize the total energy,

$$\frac{\partial E}{\partial C_{\mu i}} = 0$$

where the coefficients are variationally determined via the Roothaan equations[1] which simplifies the spatial integro-differential equation,

$$f(\underset{\sim}{r}_1)\ \Psi_i(\underset{\sim}{r}_1) = \varepsilon_i\ \Psi_i(\underset{\sim}{r}_1) \qquad ,$$

(f is the Hartree Fock operator) to a single matrix equation

$$\mathbf{F}\ \mathbf{C} = \mathbf{S}\ \mathbf{C}\ \boldsymbol{\varepsilon}$$

which, in turn, can be solved by standard matrix techniques.

In the past two decades many electronic structure calculations were successful with the use of an SCF wave function[1,2]. The systems studied were mainly composed of main-group elements. As molecules of interest became more complicated (for example, transition metal-containing systems where correlation effects had not been addressed), solutions of more than one determinant were needed. We have

seen before that the overall molecular wavefunction, Ψ, can be expanded by a linear combination of all possible arrangements of Φ's (configurations), but for practical purposes, this too, must be limited to a finite expansion. The best possible solution (lowest energy) under these conditions is obtained by optimally determining the coefficients of each configuration. The selection of which configurations are included in this finite expansion merits extreme care. There are two types of expansions which will be discussed here: Multi-Configuration-SCF (MCSCF) and Configuration Interaction (CI) wavefunctions. Variations of each of these wavefunctions will also be considered.

A complete expansion for an N-electron system in terms of Slater determinants has the form:

$$\Psi = \sum_{i,j,\ldots n} C_{i,j,\ldots,n} \mathcal{A} \left[\Phi_i(\underset{\sim}{q}_1)\, \Phi_j(\underset{\sim}{q}_2) \ldots \Phi_n(\underset{\sim}{q}_N) \right]$$

and the individual one-electron orbitals have the expansion:

$$\Phi_i(\underset{\sim}{r}) = \sum_{\mu} C_{i\mu}\, \chi_{\mu}(\underset{\sim}{r})$$

This is approximate because the expansion is finite. When only the coefficients of the configurations are optimized variationally then we have a Configuration Interaction (CI) wavefunction[4]. If both the coefficients of the configurations and the orbitals are optimized, we have a Multi-Configuration-SCF (MCSCF) wavefunction[5]. The determination of these optimized functions is an immense task. Since large expansions of each of these wavefunctions can lead to computational difficulties, one attempts to choose only those configurations and basis functions expected to be of importance to the overall structure of the system.

The above molecular wave function is often written as,

$$\Psi = \sum_{\nu=0}^{n} C_\nu \Phi_\nu \qquad \text{where} \quad \Phi_\nu = \mathcal{A}\,[\phi_i \phi_j \ldots \phi_n]$$

i.e., Ψ is a linear combination of Slater determinents, Φ_ν. Φ_0 is taken as the SCF function and higher order Φ_ν's are configurations which represent electron excitations (single excitations, double excitations, ..., etc.) from the SCF configuration.

One of the main disadvantages of using an SCF wavefunction is its inability to properly describe the dissociation process of a molecule into its atomic fragments. In a diatomic molecule with a simple single bond, the dissociation into the homolytic components is not possible with this wavefunction, leading to large errors in calculated dissociation energies. This is an example where additional correlation is needed. Take a hypothetical diatomic system with only a single bond, A-B. A single bond is commonly described by a doubly occupied molecular orbital, e.g. σ_g^2, while other electrons in the system are placed in what we will consider as core orbitals. Core orbitals are usually considered as doubly occupied ("inner-shell") orbitals not involved in the overall chemistry of the molecular system. Designations of types of orbitals vary according to what is sought in a molecular study. For example, in our study of dilithiomethane, CH_2Li_2, we are interested in the interaction of carbon with the two lithium atoms and the C-H bonding orbitals were taken as core orbitals.

According to the SCF description, as the distance between atoms A and B increases ($R \rightarrow \infty$), the doubly occupied σ_g^2 (which was shared among A and B at the equilibrium distance, $\sigma_g^2 \approx (\sigma_A + \sigma_B)^2$) can then be centered on atom A ($\sigma_g^2 \rightarrow \sigma_A^2$), on atom B ($\sigma_g^2 \rightarrow \sigma_B^2$), and on both A and B ($\sigma_g^2 \rightarrow \sigma_A\sigma_B$). If the proper description of the fragments requires an equal splitting of the two electrons among atoms A and B (with no ionic terms), then the SCF energy will be too high. Suppose we included another configuration where the two electrons in σ_g are "excited" in an orthogonal antibonding orbital, e.g. σ_u.

$$\Psi_{MCSCF} \approx C_0 \mathcal{A} \mid (\text{core})^2 \sigma_g^2 \alpha\beta > + C_1 \mathcal{A} \mid (\text{core})^2 \sigma_u^2 \alpha\beta >$$

The coefficients, C_i's, and all orbitals are optimized in this 2X2 MCSCF wavefunction and when rewritten as follows:

$$\Psi_{MCSCF} \approx C_0 \mathcal{A} \mid (\text{core})^2 [\, \sigma_g^2 - \lambda\, \sigma_u^2 \,]\, \alpha\beta >$$

$$\text{where} \qquad \lambda = - \frac{C_1}{C_0}$$

the extent by which the two configurations "mix" is monitored by the parameter λ. Orbitals σ_g and σ_u can be combined to form two localized orbitals:

$$\zeta_+ = \sqrt{\frac{1 + S}{2}} \mid \sigma_g > + \sqrt{\frac{1 - S}{2}} \mid \sigma_u >$$

$$\zeta_- = \sqrt{\frac{1 + S}{2}} \mid \sigma_g > - \sqrt{\frac{1 - S}{2}} \mid \sigma_u >$$

$$\text{where} \quad S = < \zeta_+ \mid \zeta_- > = \frac{1 - \lambda}{1 + \lambda}$$

These localized ζ_+, ζ_- orbitals are known as Generalized Valence Bond (GVB)[6] orbitals. They are non-orthogonal to each other but the orbitals as a pair are orthogonal to other orbitals in the system. Since ζ_+ and ζ_- are non-orthogonal to each other, the integral $< \zeta_+ \mid \zeta_- >$ is non-zero and the resulting value, S, is called the overlap of these two orbitals. Note the transformation between the (natural) molecular orbitals and the localized GVB orbitals:

$$(\, \sigma_g^2 - \lambda\, \sigma_u^2 \,)\, \alpha\beta \implies (\, \zeta_+ \zeta_- + \zeta_- \zeta_+)\, (\alpha\beta - \beta\alpha)$$

Note the similarities of the GVB expression to what we know as the Valence Bond model. The GVB orbitals as a pair are optimized as are the rest of the orbitals. One observation to keep in mind: λ monitors the "need" for the extra configuration in the wavefunction, i.e., if at the molecular level, σ_u plays a small role, λ is small; if at $R=\infty$, σ_u is equally important, then $\lambda=+1$.

The GVB (2X2 MCSCF) wavefunction behaves properly at all distances if the spin states of the individual fragments lead to doublet states. For example, H_2 separates correctly to a ^2S spin state for each hydrogen atom. This is not the case for fragments with open shell electrons having a total spin more than 1/2 (doublet state). The GVB (2X2 MCSCF) wavefunction can not satisfactorily separate, e.g. a C-H ($^2\Pi$) radical to the low energy ^3P carbon and ^2S hydrogen atoms. To insure that the separated fragments have the proper spin states, extra configurations are added (spin eigenfunctions) resulting in a Spin-Optimized GVB (SOGVB) wavefunction.

In Figure 1, we have an example of a Spin Eigenfunction Branching Diagram where the number of linearly independent spin eigenfunctions is determined by the number of unpaired electrons and the overall multiplicity of the molecular system. Beyond the 2-configuration MCSCF (GVB) wavefunction needed to break the bond, we need to include 2 more configurations for a wavefunction (SOGVB) that can partition the C-H molecule in a $^2\Pi$ state to the correct ^3P carbon and ^2S hydrogen spin states (two unpaired electrons on C and one unpaired electron on H gives a total of 3

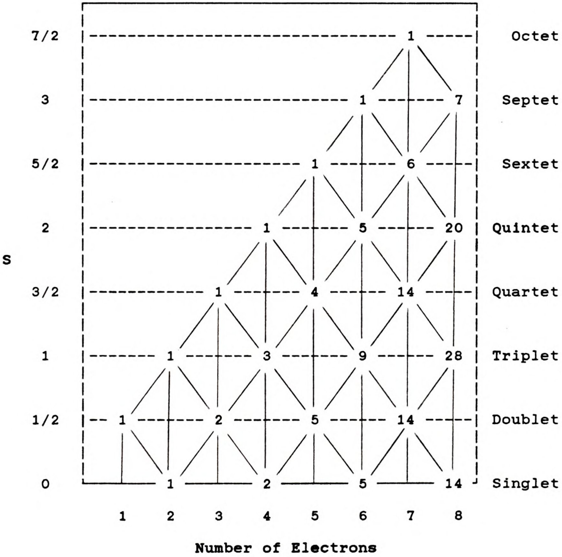
7/2
3
5/2
2
S
3/2
1
1/2
0
Octet
Septet
Sextet
Quintet
Quartet
Triplet
Doublet
Singlet
1
1 7
1 6
1 5 20
1 4 14
1 3 9 28
1 2 5 14
1 2 5 14
1 2 3 4 5 6 7 8
Number of Electrons

Figure 1. Spin Eigenfunction Branching Diagram
Number of linearly independent spin eigenfunctions one can form from a given allotment of electrons. S is the total spin and the corresponding multiplicity is on the right hand side.

unpaired electrons for the separated system which needs to be coupled for an overall doublet state). The SOGVB wavefunction adjusts spin recouplings upon fragment separation.

All molecular systems under study in this dissertation were done by the use of an MCSCF (SOGVB) wave function. This function is then used as an initial estimate for further extensive CI studies. The analysis for the construction of a wavefunction describing multiple bonding follows the same procedure (and requirements) as the single bonded systems which, in addition to higher levels of correlation beyond those addressed here, will be discussed in the main text.

As mentioned before, only the coefficients of the configuration expansion are optimized in a CI function; not the coefficients for the basis functions used for defining the orbitals. Generally, the procedure for constructing CI functions is by using an optimized SCF orbital set and expand the function with configurations which represent all possible excitations from the valence orbitals of this set. This is considered a Full (Valence Electron) CI. Excitations from the core orbitals are not considered (i.e., kept "frozen").

Of the many levels of excitations (single, double, triple, ..., etc.), single and double excitations account for ~90% of the correlation needed to improve the SCF wavefunction for many molecular systems. A CI wavefunction consisting of single and double excitations from an SCF

valence reference space is called an SCF+1+2 wavefunction. The electrons in the optimized (SCF) orbitals are excited into unoccupied virtual orbitals. Calculations done by this method are far better (lower energy) than a simple SCF wavefunction[4], but unfortunately this wavefunction is still not size consistent[1], i.e., the energy of the molecule when the fragments are far apart is not the sum of the energies of the individual fragments.

An appropriate extension to this SCF+1+2 (CI) wavefunction is a wavefunction based on single and double excitations from an optimized MCSCF valence orbital reference space: MCSCF+1+2. As discussed previously, the MCSCF function by which this CI function is based on, allows for proper dissociation of the system (with the proper spin characteristics). This type of wavefunction is used in our studies and has the important characteristic of being, essentially, size consistent.

LIST OF REFERENCES

LIST OF REFERENCES

1. A. Szabo and N.S. Ostlund, "Modern Quantum Chemistry: Introduction to Advanced Electronic Structure Theory", Macmillan Pub. Co., Inc., New York, N.Y., 1982.

2. H.F. Schaefer III, "The Electronic Structure of Atoms and Molecules", Addison-Wesley Pub. Co., Reading, Mass., 1972.

3. T.H. Dunning, Jr. and P.J. Hay, "Gaussian Basis Sets for Molecular Calculations" in "Methods of Electronic Structure Theory", edited by H.F. Schaefer III, Plenum Press, New York, 1977, p.1.

4. I. Shavitt, "The Method of Configuration Interaction" in "Methods of Electronic Structure Theory", edited by H.F. Schaefer III, Plenum Press, New York, 1977, p.189.

5. a) A.C. Wahl and G. Das, "The Configuration Self-Consistent Field Method" in "Methods of Electronic Structure Theory", edited by H.F. Schaefer III, Plenum Press, New York, 1977, p.51.

   b) R. Shepard, "The MCSCF Method" to appear in Advances in Chemical Physics, "Ab Initio Methods in Quantum Chemistry", edited by K. Lawley, 1986.

   c) T.H. Dunning, Jr., "Multiconfiguration Wavefunction for Molecules: Current Approaches" in "Advanced Theories and Computational Approaches to the Electronic Structure of Molecules", edited by C.E. Dykstra, Reidel Pub. Co., 1984, p.67.

6. a) F.W. Bobrowicz and W.A. Goddard III, "The Self-Consistent Field Equations for Generalized Valence Bond and Open-Shell Hartree-Fock Wave Functions" in in "Methods of Electronic Structure Theory", edited by H.F. Schaefer III, Plenum Press, New York, 1977, p.79.

   b) W.A. Goddard III, T.H.Dunning, Jr., W.J. Hunt, P.J. Hay, J. Acc. Chem. Res., 6, 368 (1973).

   c) W.A. Goddard III and L.B. Harding, Ann. Rev. Phys. Chem., 29, 363 (1978).

7. Discussions with J.F. Harrison.

APPENDIX B

APPENDIX B

LISTING OF PUBLICATIONS

Included here is a listing of the publications resulting from this dissertation:

1. "The Bonding, Dipole Moment, and Charge Distribution in the Lowest Singlet and Triplet States of CH_2Li_2." Aileen E. Alvarado-Swaisgood and James F. Harrison, J. Phys. Chem., 1985, 89, 62.

2. "Electronic and Geometric Structures of the Chromium Cations CrH^+, $CrCH_3^+$, $CrCH_2^+$, and $CrCH^+$." Aileen E. Alvarado-Swaisgood, John Allison, and James F. Harrison, J. Phys. Chem., 1985, 89, 2517.

3. "Electronic and Geometric Structures of ScH^+ and ScH_2^+." Aileen E. Alvarado-Swaisgood and James F. Harrison, J. Phys. Chem., 1985, 89, 5198.

4. "The Electronic and Geometric Structures of the Transition-Metal Carbyne Cations $ScCH^+$, $TiCH^+$, VCH^+, and $CrCH^+$." A. Mavridis, A.E. Alvarado-Swaisgood and J.F. Harrison, J. Phys. Chem., 1986, 90, 2584.

5. "Electronic and Geometric Structures of the Scandium Cations ScH^+, $ScCH_3^+$, $ScCH_2^+$, and $ScCH^+$." Aileen E. Alvarado-Swaisgood and James F. Harrison, Submitted to J. Phys. Chem.

6. "The Electronic and Geometric Structure of the Lowest $^5\Sigma^+$ and $^5\Pi$ States of $CrCl^+$." Aileen E. Alvarado-Swaisgood and James F. Harrison, Submitted to J. Phys. Chem.

MICHIGAN STATE UNIV. LIBRARIES
31293006343226